Moisture and chloride transport in porous materials

THEORETICAL AND EXPERIMENTAL STUDIES

Azee Taher

Bouwstenen 375

MOISTURE AND CHLORIDE TRANSPORT IN POROUS MATERIALS

Theoretical and experimental studies

PROEFSCHRIFT

ter verkrijging van de graad van doctor
aan de Technische Universiteit Eindhoven,
op gezag van de rector magnificus prof.dr. S.K. Lenaerts,
voor een commissie aangewezen door het College voor Promoties,
in het openbaar te verdedigen op dinsdag 20 februari 2024 om 13:30 uur

door

Azee Taher

Geboren te Arbil, Irak

Dit proefschrift is goedgekeurd door de promotoren en de samenstelling van de promotiecommissie is als volgt:

Voorzitter:	prof.dr.ir. M.C.J. Hornikx
Promotor:	prof.dr.ir. H.J.H. Brouwers
Co-promotor:	dr.ir. P. Spiesz (Heidelberg Materials Benelux)
Promotiecommissieleden:	prof.dr. H. Justnes (Norwegian University of Science and Technology)
	prof.dr.ir. J.C. Walraven (Delft University of Technology)
	prof.dr. I.S. Pop
	prof.dr.ir. D.M.J. Smeulders
	dr.ir. G.J.L. van der Wegen (SGS INTRON)

Het onderzoek of ontwerp dat in dit proefschrift wordt beschreven is uitgevoerd in overeenstemming met de TU/e Gedragscode Wetenschapsbeoefening.

Dedicated to my father: Jamal Taher

Moisture and chloride transport in porous materials - Theoretical and
experimental studies / by Azee Taher
A catalogue record is available from the Eindhoven University of Technology Library
ISBN 978-90-386-5953-4
Bouwstenen 375
NUR 924

Ph.D. Thesis, Eindhoven University of Technology, the Netherlands
Cover photo by Dirk Pero
Cover design by Azee Taher
Printed by TU/e print service ADC Dereumaux, Eindhoven, the Netherlands

Preface

This thesis would not have been possible without the help and support of many people.

First and foremost, my profound respect and gratitude are directed towards prof. dr.ir. H.J.H. Brouwers, my supervisor and promotor, for the opportunity to conduct my PhD research in the chair Building Materials, and for his support and sharing of experience and knowledge. Without his significant contributions, the completion of this thesis would have been impossible.

I would like to thank my co-promotor, dr.ir. Przemek Spiesz for his support, and encouragement throughout various stages of this work. It is a privilege to have benefited from his expertise, and I sincerely thank him for his dedication.

Dr.ir. Ton van der Zanden, my initial co-promotor, deserves a special mention for his dedication and support during the early years of my research journey leading up to this doctoral thesis.

I would like to extend my gratitude to the members of my promotion committee: prof.dr.ir. T.A.M. Salet from Eindhoven University of Technology (TU/e), prof.dr. H. Justnes from the Norwegian University of Science and Technology, prof.dr.ir. J.C. Walraven from Delft University of Technology, dr.ir. G.J.L. van der Wegen from SGS INTRON, prof.dr. I.S. Pop and Prof.dr.ir. D.M.J. Smeulders from TU/e. Their observations and invaluable suggestions have enriched my work immeasurably.

I must also acknowledge the indispensable roles played by the laboratory technicians and supporting staff who have been a beacon of guidance for the experimental work within the laboratory. Also to the phenomenal staff of the secretariat who have worked behind the scenes, ensuring smooth administrative operations and fostering a harmonious workspace.

It would be an oversight on my part if I did not express my profound gratitude to dr.ir. Hamid Montazari. Throughout this journey, he has been a constant pillar of support, providing invaluable counsel and friendship that were indispensable.

During my stay at the TU/e I have met some wonderful colleagues and I would like to address my appreciation to some former and current colleagues for their help and support: A.C.J. de Korte, M.V.A. Florea, A. Lázaro, G. Quercia, S. Lorencik, R. Yu, P. Tang, C. Straub, P.M.F. van de Wouw, X. Gao, B. Yuan, K. Schollbach, Q. Alam, H. Karimi and M. Ahmed.

In addition, I had the chance during my PhD to supervise two special master students: Thomas Arends and Jasper Hofstede with whom I shared the passion for working and who contributed to this thesis, opening new perspectives. Thank you for your help in assisting my research and hopefully my supervision has been helpful for your professional careers.

On a personal note, I would like to express my deepest appreciation to my family. My father, Jamal Taher, has been a bastion of strength, having dedicated his entire life to ensuring the well-being of his family. My mother, Saada Sultan's unending love and sacrifices, have been a guiding force throughout my journey.

I reserve a special acknowledgment for my beloved wife, Zhela Tahir her steady support and love made it possible for me to see this through. To my cherished daughters, Zara and Yara, the shining lights of my life. I love you both immeasurably.

I am also deeply indebted to my brothers, Rawa, Rashwan, Ari and Ahmad whose steadfast support and belief in me have been a source of continuous motivation. Furthermore, gratitude goes to, Demet, Ziela, Saz and their lovely children Nali, Maan, Inara, Mila and Aran for their support during the years of my PhD.

Every chapter of this thesis carries the imprints of the contributions, guidance, and unwavering support from each individual mentioned and many more. For all these and more, I remain eternally thankful.

Azee Taher

Arnhem, January 2024

Table of Contents

List of Figures

List of Tables

Nomenclature

a	Specific exchanging surface area	$[m^2/m^3]$
a_w	Water activity	[-]
b	Chloride binding intensity parameter	[-]
C	Water concentration	$[kg/m^3]$
C_m	Moisture concentration	$[kg/m^3]$
$C_{x=0}$	Water concentration at x=0	$[kg/m^3]$
$C_{t=0}$	Begin water concentration	$[kg/m^3]$
D	Diffusion coefficient of water in concrete	$[m^2/s]$
D_a	Arithmetic mean of the diffusion coefficients	$[m^2/s]$
D_g	Geometric mean of the diffusion coefficients	$[m^2/s]$
D_a	Diffusion coefficients for wetting	$[m^2/s]$
D_a	Diffusion coefficients for drying	$[m^2/s]$
D_m	Molecular diffusion coefficient of chloride in water	$[m^2/s]$
D_s	Dispersion coefficient of chloride in concrete	$[m^2/s]$
d_i	Distance from the rotation axis	[m]
F	Cumulative volume fraction	[-]
F_{max}	Porosity	[-]
g	Gravitational acceleration	$[m\ s^{-2}]$
K	Chloride binding capacity	$[m^{3n}/kg^n]$
k_r	Relative permeability	[-]
L	Length of the sample	[m]
M	Mass	[kg]
M_{Cl}	Molar mass of chloride	$[kg_{Cl}/mol_{Cl}]$
M_L	Mass of left side	[kg]
M_R	Mass of right side	[kg]
M_f	Mass flow	[kg/d]
M_l	Mass loss	[kg]
m	Moisture concentration	$[kg/m^3]$
m_s	Mass of the sample	$[kg_{solid}]$
m_s	Surface dried mass of sample	[g]
m_w	Mass of water-saturated sample	[g]
m_d	Mass of oven dried sample	[g]
m_{air}	Amount of water in the air	[g]
m_{total}	Amount of water in the system	[g]
N	Number of grid points	[-]
N_{AgNO3}	Molarity of silver nitrate solution	$[mol_{AgNO3}/m^3_{AgNO3}]$
n	Mass flux	$[kg/s\ m^2]$

n_m	Moisture flux	[kg/s m^2]
n_w	Water flux	[kg/s m^2]
$n_{s,w}$	Chloride flux in water	[kg/s m^2]
$n_{v,w}$	Volume flux	[m^3/s/m^2]
p	Pressure	[N/m^2]
p_c	Capillary pressure	[kg/m s^2]
R	Universal gas constant	[N m/K mol]
RH	Relative humidity	[%]
r	Pore radius	[m]
S	Chloride concentration in concrete	[kg/m^3]
S_t	Total concentration of chlorides	[kg_{Cl}/100 kg_{solid}] or [%]
s	Chloride concentration in water	[kg/m^3]
s_f	Free-chloride concentration	[kg_{Cl}/$m^3_{solution}$]
s_B	Bound-chlorides concentration	[kg_{Cl}/kg_{solid}]
$s_{outside}$	Chloride concentration in the water from the outside world	[kg/m^3]
T	Temperature	[°C] or [K]
t	Time	[s] or [h] or [d]
U	Water saturation	[-]
U_i	Initial saturation	[-]
U_b	Saturation at boundary	[-]
V	Volume	[m^3]
V_{AGNO3}	Volume of the titrated silver nitrate solution	[m^3_{AgNO3}]
v	Velocity	[m/s]
v_i	Molar volume of liquid	[m^3/mol]
w	Moisture concentration	[kg/m^3]
x	Position coordinate	[m]
z	Dimensionless length scale	[-]
Greek:		
ε	Elapsed time of blowing air	[s]
μ	Viscosity	[kg/m s]
ρ	Density	[kg/m^3]
ρ_m	Apparent density of liquid-saturated mortar	[kg_{solid}/m^3_{mortar}]
ρ_s	Specific density of mortar	[kg_{solid}/m^3_{solid}]
σ	Surface tension	[N/m]
τ	Tortuosity	[-]
Φ	Contact angle	[deg]

ϕ	Porosity	[$m^3_{solution}$/100 m^3_{mortar}] or [%]
φ	Volume fraction	[-]
ω	Angular velocity	[rad/s]

1. Introduction

1.1 Problem statement

Concrete is one of the oldest building materials in the world [1]. It usually consists of cement, aggregates and water. Concrete is characterized with high compressive strength, but rather low tensile strength. This disadvantage can be addressed by the addition of steel reinforcement.

In recent years, there is a clear trend towards design for sufficient durability (service lifetime) of concrete structures [2]. This requires the development and subsequent introduction of performance criteria as a design tool for practice. Corrosion of steel reinforcement induced by chlorides penetrating from the exposed concrete surface is considered as the major threat to the durability of concrete structures.

Concrete is a durable material, but there are a number of factors which influence concrete durability [3]. Chloride ingress into concrete is one of the most commonly found damage mechanisms [4]. When chloride reaches the rebars, corrosion can onset and that decreases the service lifetime of the structures. The steel reinforcement in concrete is normally well protected against corrosion. This protection is based on the alkalinity of the pore water of concrete [5]. The high pH generates a thin protective layer on the steel surface. This passivation layer inhibits the corrosion process. This layer can vanish due to the chloride.

Chloride penetrates into concrete with water. That is especially the case when concrete structure comes in contact with seawater (Figure 1.1). Because of the presence of chloride in seawater, chloride can intrude in concrete and affect the reinforcement [6]. The corrosion of the reinforcements is often detected in marine structures, especially in the splash and tidal zones [7-9]. The chloride penetration into marine structures begins with the wetting phase, in which the external layer of concrete is saturated with a chloride solution by capillary adsorption. In the drying phase, the water evaporates leaving chloride behind [10]. During the next wetting phase, the pores are again filled with seawater, which dissolves salts already present in the pore. Therefore, the concentration of chloride rises. Once the chloride concentration at the level of rebars exceeds the critical value, corrosion of the steel reinforcement will occur [11-13].

Another example of damage caused by chloride is clearly visible in tunnels and parking garages [14]. The corrosion in tunnels and parking garages occurs because, in winter, de-icing salt is used on the roads to prevent them from freezing. This de-icing salt dissolves in the water present on the roads. The water spray

Figure 1.1: Rebar corrosion in a concrete pile in a marine structure in the splash and tidal zones[1].

[1] Retrieved from https://www.portstrategy.com/news101/port-operations/marine-engineering/treating_your_piles

containing chloride is being transported to the bottom of bridge decks, columns of viaducts and tunnel walls, and this leads to chloride penetration in those structures, as shown in Figure 1.2. The floor of parking garages can also be exposed to chlorides, because of the de-icing salt that is brought in by cars. For all these reasons, further research needs to be performed to better understand the individual and combined impacts of moisture transport and chloride transport in concrete.

Research on moisture transport in concrete can be performed by experimental tests [15] or theoretical models [16-22]. Experimental tests offer the advantage that the real situation is studied and the full complexity of the problem is taken into account. However, they are normally rather expensive and time-consuming. In addition, there is no or only limited control over the boundary conditions in order to be in accordance with practice.

Also, important parameters cannot be measured easily and accurately. For example, measuring moisture profiles in concrete is a difficult task, and can only be accurately conducted using advanced methods such as the magnetic resonance imaging (MRI) technique [15]. However, this is an expensive approach and can only be used for very small samples. This technique, therefore, cannot explicitly represent the moisture transport in large scales as it occurs in practice. Therefore, the need for a simple and inexpensive experiment set-up is of great importance [23].

Theoretical approaches, on the other hand, are simple and rather fast. In addition, they easily allow efficient parametric studies. This approach allows full control over the boundary conditions. However, the accuracy and reliability of such as approach are of concern.

Given the complexity involved in determining the impact of different parameters on moisture transport, different coefficients are normally developed and used in theoretical models. The accuracy of these models therefore highly depends on the accuracy of these coefficients. Nevertheless, the accuracy of these coefficients depends on the availability and accuracy of experimental tests. For example, given the complexity involved in measuring sorption isotherm curves for concrete, these curves are normally developed based on a limited number of measured points that could not be sufficient to accurately describe the correlation between moisture content and relative humidity of the environment. This can, therefore, significantly influence the accuracy of moisture transport models [24].

Figure 1.2: Corrosion of steel reinforcement due to de-icing salts in a parking garage[2].

[2] Retrieved from https://rbconspro.wordpress.com/tag/aditivo-inhibidor-de-corrosion

A detailed review of the literature reveals that several studies have been performed to investigate the individual impacts of moisture and chloride transport in concrete. Nevertheless, the interaction between the moisture and chloride has not yet been systematically investigated [25].
While the focus in most of the previous studies has been on moisture and chloride transport either by diffusion and capillary suction or convection, the interaction between the three different transport mechanisms (i.e., natural diffusion, capillary suction and convection) should be further studied.
The research gaps can, therefore, be summarized as follows:

- Lack of detailed research on the performance of different moisture transport models.
- Lack of simple and cheap experimental set-up for measuring moisture transport in concrete.
- Lack of high-resolution data for sorption isotherm.
- Lack of knowledge on the combined impacts of moisture and chloride.
- Lack of knowledge about the interaction between different transport mechanisms (diffusion, capillary suction and convection).

Based on the above-mentioned research gaps, the main objectives of this thesis are:

- Compare the performance of different moisture transport models.
- A detailed description of measuring procedure of moisture transport in concrete.
- A detailed evaluation of the impact of sorption isotherm on moisture transport in concrete.
- A detailed evaluation of the combined impacts of moisture and chloride.
- A detailed evaluation of the interaction between different transport mechanisms (diffusion, capillary suction and convection).

1.2 Thesis outline

This thesis is based on five journal papers and conference papers:

- **Chapter 2:** Taher, A. Cao, X. Pop, I.S. van der Zanden, A.J.J. & Brouwers, H.J.H. (2013). Moisture transport in concrete during wetting/drying cycles. *Chemistry and Materials Research*, 5, 86-90.
- **Chapter 3:** van der Zanden, A.J.J. & Taher, A. (2014). A gravitational procedure to measure the diffusion coefficient of mater in porous materials: a case study on concrete. *Drying Technology*, 32(6), 708-712.
- **Chapter 4:** Taher, A. & Brouwers, H.J.H. (2023). Sorption isotherm measurements for porous materials: A new hygroscopic method. *Construction and Building Materials*, 379, 131166.
- **Chapter 5:** van der Zanden, A.J.J. Taher, A. & Arends, T. (2015). Modelling of water and chloride transport in concrete during yearly wetting/drying cycles. *Construction and Building Materials*, 81, 120-129.

- **Chapter 6:** Taher, A. van der Zanden, A.J.J. & Brouwers, H.J.H. (2013). Chloride transport in mortar at low moisture concentration. *Chemistry and Materials Research*, 5, 53-56.
- **Chapter 7:** Taher, A. Hofstede, J.M. van der Zanden, A.J.J. & Brouwers, H.J.H. (2014). The influence of air in mortar on the results of the RCM test. Proceedings of the 5th International Conference on Non-Traditional Cement and Concrete (NTCC2014), June 16-19 2014, Brno, Czech Republic (pp. 245-248) & Taher, A. Qu, Z. & Brouwers, H.J.H. (2017). Influence of air on the chloride penetration in concrete. Proceedings of the 9th International Symposium on Cement and Concrete (ISCC 2017), November 1-4 2017, Wuhan, China.

The correlation between the 8 chapters of this thesis is presented in Figure 1.3. In Chapter 2, two methods that are used and compared theoretically to describe moisture transport in concrete structures during drying/wetting cycles. In addition, an experimental setup is proposed to validate the models. In Chapter 3, a measuring procedure is proposed to obtain the diffusion coefficient of water in porous materials. In this procedure, a centrifuge is used to create a non-homogenous water distribution inside a porous material. In addition, an equation is derived with which the concentration gradient of a partially saturated sample in a gravity field can be determined. Chapter 4 presents a novel experimental setup to measure the sorption isotherm in which more points can be measured with an adjustable measurement resolution. Two porous materials are considered: mortar and sand-lime, where the results are compared with the results found in the literature. In addition, the effect of chloride on the sorption isotherm is investigated and compared with the case without chloride. Chapter 5 presents a model for the transport of chloride in concrete that is not saturated with water. The transport of water is described with a diffusion coefficient. The transport of chloride includes the transport of chloride dissolved in the pore water moving through the concrete and the transport of chloride caused by a gradient in the pore water chloride concentration. Two processes are taken into account: (i) chloride convection, and (ii) chloride diffusion (modelled with the Fick's law). The model is applied to concrete with a daily and yearly cycle of drying and wetting. Chapter 6 investigates the impact of chloride on moisture transport in concrete for low moisture concentration. An experimental setup is developed to measure moisture transport in thin specimens. Two materials are considered, mortar and sand-lime, where the measurements are performed for samples with and without chloride. Chapter 7 experimentally studies the chloride transport in unsaturated concrete to better understand the capillary suction mechanism of the chloride transport in the surface layers of unsaturated concrete. The measurements are performed in two stages. The first experiment compares two transport mechanisms, i.e. natural diffusion and capillary suction, while the second experiment is performed to evaluate forced migration and capillary suction in unsaturated concrete. Chapter 8 gives the conclusions of the research.

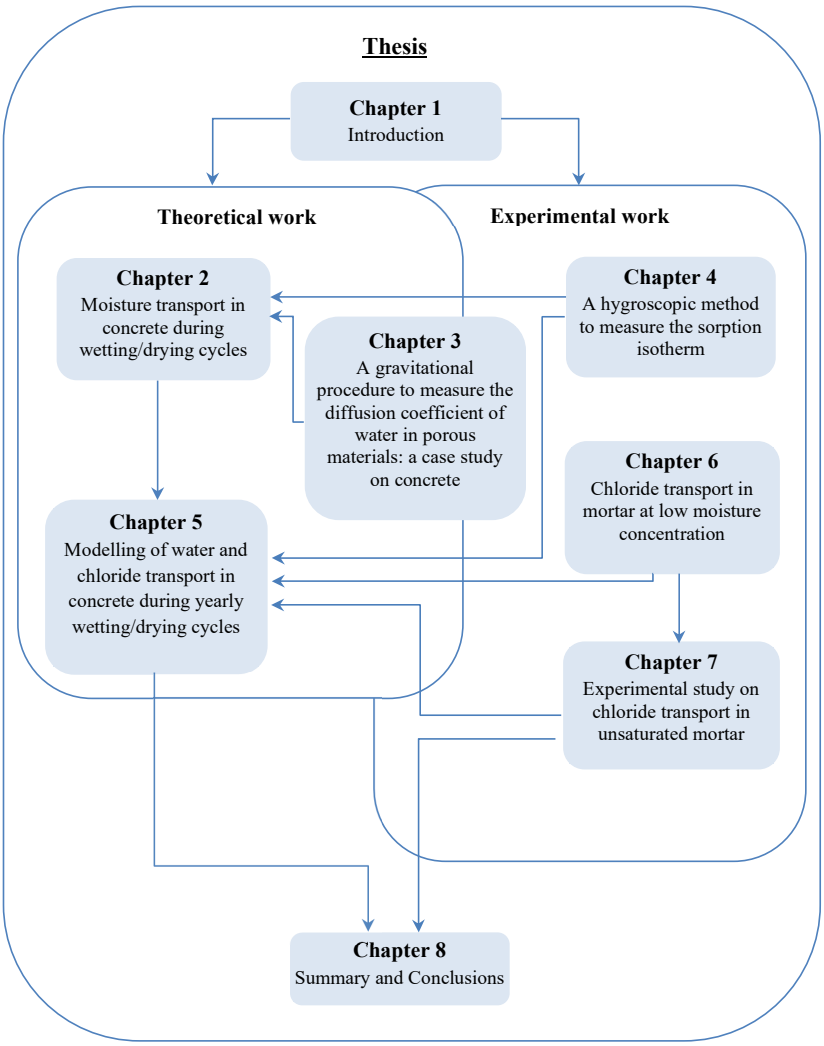

Figure 1.3: Outline of this thesis.

1.3 References

[1] Forty A., Concrete and culture: A material History, Reaktion Books LTD, UK (2012).

[2] Ho D.W.S. and Chirgwint G. J., A performance specification for durable concrete, Construction and Building Murerials 10 (1996) 375-319.

[3] A1-Rabiah A.R., Baggott R., Durability Requirements for Reinforced Concrete Construction in Aggressive Marine Environments, Marine Structures 3 (1990) 285-300.

[4] Glass G.K., Buenfeld N.R., The presentation of the chloride threshold level for corrosion of steel in concrete, Corrosion Science 39 (1997) 1001-1013.

[5] Martín-Pérez B., Zibara H., Hooton R.D., Thomas M.D.A., A study of the effect of chloride binding on service life predictions, Cement and Concrete Research 30 (2000) 1215-1223.

[6] Carrozzino S., Righini F., Ion chromatographic determination of nutrients in sea water, Journal of Chromatography A (1995) 277-280.

[7] Bohno H., Corrosion in reinforced concrete structures, Woodhead publishing Ltd and CRC (2005).

[8] CUR, Durability of concrete structures in marine environments, CUR Report 215, Stichting CUR (2005).

[9] Moonen M.R., Chloride-indringing in beton, Master thesis Civil Engineering, University of Twente, The Netherlands (2005).

[10] Hong K., Hooton R.D., Effects of cyclic chloride exposure on penetration of concrete cover, Cement and Concrete Research 29 (1999) 1379-1386.

[11] Pel L., Sawdy A., Voronia V., Physical principles and efficiency of salt extraction by poulticing, Journal of Cultural Heritage 11 (2010) 59-67.

[12] Uji K., Matsuoka Y., Maruya T., Formation of an equation for surface chloride content of concrete due to permeation of concrete, Corrosion of reinforcement of concrete (1990) 58-267.

[13] Ann K.Y., Ahn J.H., Ryou J.S., The importance of chloride content at the concrete surface in assessing the time to corrosion of steel in concrete structures, Construction and Building Materials 23 (2009) 239-245.

[14] Zuquan J., Xia Z., Tiejun Z., Jianqing L., Chloride ions transportation behavior and binding capacity of concrete exposed to different marine corrosion zones, Construction and Building Materials 177 (2018) 170–183.

[15] Pel L., Moisture transport in porous building materials, PhD Thesis, Eindhoven University of Technology, the Netherlands (1995).

[16] Haupl P. and Stopp H., Feuchtetransport in baustoffen und bauwerksteilen, PhD Thesis, TU Dresden (1987).

[17] Haupl P., Fechner H., Hygric material properties of porous building materials, Journal of Building Physics 26 (2003) 259-284.

[18] Pel L., Brocken H., Kopinga K., Determination of moisture diffusivity in porous media using moisture concentration profiles, Heat and Mass Transfer (1996) 1273-1280.

[19] Kunzel H.M., Verfahren zur ein-und zweidimensionalen Berechnung des gekoppelten Feuchte- und Warmetransports in Bauteilen mit einfachen Kennwerten, PhD Thesis, Stuttgart University (1994).

[20] Krus M., Holm A., Simple methods to approximate the liquid transport coefficients describing the absorption and drying, Proceedings of sympossium: Physics in the Nordic Countries', Göteborg (1999).

[21] Janssen H., Blocken B., Carmeliet J., Conservative modelling of the moisture and heat transfer in building components under atmospheric excitation, International Journal of Heat and Mass Transfer 50 (2007) 1128-1140.

[22] Pinder F.G., Gray G.W., Essentials of Multiphase Flow and Transport in Porous Media, John Wiley & Sons, Inc, New Jersey (2008).

[23] Belhamri A., Characterization of the first falling rate period during drying of a porous material, Drying Technology 21 (2003) 1235-1252.

[24] Zhang Z., Modelling of sorption hysteresis and its effect on moisture transport within cementitious materials, PhD Thesis, Université Paris-Est (2014).

[25] Homan L., Ababneh A., Xi Y., The effect of moisture transport on chloride penetration in concrete, Construction and Building Materials 125 (2016) 1189-1195.

2

2. Moisture transport in mortar and concrete during wetting/drying cycles

This chapter has been published as:

Taher, A. Cao, X. Pop, I.S. van der Zanden, A.J.J. & Brouwers, H.J.H. Moisture transport in concrete during wetting/drying cycles. Chemistry and Materials Research 5 (2013) 86-90.

2.1 Introduction

Durability of concrete is strongly related to the moisture transport. Moisture transport in marine environment, where drying and wetting cycles occur, leads chloride to penetrate into reinforced concrete structures. When chloride reaches the rebars, corrosion can appear and that decreases the service life time of the structures. By describing the moisture transport in such a structure, the service life can be determined. Many descriptions of moisture transport in concrete can be found in the literature. For example, the authors [1-5] describe moisture transport in concrete structures by using a single diffusion coefficient. In [6-8], the same by using two different diffusion coefficients for drying and wetting. The purpose of this study is to compare these two methods of describing moisture transport in concrete structures during drying/wetting cycles. In addition to the modelling, an experimental set-up is proposed to validate the models.

2.2 Moisture transport in concrete

The diffusivity equation is a commonly used equation in building physics for both vapour and liquid moisture transport. Prior to the availability of numerical simulation, analytical solutions had to be applied to determine both heat and mass transfer. Generally, diffusivity approaches are derived from moisture profiles of water uptake or drying experiments. Inserting the diffusion equation into the balance equation leads to calculating the volumetric water content. In the following subsections, various diffusivity approaches are outlined.

2.2.1 Diffusivity approach according to Häupl

Häupl and Stopp's standard diffusivity function [9] provides an analytic solution for the water uptake problem (Figure 2.1 a), where the parameter k is a shape factor moving the strong slope of the diffusivity function. A second diffusivity approach by Häupl and Fechner [10] introduced a fixed water content as an additional parameter at which liquid water transport inside the material begins, this is specified to be the sorption moisture content with values of 35% and 80% relative humidity (Figure 2.1 b). The value for sorption moisture content is dependent on available material data and has to be adjusted or chosen accordingly. The standard diffusivity function is very flexible and can therefore be applied to most building materials. However, the practical application of this function is hampered by difficulties in parameter identification. In addition, the standard diffusivity function is sensitive to lower moisture levels which may result in an overestimation of liquid water transport. This issue may be resolved by applying the modified diffusivity function. However, this approach can only be applied for a limited selection of materials.

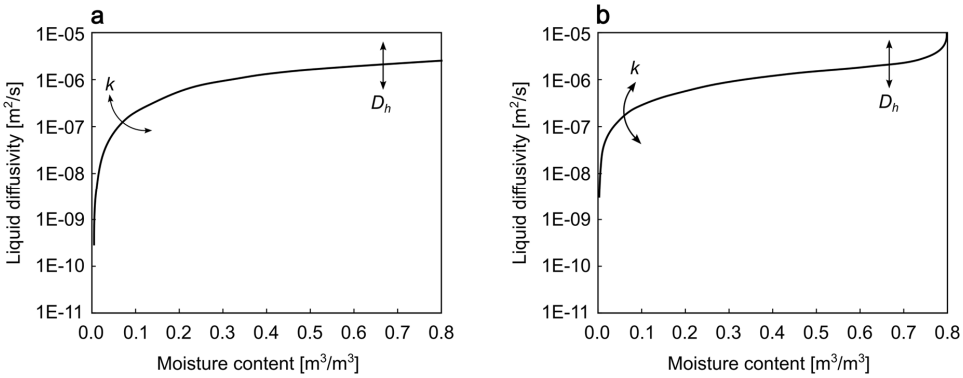

Figure 2.1: Water diffusivity in porous materials according to [9, 10].

2.2.2 Diffusivity approach according to Pel

Pel [11] specifies a vapor diffusivity function with several parameters considering an increase due to effects of hysteresis and the influence of surface diffusion and liquid water islands on vapor transport. Pel defines a moisture diffusivity which accounts for liquid and vapor transport as shown in Figure 2.2, where β is the slope of the function. The approach has good flexibility but is hampered by the requirement for measurements of moisture profiles or a combination of measured data and numerical simulation in order to make appropriate adjustments to the parameters. Pel has provided examples of parameter values that can be used for certain materials. Should these examples not be applicable, and measured data or numerical simulations are not available, then Pel's approach cannot be used.

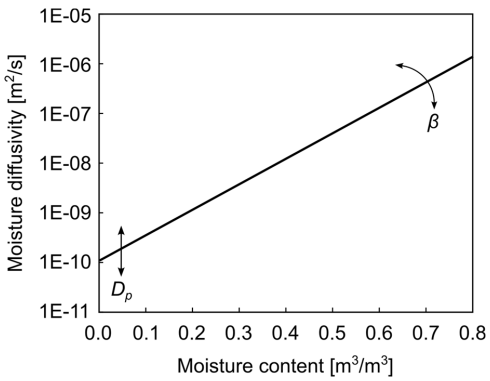

Figure 2.2: Moisture diffusivity in porous materials according to Pel [11].

2.2.3 Diffusivity approach according to Künzel

Künzel [12] has modelled heat and moisture transport phase separately, whereby he defined several transport coefficients for liquid water and water vapor transport without any elaboration on the practical determination of these parameters. Interestingly, whereas Künzel described a moisture content dependent vapor diffusion coefficient which is restricted to a certain range of values due to short-cuts at capillary water islands, Künzel uses a constant vapor diffusion coefficient which is independent from moisture content (Figure 2.3). In essence, Künzel provided a simplified approach to determine the material coefficients. In addition, he proposes to consider the impact of the hysteresis and highlights the need to define two diffusivity functions.

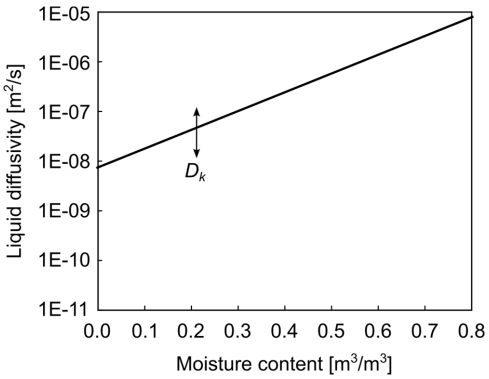

Figure 2.3: Water diffusivity in porous materials according to Künzel [12].

2.2.4 Diffusivity approach according to Krus and Holm

Krus and Holm [13] described experimental methods for determination of material properties. Based on the approaches from Künzel (described above) a more flexible diffusivity approach was developed by Krus and Holm. They propose the use of two diffusivity functions, one for capillary suction under water contact D_{cp} and one for liquid water transport without water contact D_{wc} (Figure 2.4).

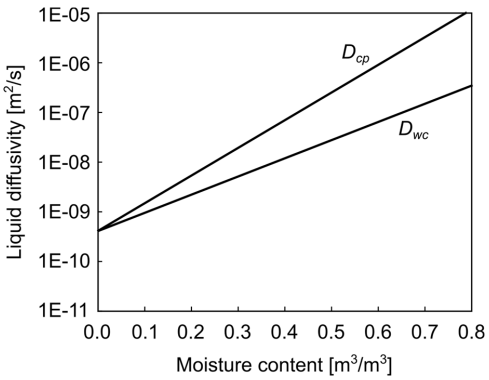

Figure 2.4: Water diffusivity in porous materials according to Krus and Holm [13].

2.2.5 Diffusivity approach according to Carmeliet and Janssen

Two further diffusivity approaches have been described and have been further improved upon by Carmeliet and Janssen [14]. The first one is a general exponential function, i.e. simplified diffusivity approach, which is comparable to Pel's approach and accounts for the liquid water diffusivity. This function includes only one adjustable parameter, and therefore does not require much input data. The second one is a sum of a function in the lower moisture range and an increasing exponential function in the higher moisture range as shown in Figure 2.5. This approach has a high flexibility, especially in the lower moisture content range; however, there are many parameters that need to be adjusted. A particular issue with this approach is that the function is only reliable if its parameters are adjusted correctly based on material data, which may not be available.

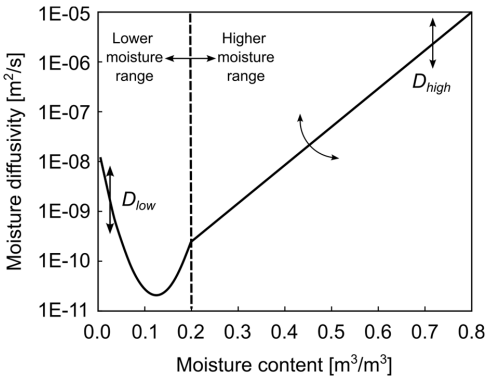

Figure 2.5: Improved moisture diffusivity in porous materials according to Carmeliet and Janssen [14].

2.2.6 Summary and Conclusions

After reviewing the various diffusivity approaches for moisture transport in building materials, it can be concluded that each method has its unique strengths and limitations.

1. Häupl's standard diffusivity function is versatile and applicable to a wide range of materials, but its practical application is hindered by difficulties in parameter identification and sensitivity to lower moisture levels. The modified version of Häupl's function offers a solution to the overestimation of liquid water transport but is limited in its applicability to specific materials.
2. Pel's vapor diffusivity function offers good flexibility and considers the effects of hysteresis and surface diffusion. However, its application is limited by the need for measured moisture profiles or a combination of measured data and numerical simulation for parameter adjustments.
3. Künzel's approach models heat and moisture transport separately, but it lacks elaboration on the practical determination of transport coefficients. Künzel's simplification of the vapor diffusion coefficient disregards moisture content dependence, potentially limiting its accuracy.
4. Krus and Holm's diffusivity approach builds upon Künzel's work and offers more flexibility with the introduction of two separate diffusivity functions. This method is better suited for experimental determination of material properties but might require additional complexity in its application.
5. Carmeliet and Janssen's diffusivity approaches provide high flexibility, particularly in the lower moisture content range. The simplified approach requires minimal input data, while the more complex approach needs careful parameter adjustments based on material data that may not always be available.

In conclusion, the selection of a suitable diffusivity approach depends on the specific materials being studied, the availability of material data, and the required level of accuracy. Researchers and practitioners should carefully consider these factors when choosing an appropriate method for their moisture transport analysis in building materials.

2.3 Mathematical model

In this study, the moisture transport (one phase flow) in concrete is described based on the Darcy's law and mass balance [15]:

$$v = -\frac{\bar{k}}{\mu} k_r \nabla p_c \tag{2.1}$$

$$\frac{\partial}{\partial t}(\phi\ U) + \nabla \cdot v = 0 \tag{2.2}$$

where v is the volumetric velocity, $\bar{k}$ the intrinsic permeability of the concrete, k_r the relative permeability (-), μ the viscosity, p_c the capillary pressure, ϕ is the porosity of the concrete, U the water saturation, and t the time. Commonly, k_r and p_c are increasing functions of the saturation U, see [15]. By substituting Eq. (2.1) into Eq. (2.2),

$$\frac{\partial}{\partial t}(\phi U) - \nabla \cdot \left(\frac{\bar{k}}{\mu} k_r \nabla p_c\right) = 0 \tag{2.3}$$

Furthermore, the following is assumed in this study:

- The sample is homogeneous.
- One-dimensional transport.
- There is no flow at the boundaries except one open boundary.
- The initial saturation is constant.

For the boundary at the right, a periodic repetition of wetting and drying cycles is assumed. In view of these assumptions, the lateral flow is 0. This allows reducing the model to one dimension. The sample occupies then the interval $(0, L)$. The following conditions are imposed,

$$at \quad t = 0: \quad U = U_i, \qquad \text{in } (0, L) \tag{2.4}$$

$$at \quad x = 0: \quad \frac{\bar{k}}{\mu} k_r \frac{\partial p_c}{\partial x} = 0, \qquad t > 0 \tag{2.5}$$

$$at \quad x = L: \quad U = U_b(t), \qquad t > 0 \tag{2.6}$$

where U_i is the initial saturation, $U_b(t)$ the saturation at the right boundary. In the context of the one-dimensional model, Eq. (2.3) becomes

$$\frac{\partial}{\partial t}(\phi\ U) - \frac{\partial}{\partial x}\left(\frac{\bar{k}}{\mu} k_r \frac{\partial p_c}{\partial x}\right) = 0 \tag{2.7}$$

To make the equation dimensionless, the following notations are introduced:

$$x := \frac{x}{L}, \quad t := \frac{t}{T}, \quad p_c := \frac{p_c}{P} \tag{2.8}$$

where *L, T, P* are characteristic values for the length, time, and capillary pressure. Substituting Eq. (2.8) into Eq. (2.7) and setting

$$\frac{T}{L^2} = \frac{\phi \mu}{\bar{k} P} \tag{2.9}$$

then Eq. (2.7) transforms into

$$\frac{\partial U}{\partial t} = \frac{\partial}{\partial x}\left(D(U)\frac{\partial U}{\partial x}\right) \tag{2.10}$$

Here

$$D(U) = k_r(U) \cdot \frac{dp_c(U)}{dU} \tag{2.11}$$

By using the Kirchhoff transformation

$$\beta(U) = \int_0^s D(v)dv \tag{2.12}$$

Eq. (2.10) becomes

$$\frac{\partial U}{\partial t} = \partial_{xx}\beta(U) \tag{2.13}$$

while the initial and boundary conditions are,

$$U(x,0) = U_i, \quad \frac{\partial U}{\partial x}(0,t) = 0, \quad U(1,t) = U_b(t) \tag{2.14}$$

where U_i is a constant number between 0 (in case of dried concrete) and 1 (in case of water saturated concrete). $U_b(t)$ is a periodic function, which simulates wetting/drying cycles,

$$U_b(t) = \begin{cases} 1 & t \in (0, T_w] + k \cdot T_p, \\ 0 & t \in (T_w, T_p] + k \cdot T_p, \end{cases} \tag{2.15}$$

where T_d is the dimensionless drying time, T_w is the dimensionless wetting time, $T_p = T_d + T_w$, is the period of one cycle, and k is any natural number.

2.4 Approaches

Two modelling approaches for the moisture transport in concrete are compared in this work. The first model uses the same diffusion coefficient for both wetting and drying phase. The second model uses two diffusion coefficients, one for the drying $D^-(U)$ and one for the wetting $D^+(U)$. In [8], the following coefficients are determined experimentally:

$$D^+(U) = 10^{-10} \cdot e^{6 \cdot U} \tag{2.16}$$

$$D^-(U) = 10^{-10} \cdot \left(0.025 + \frac{0.975}{1 + \left(\frac{1-U}{0.208}\right)^6}\right) \tag{2.17}$$

which are plotted in Figure 2.6.

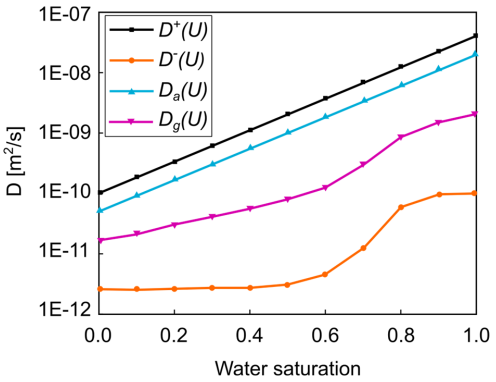

Figure 2.6: Various diffusion coefficients as a function of saturation.

2.4.1 Standard model: one diffusion coefficient

A standard model considers the same diffusion coefficient for both wetting and drying, in view of Eq. (2.16) and Eq. (2.17), the following averages are considered:

$$D_a(U) = \frac{D^+(U) + D^-(U)}{2} \tag{2.18}$$

$$D_g(U) = \sqrt{D^+(U) \cdot D^-(U)} \tag{2.19}$$

Here $D_a(U)$ is the arithmetic mean of the diffusion coefficients, $D_g(U)$ the geometric mean of the diffusion coefficients, $D^+(U)$ the diffusion coefficient for wetting and $D^-(U)$ the diffusion coefficient for drying, see Eqs. (2.16) and (2.17). The coefficients introduced in Eqs. (2.18) and (2.19) are then used for the Kirchhoff transformation in Eq. (2.10). For the resulting model, Eq. (2.12), an implicit numerical scheme [16] is combined with a linear iterative procedure [17].

2.4.2 Hysteretic model

Here the hysteretic model in [18] is adapted,

$$\frac{\partial U}{\partial t} = \partial_{xx} p(U) \tag{2.20}$$

In the above, $p(U)$ has to include the switch between two diffusion coefficients, in this case, $p(U)$ reads

$$p(U) = p_e(U) + \gamma(U) \cdot sign(\partial_t U) \tag{2.21}$$

where $p_e(U)$, $\gamma(U)$ and $sign(\partial_t U)$ are defined as

$$p_e(U) = \frac{\beta^+(U) + \beta^-(U)}{2} \tag{2.22}$$

$$\gamma(U) = \frac{\beta^+(U) - \beta^-(U)}{2} \tag{2.23}$$

and

$$sign(\partial_t U) = \begin{cases} 1 & if \quad \partial_t U > 0 \\ -1 & if \quad \partial_t U < 0 \end{cases} \tag{2.24}$$

$\beta^{+/-}(U)$ are the Kirchhoff transformations for the wetting/drying diffusion coefficients,

$$\beta^{+/-}(U) = \int_0^U D(z)^{+/-} dz \tag{2.25}$$

When solving the system, $sign(\partial_t U)$ is replaced by the regularization $sign_\delta(\partial_t U)$ (Figure 2.7),

$$sign_\delta(\partial_t U) = \begin{cases} \delta\partial_t U + \delta^2 - 1 & if \quad \partial_t U < \delta \\ \dfrac{\partial_t U}{\delta} & if -\delta < \partial_t U < \delta \\ \delta\partial_t U - \delta^2 + 1 & if \quad \partial_t U > \delta \end{cases} \tag{2.26}$$

where $0 < \delta << 1$ is the regularization parameter.

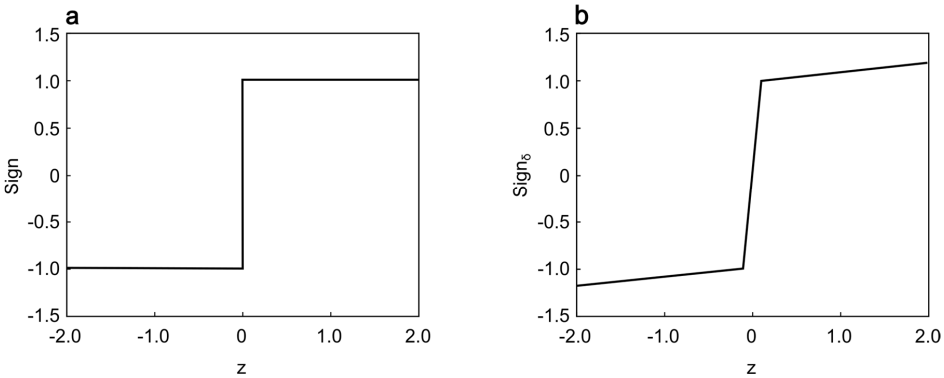

Figure 2.7: The graphs of (a) $sign$ and (b) $sign_\delta$.

Solving the above equations directly using the finite difference method leads to incorrect results. Alternatively, the inverse $\phi_\delta(r)$ of the regularized $sign_\delta$ is used as considered in [19],

$$\phi_\delta(r) := \begin{cases} -\delta + \dfrac{r+1}{\delta} & if \quad r < -\delta, \\ \delta r & if \quad r \in [-\delta, \delta], \\ \delta + \dfrac{r-1}{\delta} & if \quad r > \delta, \end{cases} \tag{2.27}$$

For the time discretization, let Δt be the time step, and $p^m \approx p(m \cdot \Delta t)$, $U^m \approx U(m \cdot \Delta t)$
The implicit discretization's of Eq. (2.20) and Eq. (2.21) are:

$$\begin{aligned} \frac{U^{m+1} - U^m}{\Delta t} &= \partial_{xx} p^{m+1} \\ \frac{U^{m+1} - U^m}{\Delta t} &= \phi_\delta\left(\frac{p^{m+1} - p_e(U^{m+1})}{\gamma(U^m)}\right) \end{aligned} \tag{2.28}$$

where $m = 0,1,\ldots$ initially, $U^0 = U_i$. Further, at $x = 0$, $\partial_x p^{m+1} = 0$, and at $x = L$, $U^{m+1} = U_b((m+1)\Delta t)$.

In the equations above, Eq. (2.28) and the left side of Eq. (2.29) are explicit for U^{m+1}. The right side of Eq. (2.29) is implicit for U^{m+1}, due to the nonlinear function of $P_e(U)$. Therefore, $P_e(U^{m+1})$ is simplified for a linear function as investigated in [20] by a Taylor expansion given by

$$p_e(U^{m+1}) = p_e(U^m) + p_e'(U^m) \cdot (U^{m+1} - U^m) \tag{2.29}$$

Then the discretized form becomes

$$\begin{aligned} \frac{U^{m+1} - U^m}{\Delta t} &= \partial_{xx} p^{m+1}, \\ \frac{U^{m+1} - U^m}{\Delta t} &= \phi_\delta \left(\frac{p^{m+1} - p_e(U^m) - p_e'(U^m) \cdot (U^{m+1} - U^m)}{\gamma(U^m)} \right) \end{aligned} \tag{2.30}$$

For discretizing the spatial derivatives, finite differences on a grid with $\Delta x = 1/N$ $(N \in \mathbb{N})$ are used.

2.5 Numerical results

The model is implemented in Matlab. Here, only one cycle is computed, which is one day for wetting and six days for drying. The initial condition (U_i) in this case is assumed to be 50% saturation. Further, the following is used in the numerical scheme: $\delta = 10^{-5}$, and $\Delta x = 10^{-3}$, $dt = 10^{-6}$.
The comparison between the results of the standard model with one diffusion coefficient and the results of the hysteretic model with two diffusion coefficients are shown in Figure 2.8.

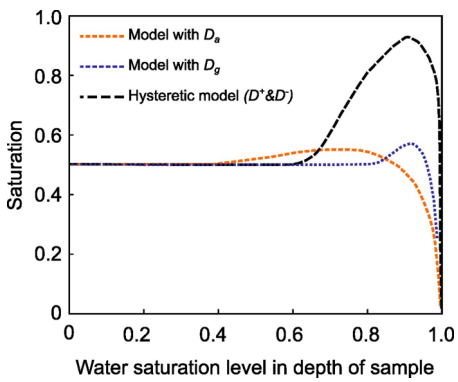

Figure 2.8: Comparison of the models.

The results show that there is a large difference between the three models, especially at the surface layers. The hysteretic model shows a higher concentration at the surface than the standard models. The experimental work in the next section, gives an explanation about the difference in results between the approaches.

2.6 Experimental work

Designing an experimental set-up which imitates the numerical work is often very challenging. These difficulties lie in the reproducing of the boundary conditions. In addition, measuring the water concentration profiles in a sample is also challenging and very costly, being Magnetic Resonance

Imaging (MRI) one of the suitable non-destructive methods. Due to these reasons a simple experiment set-up is designed to validate the numerical work. Cylindrical mortar samples with a diameter of 10 cm, 2.5 cm thickness and the properties as shown in Table 2.1 are used in this experiment. The sample is saturated using the vacuum method and dried with air for a certain period of time and then wetted again by simply placing it in water. During this process the weight of the sample is monitored. Figure 2.9 shows the results obtained on the mortar sample.

Table 2.1: Main characteristics of mortar.

Materials	**Mortar**	
	Volume [m³]	**Mass [kg]**
CEM I 42,5N	159.5	502.2
Sand	568.5	1506.5
Water	251.1	251.1
Superplasticizer	0.9	1
Air	20	-
w/c	0.5	
Porosity / 28-day	17 %	
Compressive strength / 28-day	56.8 MPa	
Flexural strength / 28-day	8.9 MPa	

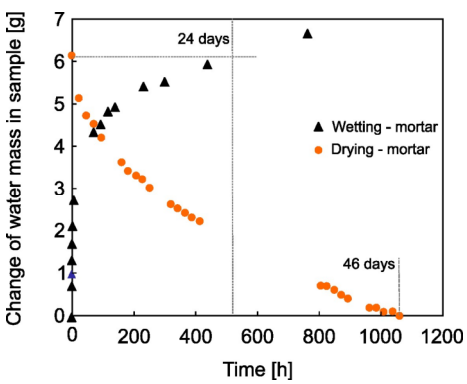

Figure 2.9: The measured mass of water in a mortar sample in the present study.

The saturated sample is dried by blowing dry air on the surface for 46 days. This is done to simulate drying. The weight of the samples during this period of time decreases by 6 grams. This means that 6 grams of water is transported out the sample during 46 days. Directly hereafter, the same sample is put into water to simulate wetting. The weight of the sample is also measured in this case. To increase the weight of the sample by 6 grams, placing the sample for 24 days in water is needed. This suggests that the water transport in a mortar sample is different during wetting and drying. From this experiment it can be concluded that numerical models with hysteresis are needed for a more accurate description of this process.

2.7 Conclusions

Two various methods (standard method and hysteretic method) to describe moisture transport in concrete during wetting/drying cycles are implemented in Matlab and the results are compared. Diffusion

coefficients measured in the literature are used in these models. One cycle of wetting/drying is compared. The duration of the wetting phase is one day and drying is six days. From the obtained numerical results, it can be concluded, that using the standard model with one diffusion coefficient or using the hysteretic model with two diffusion coefficients, can have a large influence on the results. After one cycle, the hysteretic model clearly gives a higher amount of moisture content in the structure, as it is shown in Figure 2.8. A simplified experiment is performed for validation. From the experimental results it can be concluded that models with hysteretic approaches describe the water transport during wetting and drying cycles better.

2.8 References

[1] Meijers S.J.H., Bijen J.M.J.M., Borst de R., Fraaij A.L.A., Computational results of a model for chloride ingress in concrete including convection, drying-wetting cycles and carbonation. Materials and structures 38 (2005) 145-154.

[2] Arfvidsson J., A new algorithm to calculate the isothermal moisture penetration for periodically varying relative humidity at the boundary, Nordic Journal of Building Physics 2 (1999) 11-21.

[3] Cunningham M.J., Moisture diffusion due to periodic moisture and temperature boundary conditions Çöan approximate steady analytical solution with non-constant diffusion coefficients, Building and Environment 27 (1992) 367-377.

[4] Pel L., Moisture transport in porous building materials, PhD Thesis, Eindhoven University of Technology, the Netherlands (1995).

[5] Selander A., Hydrophobic Impregnation of Concrete Structures: Effects on Concrete Properties, PhD Thesis, Sweden (2010).

[6] Torrenti J.M., Granger L., Diruy M., Genin P., Modeling concrete shrinkage under variable ambient conditions, ACI Materials Journal 96 (1999) 35-39.

[7] Baroghel-Bouny V., Caractérisation des pâtes de ciment et des bétons-Méthodes, analyse, interpretations, Laboratoire central des Ponts et Chaussées, France (1994).

[8] Li C., Li K., Chen Z., Numerical analysis of moisture influential depth in conrete during drying-wetting cycles, Tsinghua Science & Technology 13 (2008) 696-701.

[9] Haupl P. and Stopp H., Feuchtetransport in baustoffen und bauwerksteilen, PhD Thesis, TU Dresden, (1987).

[10] Haupl P., Fechner H., Hygric material properties of porous building materials, Journal of thermal envelope and building science 26 (2003) 259-284.

[11] Pel L., Brocken H., Kopinga K, Determination of moisture diffusivity in porous media using moisture concentration profiles, Heat Mass Transfer 39 (1996) 1273-1280.

[12] Künzel H.M., Verfahren zur ein-und zweidimensionalen Berechnung des gekoppelten Feuchte- und Warmetransports in Bauteilen mit einfachen Kennwerten, PhD Thesis, Stuttgart university, (1994).

[13] Krus M., Holm A., Simple methods to approximate the liquid transport coefficients describing the absorption and drying, Proceedings of sympossium: Physics in the Nordic Countries' (1999) 241-248.

[14] Janssen H., Blocken B., Carmeliet J., Conservative modelling of the moisture and heat transfer in building components under atmospheric excitation, International Journal of Heat and Mass Transfer 50 (2007) 1128-1140.

[15] Pinder F.G., Gray G.W., Essentials of Multiphase Flow and Transport in Porous Media, John Wiley & Sons, New Jersey (2008).

[16] Radu F.A., Pop I.S., Knabner P., Error estimates for a mixed finite element discretization of some degenerate parabolic equations, Numerische Mathematik 109 (2008) 285-311.

[17] Radu F.A., Pop I.S., Knabner P., Newton type methods for the mixed finite element discretization of some degenerate parabolic equations, Numerical Mathematics and Advanced Applications (2006) 1192-1200.

[18] Beliaev A.Y., Hassanizaeh S.M., A theoretical model of hysteresis and dynamic effects in the capillary relation for two-phase flow in porous media, Transport in Porous Media 43 (2001) 487-510.

[19] Schweizer B., Instability of gravity wetting fronts for Richards equations with hysteresis, Interfaces and Free Boundaries 14 (2012) 37-64.

[20] Rätz A., Schweizer B., Hysteresis models and gravity fingering in porous media, ZAMM - Journal of Applied Mathematics and Mechanics 94 (2012) 645-654.

3

3. A gravitational procedure to measure the diffusion coefficient

This chapter has been published as:

Van der Zanden, A.J.J. & Taher, A. A gravitational procedure to measure the diffusion coefficient of water in porous materials. Drying Technology 32 (2014) 708-712.

3.1 Introduction

Many materials are porous and can absorb water. The presence of water and accompanied deleterious substance can lead to the damage of the materials. It is therefore important to understand the processes involved in the transport of water in porous materials. Many theoretical models can be found in literature, for instance [1]. These processes are studied very often experimentally, because every porous material has its own characteristics. The most obvious physical property that can be measured during a process is the mass of a sample (see, for example, Legros et al. [2]) where a drying sample loses weight. Another valuable experimental technique is nuclear magnetic resonance (NMR), where the mass distribution inside a sample can be measured. For instance, Pel et al. [3] measured the water distribution inside a fired-clay brick during the drying process. The advantage of this technique is that the water distribution can be measured inside a sample as a function of time. Two important disadvantages of this technique are that it is expensive and that much knowledge is needed to use it. Other techniques used to obtain moisture transport properties are measuring the surface temperature and saturation values using an optical metrology (see [4]) or using interior humidity measurements [5].

Another technique has been proposed to determine the diffusion coefficient of water in porous materials by van der Zanden and Aghaei [6]. In this technique, a sample is dried on one side, while it is hanging from two cables, which are each connected to a balance. In this way, more information is obtained from the drying experiment compared to the situation where only the total mass is measured with one balance. Van der Zanden and de Wit [7] studied the accuracy of this drying procedure when the used balances have a given inaccuracy. This technique is similar to the technique proposed by Gaffner [8] who measured the mass at one end of a sample, while the other end was resting on a support. He sealed the sample on all sides and created a non-equilibrium situation inside the sample by placing two differently conditioned sample halves against each other. The main disadvantages of this technique are that both sample halves can have different characteristics and that the connection between the sample halves can introduce resistance against mass transport.

The present chapter proposes another measuring procedure to obtain the diffusion coefficient of water in porous materials. In the procedure, a centrifuge is used to create a non-homogeneous water distribution inside a porous material. The material is then taken out of the centrifuge and the method of van der Zanden and Aghaei [6] can then applied to measure how fast the water reaches the equilibrium distribution again.

In the second section, the proposed measuring procedure is described in detail. Next, an equation is derived with which the concentration gradient of a partially saturated sample in a gravity field can be obtained. How the diffusion coefficient is obtained from the measured masses is not described in the present study, but is presented by van der Zanden and de Wit [7]. Finally, the proposed procedure is examined theoretically for a sample of concrete.

3.2 Measurement procedure

In this paragraph, the method of sample preparation and how the measurements are performed are described in detail.

The first step is the sample preparation. The sample is most often cut from a larger piece of material. For the presented procedure, a length of 0.1 m is convenient, and a height and a width of both 0.05 m are convenient. Of course, these values are somewhat arbitrary. The measuring procedure assumes that no

water can leave or enter the sample during the mass measurements. To ensure this, the sample must be sealed completely, except for a small surface area of the sample, which is used to condition the sample with some average water content. Thus, after the partial sealing, the sample is conditioned. The first part of the conditioning of the sample is adding a known amount of water to the sample. After all, the diffusion coefficient depends very often strongly on the water content. Thus, for each meaningful measurement of the diffusion coefficient, the water content at which the diffusion coefficient is measured must be known. The second part of the conditioning is creating a homogeneous water distribution throughout the sample. This takes just time. After this, the remaining open surface area of the sample is sealed too. The waiting on a homogeneous water distribution can also be done after the sealing of the sample. The result is a sample with some water content, which is sealed on all sides. During the sample preparation, the mass is measured after every production step. Thus, the mass of the dry sample, the sealing material and the added water are known.
The second step is that the sample is placed in a centrifuge (Figure 3.1) to create a non-homogeneous water distribution inside the sample. The time that it takes to reach this non-homogeneous water distribution depends on the diffusion coefficient of water in the sample.

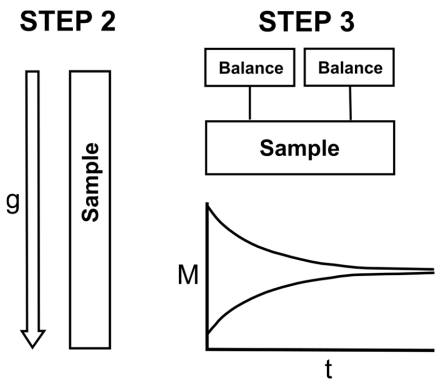

Figure 3.1: After the sample preparation, a non-homogeneous water distribution is in the second step created with a (forced) gravity field. In the third step, it is measured how the mass distribution in the sample evolves as a function of time.

The third step is the measurement of the mass on two places of the sample as proposed by van der Zanden and Aghaei [6]. Both masses are registered as a function of time. The masses as predicted from Fick's second law are fitted with the measured masses. The best fit gives the value of the diffusion coefficient. A detailed description of this method was given by Van der Zanden and De Wit [7].
It has been shown that the diffusion coefficient is very often a function of the water content for instance, for concrete [9], for parboiled rice [10], and for pineapple [11]. The preceding steps give the value of the diffusion coefficient only at one water content of the sample. The sample can be used again for another water content. In order to do so, the sealing must be removed at a small surface area and a small amount of water must be evaporated from the sample or a small amount of water must be added to the sample. The sealing must then be repaired, and then the sample is ready for a measurement at another water content. It is also possible to use the same sample upside down to investigate possible inhomogeneities of the sample.
The proposed procedure is better than the procedure proposed by van der Zanden and de Wit [7], because in their procedure, the measured masses depend on their drying flux and the diffusion coefficient, while

in the present procedure there is no drying flux. The reaching of the new equilibrium, the time evolution of the measured masses, depends on the diffusion coefficient only.

3.3 Equilibrium concentration gradient in a gravity field

When a partially saturated porous sample is placed into a gravity field, the water in the sample will sink until equilibrium is reached, where the bottom part has a higher water concentration than the upper part. In the present section, a differential equation will be derived, with which the concentration gradient in the sample can be obtained. It is based on the fact that, in an equilibrium situation, the gradient in the hydrostatic pressure is equal to the gradient in the capillary pressure.

The radius of pores in a porous material can vary a few orders of magnitude, ranging, for instance, from 0.01 to 10 μm. For an overview of the pore size distribution of different building materials, and how this distribution is measured, see, for instance, the work of Haynes [12]. When such a material is partially saturated with water, the water is, due to the capillary forces, in the smallest pores. This has been observed experimentally by Engøy et al. [13]. The larger pores are still filled with air. It is assumed here that both phases, i.e., the water and the air phase, are both continuous. This means that every geometrical point in one phase can be reached from any other point in that same phase through a path that lies also completely in that same phase.

When such a partially saturated sample is placed into a gravity field with acceleration g, the situation of Figure 3.2 arises. The water is pulled down by gravity, which results in a higher water concentration at position x than at position x+dx. At position x, more pores are filled with water than at position x+dx.

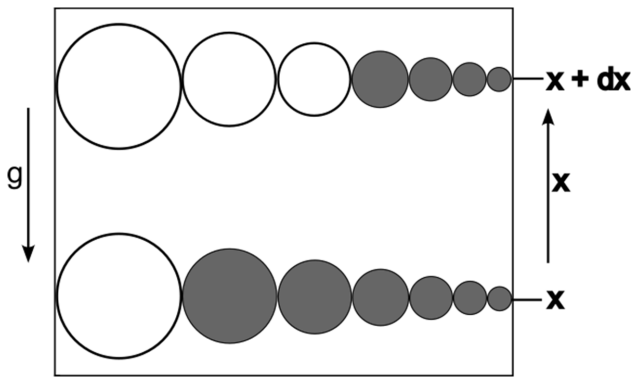

Figure 3.2: A partially saturated porous material that is placed into a gravity field has, in an equilibrium situation, more pores filled at position x than at position x+dx.

In the absence of gravity, such a concentration gradient would lead to a pressure gradient in the water phase and to water flow through the water filled pores, as is shown by the model of van der Zanden et al. [14,15]. In the presence of gravity, however, the difference between the pressure in the water phase at x and at x+dx is in equilibrium situation, because of the assumption of continuity in the water phase, the hydrostatic pressure difference, and is given by

$$p(x) = p(x + dx) + \rho \cdot g \cdot dx \tag{3.1}$$

where ρ is the density of water. An example of a cumulative pore size distribution of a fictional material is sketched in Figure 3.3. It is measured by forcing mercury under pressure into a sample, as it was already done by Ritter and Drake [16] in 1945. From the pressure in the mercury needed to force the mercury into the sample, the average pore radius can be obtained using Laplace's law (Atkins [17]) and the volume of mercury in the sample is measured. The result is given as a cumulative volume fraction, F. The maximum value of F, Fmax, is the total volume of the pores expressed as the volume fraction of the porous sample and is thus the porosity of the concrete. For the sample of Figure 3.2, at position x, the volume fraction occupied by water is F_{max} - F(x). This means that all the pores with a radius smaller than r(x) are filled with water. Likewise for F(x+dx) and r(x+dx).

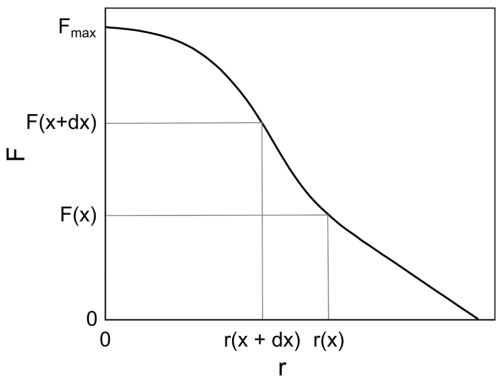

Figure 3.3: A hypothetical pore size distribution. The cumulative volume fraction is given as a function of the pore radius.

The density of air is much smaller than the density of water. The hydrostatic pressure difference is in the air phase much smaller than in the water phase and is thus neglected in the derivation below. The pressure in the air phase is set to zero [14]. This is not the real value, but only pressure differences are relevant for the present reasoning. Then, with Laplace's law [17], the water pressure can be related to the largest filled pore radius as

$$p(x) = -\frac{2\sigma}{r(x)} \tag{3.2}$$

and

$$p(x+dx) = -\frac{2\sigma}{r(x+dx)} \tag{3.3}$$

where σ is the surface tension of water. Substitution of Eqs (3.2) and (3.3) into Eq. (3.1) gives

$$\frac{-2\sigma}{r(x)} = \frac{-2\sigma}{r(x+dx)} + \rho \cdot g \cdot dx \tag{3.4}$$

which can be written as

$$\frac{-2\sigma}{r} = \frac{-2\sigma}{r+dr} + \rho \cdot g \cdot dx \tag{3.5}$$

Eq. (3.5) can be written as

$$\frac{-2\sigma}{r} = \frac{-2\sigma}{r}\left(\frac{1}{1+\frac{dr}{r}}\right) + \rho \cdot g \cdot dx \tag{3.6}$$

which can be approximated as

$$\frac{-2\sigma}{r} = \frac{-2\sigma}{r}\left(1-\frac{dr}{r}\right) + \rho \cdot g \cdot dx \tag{3.7}$$

which can be simplified to

$$\frac{dr}{dx} = \frac{-\rho \cdot g \cdot r^2}{2\sigma} \tag{3.8}$$

For F as a function of x, Eq. (3.8) can be used to obtain

$$\frac{dF}{dx} = \frac{dF}{dr} \cdot \frac{dr}{dx} = \frac{dF}{dr}\left(\frac{-\rho \cdot g \cdot r^2}{2\sigma}\right) \tag{3.9}$$

The result of this section, Eq. (3.9), gives the gradient of the cumulative volume fraction *F* and, because the water concentration is given by ρF, essentially also the concentration gradient in a partially saturated porous material that is placed into a gravity field. If this gravity field is artificially created with a rotating motion, the acceleration g is a function of position *x*.

3.4 Theoretical application to a concrete sample

A hypothetical experiment is considered on a sample with length L, as it is sketched in Figure 3.4. The mass is measured on the left side, M_L, and on the right side, M_R. The (centrifugal) acceleration was pointing in the negative *x* direction, like in Figure 3.2. A water concentration profile is sketched with a low concentration at $x = L$ and a high concentration at $x = 0$.

An estimation will be given of the mass difference that can be expected when the sample of Figure 3.4 has been in a gravity field. The sample can be considered to consist of two halves, one on the left side and one on the right side. In each halve, there is an average water concentration, which is different for both halves. This results in a difference in the masses M_L and M_R. To obtain this mass difference, Eq. (3.9) is used to arrive at the approximation

$$\Delta F \equiv F_L - F_R \cong \frac{L}{2} \cdot \frac{dF}{dr}\left(\frac{-\rho \cdot g \cdot r^2}{2\sigma}\right) \tag{3.10}$$

from which follows

$$\Delta M \equiv M_L - M_R \cong \frac{L}{2} \cdot \frac{dF}{dr}\left(\frac{-\rho \cdot g \cdot r^2}{2\sigma}\right) \cdot \frac{V}{2} \cdot \rho \tag{3.11}$$

where V is the volume of the sample.

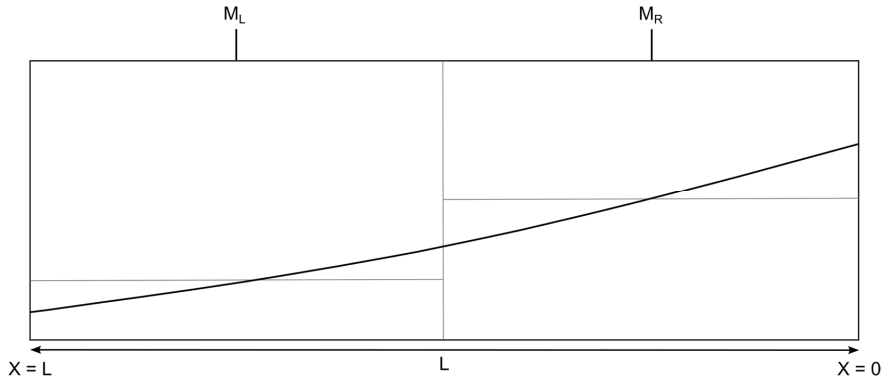

Figure 3.4: In an experiment, the total mass of the sample is divided into two parts, which are measured independently. A non-homogeneous water content is shown, and the average water content of the two halves are shown.

Eq. (3.11) has a very simple form, and it is accurate enough for an estimation of the order of magnitude. The correct equations for M_L and M_R follow from the mechanical no-rotation conditions [6,7]. If the mass difference is not large enough, it can be increased by moving the wires closer to each other. In this way, the sensitivity of the measuring procedure can be increased.

This method can now be applied theoretically on a sample of concrete. In Figure 3.5, the pore size distribution is given, as the result of a computation, presented by Ye [18]. The pores have a size typically in the range 0.2 - 2 μm. Now, an estimation will follow of the mass difference, given by Eq. (3.11), for a sample that has a size that is easy to handle in an experiment with a centrifugal velocity that can be obtained easily. The diameter of the largest filled pores is set 1 μm. From Figure 3.5 and after a little computation, it follows that dF/dr has the value - 10^5 m^{-1}. A convenient sample size is a length of 0.1 m and a width and height of 0.05 m. The density of water is 1000 kgm^{-3}. The surface tension σ of water is $73 \cdot 10^{-3}$ Nm^{-1}. A centrifuge for drying clothes can easily have a rotation velocity of 20 rps, which implies an angular velocity, ω, of 120 rad s^{-1}. If the sample is placed 0.25 m from the rotation axis, the acceleration,

$$g = \omega^2 \cdot d_i \tag{3.12}$$

with d_i the distance from the rotation axis, becomes $3.6 \cdot 10^3$ ms^{-2}. Using these values in Eq. (3.11) gives a mass difference of $3.1 \cdot 10^{-3}$ kg. This mass difference can be measured very easily. For dryer samples, the mass difference is smaller. For instance, for the same sample, but now with the pores filled unto a pore diameter of 0.1 μm, dF/dr has approximately the same value as before, but the ten times smaller pore radius leads to a 100 times smaller mass difference. For higher water concentrations, the mass difference is larger.

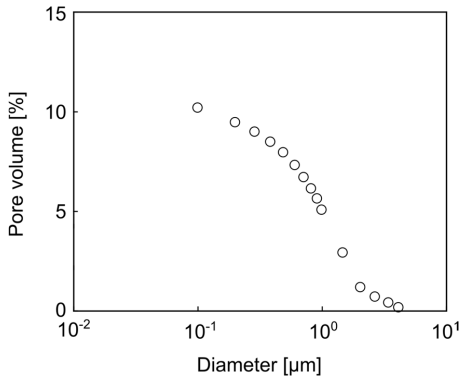

Figure 3.5: The pore size distribution as found in the literature [18].

3.5 Conclusion

A procedure to measure the diffusion coefficient of water in porous materials has been presented in this chapter. After preparation of the sample, which is the first step, the procedure consists of a second step, where a non-equilibrium situation inside a partially saturated porous sample is created using a centrifuge. In the third step, the sample is taken out of the centrifuge and how fast the water distribution inside the sample reaches its new equilibrium is measured by hanging the sample from two cables, each connected to a balance. The comparison with Fick's second law gives the diffusion coefficient.
The theoretical application on concrete shows that, for this material, the procedure can be used. In order to show the feasibility of the procedure, the pore size distribution must be known. However, to measure the diffusion coefficient with the proposed procedure on a material, the pore size distribution does not need to be known beforehand.

3.6 References

[1] Wang W., Chen G., Mujumdar A.S., Physical interpretation of solids drying: An overview on mathematical modeling research, Drying Technology 25 (2007) 659-668.

[2] Legros M., Yoshida M., Sakaguchi T., Imakoma H., Okazaki M., Determination method of variable diffusion coefficients of hygroscopic material from drying rate curves of the single particle, Drying Technology 10 (1992) 733-752.

[3] Pel L., Kopinga K., Bertram G., Lang G., Water absorption in a fired-clay brick observed by NMR scanning, Journal of Applied Physics 28 (1995) 675-680.

[4] Belhamri A., Characterization of the first falling rate period during drying of a porous material, Drying Technology 21 (2003) 1235-1252.

[5] Zhang J., Hou D., Gao Y., Wei S., Determination of moisture diffusion coefficient of concrete at early age from interior humidity measurements, Drying Technology 29 (2011) 689-696.

[6] Van der Zanden A.J.J., Aghaei A., Determination of the diffusion coefficient of water in brick with a simple mass distribution technique, Drying Technology 27 (2009) 393-402.

[7] Van der Zanden A.J.J., De Wit M.H., A procedure to measure the diffusion coefficient of water in brick as a function of the water concentration, Drying Technology 30 (2012) 526-534.

[8] Gaffner D., The moment method for measuring moisture diffusivity of porous building materials, In Proceedings of the Conference Thermal Performance for the Exterior Envelope of the Whole Building X (2007).

[9] Dietll C., George O.P., Bansal N.K., Modeling of diffusion in capillary porous materials during the drying process, Drying Technology 13 (1995) 267-293.

[10] Elbert G., Tolaba M.P., Aguerre R.J., Suarez C., A diffusion model with a moisture dependent diffusion coefficient for parboiled rice, Drying Technology 19 (2001) 155-166.

[11] Simal S., Garau M.C., Femenia A., Rossello C., A diffusional model with a moisture-dependent diffusion coefficient, Drying Technology 24 (2006) 1365-1372.

[12] Haynes J.M., Determination of pore properties of constructional and other materials, Mate´riaux et Construction 6 (1973) 169-174.

[13] Engøy T., Feder J., Jøssang T., Counter-flow in drying of competing pores, Physica Scripta 38 (1991) 99-102.

[14] Van der Zanden A.J.J., Coumans W.J., Kerkhof P.J.A.M., Schoenmakers A.M.E., Isothermal moisture transport in partially saturated porous media, Drying Technology 14 (1996) 1525-1542.

[15] Van der Zanden A.J.J., A possible revision of the results of a model for moisture transport in partially saturated porous media. Drying Technology 13 (1995) 2227-2231.

[16] Ritter H.L., Drake L.C., Pore-size distribution in porous materials, Industrial and Engineering Chemistry 17 (1945) 782-791.

[17] Atkins P.W., Physical Chemistry, Oxford University Press: Oxford, UK (1998).

[18] Ye G., Experimental Study and Numerical Simulation of the Development of the Microstructure and Permeability of Cementitious Materials, PhD thesis, TU Delft, The Netherlands (2003).

4. Sorption isotherm measurements for porous materials: A new hygroscopic method

This chapter has been published as:

Taher, A. & Brouwers, H.J.H. Sorption isotherm measurements for porous materials: A new hygroscopic method. *Construction and Building Materials* 379 (2023) 131166.

4.1 Introduction

The concrete durability is largely influenced by the level of corrosion of the steel rebars in the concrete structure. Corrosion in concrete structures usually occurs as a result of carbonation and/or chloride penetration. Chloride penetration can be very important for structures on coastal areas where chloride concentrations in the water and the air can be high. This is also the case for concrete roads and bridges when de-icing salt is used to prevent roads from icing. It is, therefore, essential to better understand water and chloride transport in concrete structures. Water and chloride transport in concrete is very complicated as it depends on several parameters such as the sorption isotherm [1-2], porosity [3], permeability, diffusion coefficient of water and chloride [4] etc.

Sorption isotherm is defined as the relationship between water content and humidity of a material at thermodynamic equilibrium. Different approaches have been implemented to investigate the sorption of water in different materials. For example, saturated salt solution method [5-10], hygroscopic method [11], manometric measuring method [12], nuclear magnetic resonance (NMR) [13-14], etc. The advantages and disadvantages of these methods are summarized in Table 4.1.

Table 4.1: Advantages and disadvantages of different sorption isotherm methods [5-19].

Method	Advantages	Disadvantages
Saturated Salt Solution	• Simple setup and operation • Inexpensive equipment • Can cover a wide range of relative humidity levels • Minimizing temperature fluctuation	• Time-consuming • Limited range of humidity levels achievable • Possible salt contamination of samples • Less accurate than some other methods
Hygroscopic	• Accurate • Can measure dynamic sorption behaviour • High-resolution data	• Time-consuming • Requires precise control of humidity levels
Manometric	• High accuracy • Suitable for a wide range of materials • Can measure sorption at very low and high humidity levels	• Requires specialized equipment • Time-consuming • Limited pressure range • More complex than some other methods • Limited sample size
Nuclear Magnetic Resonance (NMR)	• Non-destructive method • High resolution and sensitivity	• Requires advanced and expensive equipment • Limited to certain types of materials and sample sizes • Requires specialized expertise • More expensive than some other methods

The saturated salt solution, hygroscopic and manometric measuring methods are widely used for research on sorption isotherm properties of porous materials such as concrete.

The simplest method is by direct weighing of the sample (saturation salt solution method). A sample of known size and mass is kept in an environment of known humidity and weighed times as the humidity

is increased. The adsorption and desorption of water by several materials, including concrete, have been widely investigated using this technique [5-9]. Although this approach can be easily implemented, errors can often occur due to the interruption of the sorption process at each weighing. Several studies have been performed to minimize errors associated with the weighing method. For example, Crank and Park [18] used a quartz spring method in which the increase of mass of the sample due to the adsorption of vapor is obtained from the length of the spring. Other studies proposed to measure the increase in mass of the sample using a balance [19].

The hygroscopic approach is an alternative approach, which is used to measure the sorption isotherm of water in very thin layers of paint. In this approach, the sample is initially dried completely and then is placed inside a glass jar. The jar has two openings to let the air go through the jar. Water drops are injected into the jar to create various relative humidity conditions. The air temperature and relative humidity inside the jar are measured when an equilibrium between the environment and the sample is achieved. In this case, one point on the sorption isotherm curve is obtained. This procedure can be continued until the saturation is almost reached. In this approach, the desorption curve is obtained as follows: A saturated sample is placed inside the jar. Air with a relatively low relative humidity is induced into the jar with a certain flowrate and time interval duration. The sample will release water due to the decrease in relative humidity caused by the dry air. Equilibrium is reached after a while and a point on the curve is obtained the same way as described before.

The manometric technique is a volumetric measurement technique [12], in which two chambers of a known volume are used. A valve separates the chambers from each other. The pressure in the chambers is measured using a manometer, the temperature can be controlled by any temperature-controlling system. At the start of the experiment, the sample is placed in the chamber, while a valve is opened to fill the other chamber with air containing vapor to an initial pressure. Then the valve between the chambers is opened, allowing the second chamber containing the sample to fill with air containing vapor. Any drop in pressure beyond that due to the volume difference between the first chamber and the two chambers together is assumed to be the consequence of the sample adsorbing water. The amount of water adsorbed by the sample is then obtained using the real gas law.

Penetration of chloride solution into porous materials is of interest in a wide range of applications. The presence of chloride in the pores of a material can change the physical properties of the material [20]. This phenomenon can also affect the contact angle and surface tension of the water. Therefore, one can expect that the presence of chloride will significantly affect water transport in porous materials such as concrete [21, 22]. Since sorption takes place on the surface of the pores, the presence of compounds strongly influences the sorption isotherm.

Rijniers [23] has measured the sorption isotherm of bulk salts, one of which was NaCl. It is found that the sodium chloride adsorbs no water vapor up until a high relative humidity (±75%). At this high relative humidity, the salt turns into a salt solution and adsorbs a large amount of water vapor. Franzen and Mirwald [24] have investigated the effect of chloride on the water uptake in sand-lime samples. From humidity sorption experiments, it is concluded that samples treated with different chloride mixtures have an extremely increased water uptake. At a relative humidity of about 70%, the samples tend to absorb a large amount of water. Koniorczyk and Wojciechowski [25] measured the sorption isotherm of cement mortar with different sodium chloride contents and created a model based on neural networks. The results showed that the higher the chloride content, the more water is absorbed. It was also observed that the presence of chloride can affect the drying time of the material. In this case, the

drying time of the material containing chloride, compared with the case with water, was longer. This can be explained with the effect of chloride on the hygral state of the material. It should be noted that chloride can also change the effective conductivity, but also the thermal capacity of the multiphase domain, which influences the energy transport. Additionally, energy is released or consumed during phase change. Villani et al. [26] predicted and measured the diffusivity of deionized water and various chloride solutions in mortar. It is seen that the diffusivity of a 17% NaCl-solution is larger than the diffusivity of deionized water, particularly at high relative humidities.

In the present study, the hygroscopic method described by Van der Zanden and Goossens [11] is chosen, because it allows measuring more points of the sorption isotherm than other techniques. The accuracy of the measurements is also adjustable by adding extra water in the experiment. Adjusting the accuracy of the results is important for materials with a complicated pore structure such as concrete. Here, the sorption isotherm of two porous materials, mortar and sand-lime, are measured and compared with literature. The effect of chloride in mortar samples is also studied by comparing the sorption isotherms of a sample containing chloride and a sample free of chloride.

4.2 Materials and sample preparation

4.2.1 Sample preparation

In this experiment, two porous materials are studied: (i) cement-based mortar specimens and (ii) sand-lime specimens. The cement in this study has a chloride content of ≤ 0.1% by the mass of the final cement according to EN 197-1 and that is neglected, because of the very small quantity. PVC cylinder tubes with a diameter 100 mm are used to cast the mortar. After curing the mortar for 28 days, the cylinder samples are cut in pieces with a thickness of 10 mm. The total porosity of the samples is measured using the vacuum-saturation technique following the standards NT Build 492 [27] and ASTM C1202 [28]. More detailed information about the test procedure is provided in Yu and Brouwers [29]. Therefore, only highlights are briefly presented here:

1. The samples are placed in a desiccator and a pressure of 4 kPa is applied for 3 hours;
2. The desiccator is filled with water gradually until the sample is completely immersed in water;
3. The vacuum is maintained for an additional hour;
4. The samples are left in water for 18 hours;
5. The mass of the surface dry samples in air is measured;
6. The mass of the samples in water is measured;
7. The sample is dried in an oven at 50 °C until a constant mass is reached. The mass of the sample is then measured.

The total porosity of the samples is calculated using equation:

$$\phi = \frac{m_s - m_d}{m_s - m_w} \times 100 \tag{4.1}$$

where ϕ is the porosity [%], m_s is the surface dried mass of water saturated sample in air [g], m_w is the mass of water-saturated sample in water [g], and m_d is the mass of oven dried sample [g]. Based on these measurements, the mortar and sand lime samples have an average porosity of 17% and 32%, respectively, as shown in Figure 4.1.

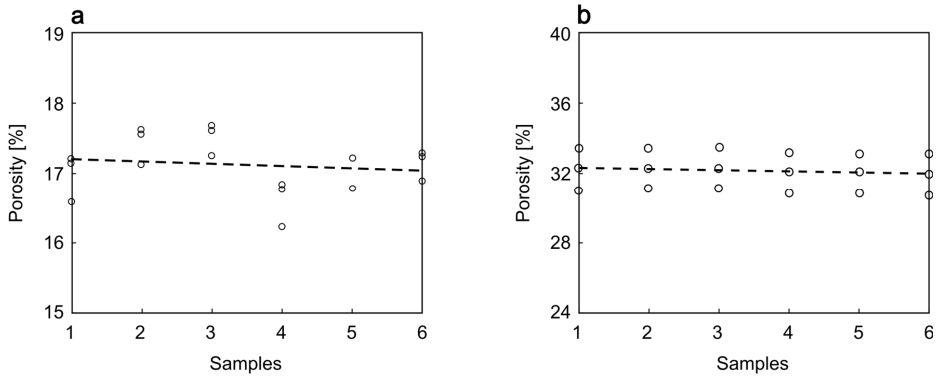

Figure 4.1: The measured porosity of (a) mortar samples, and (b) sand-line samples following the standards NT Build 492 (1999) and ASTM C1202 (2005).

Based on the measured porosity, a salt solution of four liters is prepared by dissolving 237 g sodium chloride per liter distilled water, to provide the samples with chloride concentration of 2% upon full saturation. For the sand-lime measurements, cylindrical samples were extracted from the sand-lime block. In this case, the diameter and the thickness of the samples are 100 mm and 10 mm, respectively. Figure 4.2 shows the measured compressive and flexural strength of the mortar sample. The specifications of the two porous materials are presented in Table 4.2.

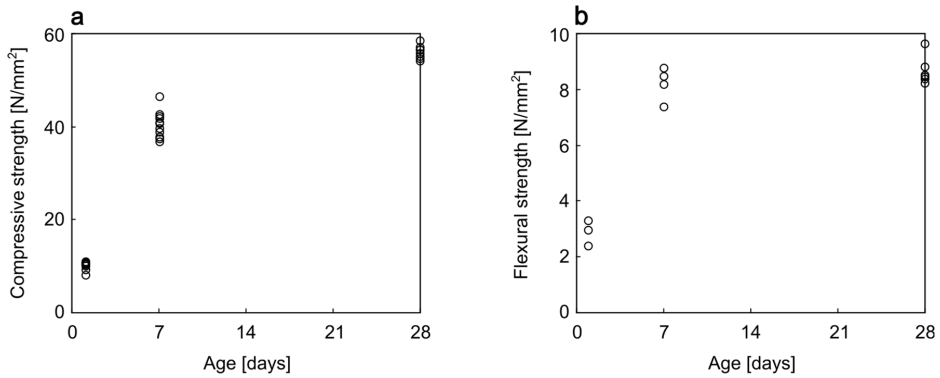

Figure 4.2: (a) Compressive strength, and (b) flexural strength of mortar samples.

Table 4.2: Main characteristics of mortar and sand-lime.

Materials	Mortar		Sand-lime
	Volume [m³]	Mass [kg]	
CEM I 42,5N	159.5	502.2	-
Sand	568.5	1506.5	-
Water	251.1	251.1	-
Superplasticizer	0.9	1	-
Air	20	-	-
w/c	0.5		-
Porosity / 28-day	17 %		32 %
Class	-		CS12
Compressive strength / 28-day	56.8 MPa		12 MPa
Flexural strength / 28-day	8.9 MPa		-

After completing the preparation of the salt solution, all the samples are placed in a holder in a desiccator (Figure 4.3). The vacuum saturation method is implemented in order to saturate the samples with the chloride solution. To do so, the following steps are taken:

1. A vacuum suction (4 kPa) is applied using a pump for 3 hours for de-airing the samples.
2. The chloride solution is added in order to have an initial concentration level of chloride in the samples.
3. The vacuum suction is maintained for another hour to ensure that the air void inside the sample is entirely saturated with the chloride solution.
4. Finally, before the chloride concentration profiles are measured, the samples will be maintained in the chloride solution at the laboratory conditions for a three- day period.

Profiles of the chloride concentration are determined by titration to examine the chloride penetration into the sample.

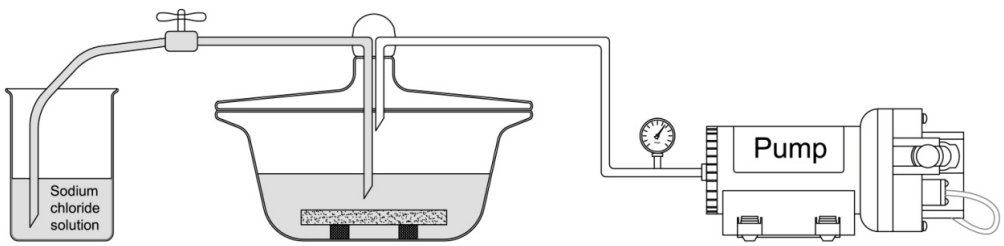

Figure 4.3: Penetrating chloride into the specimens using vacuum saturation.

4.2.2 Titration analysis

In this study, the titration analysis is used to measure the chloride concentration profiles. The titration analysis is a commonly used method for chemical analysis [30-33].

Potentiometric titration curves are obtained by plotting the potential of the chloride-selective electrode E against the volume V of the added titrant. Rapid changes in the potential signal the equivalence point of the titration. The maximum change in potential is calculated by finding the maximum slope of this graph. This is easily found by plotting the first derivative curve dE/dV against V, the equivalence point is the point where dE/dV is zero. The corresponding value for the added titrant is thus obtained, the

volume of the analysed solution is known, which is set to 10 mL, and so the concentration of the analyte is calculated. With automatic titration, these calculations are done by a computer.

4.2.3 Chloride concentration profiles

To obtain chloride concentration profiles, layers of three mortar samples (numbered 1, 2 and 3) are ground with Profile Grinder 110 as shown in Figure 4.4. On the outer 2 mm of the sample, layers of 1 mm are ground, the rest of the sample is ground into layers of 2 mm. The powder is collected in marked plastic bags.

Figure 4.4: Profile Grinder 110 device.

Due to the pressure caused by the placeholder on sample 1, the last 2 mm were cracked before grinding. Therefore, the last 2 mm is regarded as one layer.
The powder of the three samples is placed in cups per layer and dried in an oven at 100 °C for 24 hours. After the powder is dried for at least 1 day, chemical analysis is performed as follows:

1. 2 g powder of each layer is weighed and placed in a beaker.
2. 35 mL of distilled water and 2 mL nitric acid of 1M is added to the beaker.
3. The content in the beaker is mixed for 1 minute.
4. The mixture is placed on a hot plate, brought to boiling and cooled afterward.
5. The content is poured onto filter paper in order to separate solid particles from the mixture. For each set of measurements, 100 mL of the filtered mixture is captured, of which 10 mL is used to determine the chloride concentration.
6. The measurement is performed by an automatic titration device, Metrohm MET 702 in which the principle of potentiometric precipitation titration is applied (Figure 4.5). This principle determines the chloride concentration by potentiometric titration with silver nitrate (titrant) and a silver electrode (indicator electrode).

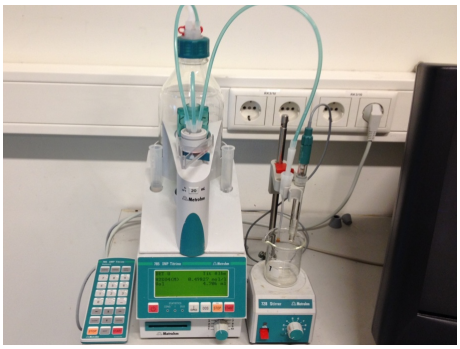

Figure 4.5: Metrohm MET 702 automatic titration device.

For each layer, two sets of measurements are done. The resulting chloride profiles are shown in Table 4.3 and Figure 4.6, in which the chloride concentration is presented as a function of distance from the surface of the samples.

It should be noted that the sample is not sealed at the top and the bottom surfaces. Therefore, the chloride can penetrate through both surfaces easily, while it was more difficult to move to the deeper level of the sample. In addition, the samples in the experiments were not completely dried before placing them in the sodium chloride solution. Therefore, it is expected that the chloride concentration would be higher throughout the samples and less sensitive to the depth of samples if the samples were firstly dried completely.

Table 4.3: The chloride concentration of ground layers from three samples, obtained from two measurements.

	Chloride concentration [%]			
	Profile [mm]	**Measurement 1**	**Measurement 2**	**Mean concentration**
Sample 1	0-1	1.246	1.241	1.244
	1-2	0.880	0.883	0.882
	2-4	0.633	0.625	0.629
	4-6	0.479	0.478	0.479
	6-8	0.606	0.611	0.609
	8-10	0.850	0.859	0.855
Sample 2	0-1	1.280	1.289	1.285
	1-2	0.942	0.928	0.935
	2-4	0.649	0.643	0.646
	4-6	0.432	0.427	0.429
	6-8	0.527	0.520	0.524
	8-9	0.771	0.769	0.770
	9-10	0.973	0.975	0.974
Sample 3	0-1	1.250	1.255	1.253
	1-2	0.897	0.898	0.898
	2-4	0.588	0.587	0.588
	4-6	0.370	0.369	0.369
	6-8	0.412	0.408	0.410
	8-9	0.583	0.593	0.588
	9-10	0.768	0.771	0.769
	10-11	1.077	1.095	1.086

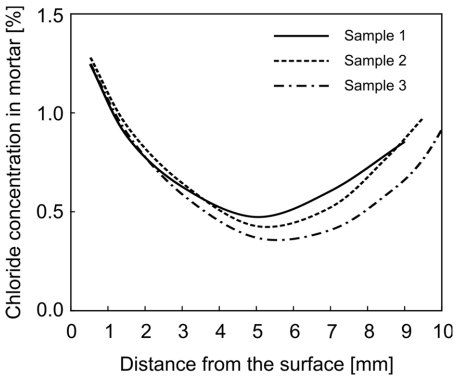

Figure 4.6: Measured concentration profiles as a function of depth for mortar samples.
For all samples, the thickness is 10 mm.

4.2.4 Chloride concentration profiles in completely dried samples

An additional experiment is performed, in which three samples are first completely dried using an oven at 50º C and relative humidity of 10%. The same procedure, as described in Section 2.3, is used to determine the chloride concentration profiles of the dried samples. From the obtained results in Figure 4.7 and Table 4.4 it is indeed seen that drying the samples completely before placing in the salt solution gives higher values and more uniform chloride concentration profiles within the depth of the samples. One can expect to see a symmetric distribution of the concentration in the samples, since the samples are assumed to be homogeneous. However, this is not the case, and differences in the chloride concentrations are clearly observed (see Figure 4.7). The main reason for these differences is not clear. But it could be probably caused in the stage of grinding layers of the samples. The samples are fixed by a holder, which disables the sample to move during the grinding process. This fixing causes stress in the sample, which causes the formation of cracks when its thickness is small, i.e., in the last layers. Cracking of the sample leads to less pulverized layers, with larger particles. Due to this rather coarse powder, the chloride bound to the surface of the pores is less dissolved when water and nitric acid are added to the powder. This yields an erroneous chloride concentration. It is thus assumed that the chloride concentration on the right side of the graph, where the obtained powder was rather coarse, is equal to the left side of the sample.

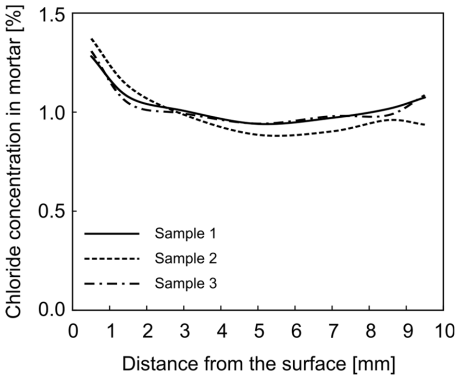

Figure 4.7: Experimentally obtained chloride concentration profiles,
where samples were completely dried before measurement.

Table 4.4: The chloride concentration of ground layers, where samples were completely dried before measurement.

	Chloride concentration [%]			
	Profile [mm]	**Measurement 1**	**Measurement 2**	**Mean concentration**
Sample 1	0-1	1.285	1.277	1.281
	1-2	1.074	1.080	1.077
	2-4	1.010	1.004	1.007
	4-6	0.940	0.942	0.941
	6-8	0.978	0.965	0.972
	8-9	1.019	1.013	1.016
	9-10	1.074	1.074	1.074
Sample 2	0-1	1.371	1.372	1.372
	1-2	1.129	1.132	1.131
	2-4	0.993	0.979	0.986
	4-6	0.876	0.892	0.884
	6-8	0.893	0.910	0.902
	8-9	0.958	0.959	0.959
	9-10	0.936	0.935	0.936
Sample 3	0-1	1.308	1.307	1.308
	1-2	1.044	1.046	1.045
	2-4	0.990	0.995	0.993
	4-6	0.944	0.939	0.942
	6-8	0.979	0.979	0.979
	8-9	0.985	0.982	0.984
	9-10	1.080	1.090	1.085

4.2.5 Determining the effectiveness of the vacuum saturation method

To verify the effectiveness of the vacuum saturation method, three mortar samples are prepared, having a thickness of 10, 20 and 40 mm. These samples are dried first using a climate chamber, in which air of 50 °C and relative humidity of 10% is blown over the samples. The samples are weighed every day until a constant mass is reached. The samples are then placed in the glass jar. The same procedure, as described in Section 2, is then followed to saturate the samples. Note that in these experiments distilled water is used (instead of chloride solution), and the samples are maintained in the water for 24 hours instead of 3 days. If the method of vacuum saturation would indeed remove all the air out of the samples, the specific increment in mass after 24 hours would be the same for each sample, regardless of its thickness. The results are shown in Table 4.5.

It can be seen that the mass increment of the three samples is almost equal, being in the order of 7% of its original mass. This result gives rise to the assumption that the vacuum saturation method removes all the air out of the samples and saturates the pores with liquid.

Table 4.5: The determination of the accuracy of vacuum suction.

	Sample 1 (10 mm)	Sample 2 (20 mm)	Sample 3 (40 mm)
Dry mass [g]	179.68	349.45	691.80
Mass after desiccation and wetting [g]	192.45	374.00	739.90
Mass increment [%]	7.11	7.03	6.95

4.3 Methodology

The sorption isotherm consists of two curves: (i) one that indicates the history of wetting, i.e. adsorption of water and (ii) one that indicates the history of drying, i.e. desorption of water. It should be noted that in some cases, depending on the properties of the material such as the porosity and permeability, these two curves are not identical. This is especially the case for concrete.

4.3.1 Adsorption isotherm

For the adsorption curve, a sample is completely dried in the climate chamber and then is placed in a glass jar with two sensors for relative humidity and temperature as shown in Figure 4.8. The glass jar is kept inside a room with a temperature-controlled environment. The temperature of the room is about 21 °C. Each data point is collected when the humidity inside the jar does not change (i.e. equilibrium). In order to prevent leakage in the system, a Teflon ring is used as a closure.

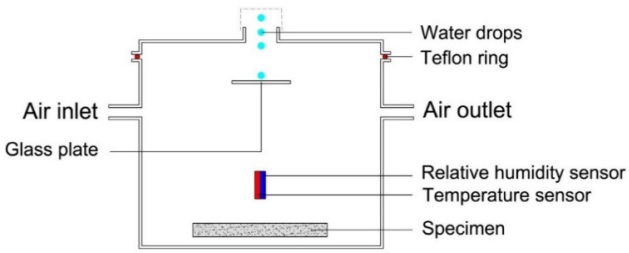

Figure 4.8: Experiment set-up to measure the sorption isotherm of porous material with a hygroscopic method.

The sample is placed first in the jar and since the sample still contains a small (unknown) amount of water, an initial equilibrium is awaited. This initial equilibrium state is the origin of the sorption curve. After the initial equilibrium is reached, a detailed sensitivity analysis is performed to assess the impact of the amount of water added to the jar on the accuracy of the experiments. To reach this goal, three quantities are tested: (i) 0.1 mL (ii) 0.3 mL and (iii) 0.5 mL of water are added to the jar. For the case with 0.1 mL of water, the experiment takes about 4 days to reach an equilibrium. However, this could provide detailed information about the adsorption behaviour of material if needed. Note that larger quantities could be used in parts of the curve where detailed information is less significant, while this could shorten the experimental duration.

The combination of using different quantities of water can be used until a final equilibrium is reached. Figure 9 shows how relative humidity changes as a function of time. It can be seen that the profile of relative humidity can be divided into three phases. The first phase is the increase of the relative humidity which is the result of the evaporation of the injected water. In the second phase, the relative humidity reduces due to the adsorption of the porous material. The final phase is the equilibrium state between the relative humidity inside the jar and the adsorbed water of the sample.

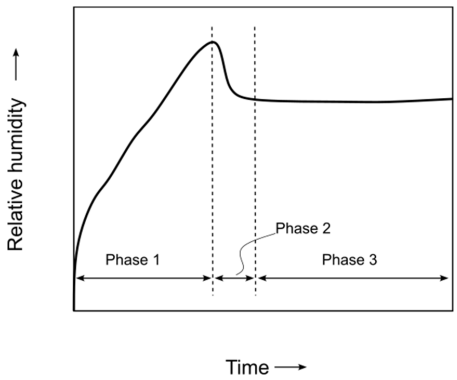

Figure 4.9: Characteristic chart of the humidity in the vessel as a function of time. The chart can be divided into three phases; the first phase is the increase of the relative humidity which is the result of the evaporation of the injected water. The second phase is the decrease of the relative humidity that results from the adsorption of the porous material. The final phase is the equilibrium state between the relative humidity inside the vessel and the adsorbed water of the specimen.

The adsorption isotherm is calculated by measuring the amount of water in the system and in the air. The relationship between these two quantities and the amount of water inside the sample is given by:

$$m_{\text{sample}} = m_{\text{total}} - m_{\text{air}} \tag{4.2}$$

Where m_{total} is the amount of water in the system, and m_{air} is the amount of water in the air that is measured based on the relative humidity. The amount of water inside the sample, m_{sample}, then can be obtained using Eq. (4.1).

By implementing the Antoine equation and the ideal gas law, the concentration of water in the saturated air, C_{sat} (kg/m^3) can be calculated as follows:

$$C_{\text{sat}} = \frac{M}{R \cdot T} \cdot e^{\left(A - \frac{B}{C+T}\right)} \tag{4.3}$$

where M (kg/mol) is the molar mass of water, R (J/(K·mol)) the gas constant and T (K) the temperature, and A (= 23.19695), B (= 3816.44) and C (= -46.13) are constants [34-35]. The concentration of water inside the jar can be computed based on the measured relative humidity (RH) inside the jar as follows:

$$C = \frac{RH}{100} \cdot C_{\text{sat}} \tag{4.4}$$

From Eqs. (4.3) and (4.4), the mass of water in the air inside the jar can be obtained using:

$$m_{\text{air}} = C.V \tag{4.5}$$

where V is the volume of the jar.

At a specific relative humidity, the water content (kg/m^3) in the sample can be obtained by dividing the mass of water in the sample (m_{sample}, obtained using Eq. (4.2)) by the volume of the sample.

4.3.2 Desorption isotherm

When the final equilibrium, at a relative humidity of approximately 90%, is reached the determination of the desorption isotherm is started. At this stage, the mass of water in the sample, as well as the mass of water in the air of the jar, are known. Figure 4.10 shows how relative humidity changes as a function of time. This graph can be divided into three phases. In the first phase, the relative humidity decreases, which is due to the blowing dry air into the jar. The second phase is the increase of relative humidity resulting from the release of water by the sample. The final phase (phase 3) is the equilibrium state between the water in the air of the jar and the water in the sample.

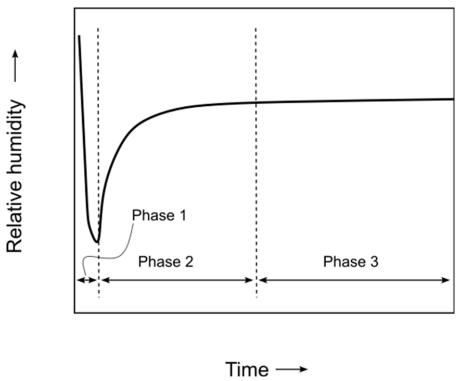

Figure 4.10: Characteristic chart of the humidity in the vessel as a function of time. This chart can be divided into three phases; the first phase is the decrease of relative humidity which results from blowing dry air in the vessel. The second phase is the increase of relative humidity resulting from the release of water by the sample. The final phase is the equilibrium state between the water in the air of the vessel and the water in the sample.

The desorption curve can be determined by pumping dry air into the jar for a certain amount of time. If the removed amount of water during the drying process is calculated, one point of the desorption curve can be determined. By using a mass balance, the mass of water removed from the jar is calculated as

$$m_{\text{out}} = \int_0^{\varepsilon} \varphi_v (C_{\text{out}} - C_{\text{in}}) dt \tag{4.6}$$

where φ_v is the volumetric flow of the dry air and ε is the elapsed time of blowing air in the jar. In this equation, C_{out} and C_{in} are water concentration for the air leaving and entering the jar, respectively. By combining Eqs. (4.3) and (4.5), m_{out} can be rewritten as follows:

$$m_{\text{out}} = \frac{C_{\text{sat}} \varphi_v}{100} \int_0^{\varepsilon} (RH_{out} - RH_{\text{in}}) dt \tag{4.7}$$

where RH_{out} and RH_{in} are the relative humidity of air leaving and entering the jar, respectively. Equilibrium is awaited, then the mass of water in the air at equilibrium is calculated with Eqs. (4.3) – (4.5). The water content in the sample is calculated from a mass balance between the mass of water in the system, and in the air inside the jar. It should be noted at each step, the mass of water in the system is obtained by subtracting the total amount of water in the jar (system) at the previous step from m_{out}, obtained by Eq. (4.6).

It is initially assumed that the jar is an ideal mixer, implying that the humidity at the outlet is the same as the humidity in the core of the jar. Therefore, the humidity of the leaving air is equal to the measured

humidity inside the jar. It is, however, observed that this assumption is associated with errors. This is because, given the location of the sensor of relative humidity in the jar, the measured values cannot be representative of the relative humidity of air leaving the jar. This error is eliminated by adding a sensor of relative humidity in the tube through which the air leaves the jar. In this case, the relative humidity is measured of air leaving the jar (RH_{out}) can be measured more accurately.

4.4 Results

Figure 11 shows the obtained sorption isotherm for the mortar sample for both cases: with and without chloride. For the case with chloride, the figure shows the adsorption and desorption behaviour of the sample. It can be seen that for the entire range of the tested relative humidity, the adsorption of the sample containing chloride is larger than the sorption of the sample containing no chloride. This is more significant for the higher values of relative humidity. For example, for RH = 20%, the absolute difference is about 4 kg/m^3, while this difference goes up to 37 kg/m^3 for RH = 70%. In addition, a closer look at Figure 4.11 reveals that the adsorption curve for the case without chloride is almost linear. On the other hand, for the sample containing chloride, a BET-Type-II curve is clearly observed [36-37]. The significant increase in the adsorption properties of the case containing chloride is due to the fact that some chloride can be bound to the surface of the pore walls. The bounded chloride is then capable of absorbing some water. This phenomenon, therefore, can significantly increase the adsorption properties of the material.

Earlier studies have shown that the presence of chloride, but also the pore size distribution can significantly influence the sorption isotherm. For example, Villani et al. [26], based on the study by Benavente [38-39] Selander [40] and Spragg [41], developed a thermodynamical model, in which an equilibrium relative humidity is derived as:

$$RH_{\mathrm{eq}}(r) = a_w e^{\frac{2\sigma v_i^0}{RTr}\cos\phi} \tag{4.6}$$

where a_w is the water activity [-], σ is the surface tension [N/m], v_i^0 is the molar volume of the liquid [m^3/mol], R is the universal gas constant [N.m/K.mol], T is the temperature [K], r is the pore radius [m] and Φ is the contact angle [deg]. According to this model, the presence of chloride can change the properties of the material such as the equilibrium relative humidity. This is mainly because the chloride content will change the surface tension of the material. It should be noted that although the surface tension of a sodium chloride solution is higher than the surface tension of pure water, the water activity is lower. For a given pore radius, this will make the equilibrium relative humidity of samples lower than that of pure water. In this perspective, if the environmental relative humidity is lower than the equilibrium relative humidity, water evaporates. If the environmental relative humidity is higher, condensation occurs. Thus, if the equilibrium relative humidity in a pore is lower, condensation occurs at lower relative humidity. This can be an explanation for the increased sorption of a sample containing sodium chloride.

It should be noted that the linear behaviour of adsorption isotherm for mortar containing no chloride can also be seen in the studies by Tada and Watanabe [42], Daina [43] and Pel [44]. Figure 4.11 also shows the desorption behaviour of the mortar sample for the case containing chloride, where the hysteresis effect can be clearly observed.

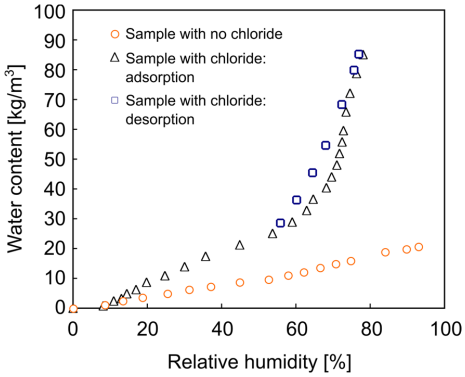

Figure 4.11: Comparison of sorption between a mortar sample containing chloride and a sample containing no chloride.

It is interesting to compare the water absorption measured here with those measured by [44] using NMR. Here the mortar samples has a water:cement:sand composition of w:c:s = 0.5:1:3, whereas in [44] the composition was w:c:s = 0.5:1:5.6. Thus, means that our sample and that of [44] have a different paste and hydrated cement content, which needs to be accounted for.

The hydrated cement volume fraction, which is the phase that absorbs water, in the cement paste can expressed with the Powers and Brownyard model as [45, 46]:

$$\varphi_{hp,p} = \frac{\alpha\left[\frac{v_c}{v_w}+\frac{w_d v_d}{v_w c}\right]}{\frac{v_c}{v_w}+\frac{w}{c}} \tag{4.9}$$

with α as degree of cement hydration, v_c/v_w and v_d/v_w the ratios of specific volume of cement and water (≈ 0.32) and of totally bound water and free water (≈ 0.81), respectively, and the w_d/c the mass of this total bound water (chemically and physically bound) per mass of cement (≈ 0.4). The volume of the cement paste in the mortar reads:

$$\varphi_{p,m} = \frac{\frac{v_c}{v_w}+\frac{w}{c}}{\frac{v_c}{v_w}+\frac{w}{c}+\frac{v_s s}{v_w c}} \tag{4.10}$$

with v_s/v_w the ratio of specific volume of sand (mostly quartz) and water (≈ 0.38). The volume fraction of hydrated cement in mortar reads:

$$\varphi_{hp,m} = \varphi_{hp,p}\,\varphi_{p,m} = \frac{\alpha\left[\frac{v_c}{v_w}+\frac{w_d v_d}{v_w c}\right]}{\frac{v_c}{v_w}+\frac{w}{c}+\frac{v_s s}{v_w c}} \tag{4.11}$$

In [44] and here, the same type of cement was used (OPC, CEM I), so with same v_c/v_w and w_d/c, and if we assume a similar degree of hydration, the present results and those of [44] become comparable by assessing their denominator of Eq. (4.11) only, being 1.96 and 2.95, respectively. The later value expresses that the paste content is lower in the mortar of [44], as more sand was mixed in.

Figure 4.12 compares the adsorption isotherm of the mortar sample without added chloride as obtained in the present study, with those of "Fig. 4.8" in [44], where the values have been multiplied by 2.95/1.96 = 1.5 to compensate for the lower cement paste content. It can be seen that for all relative humidity values, the results of the presented method and [44] are close to each other, though here slightly higher adsorption isotherm values are obtained.

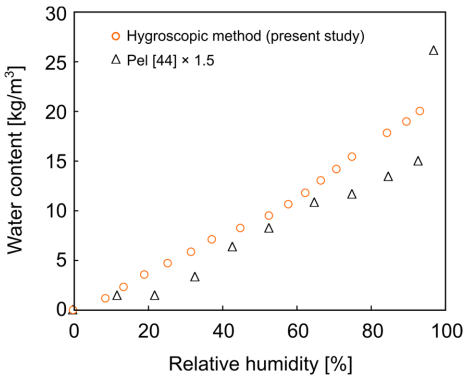

Figure 4.12: Adsorption isotherm of mortar sample containing no chloride.

Figure 4.13 shows the adsorption of sand-lime samples for both with and without chloride. The properties of the material are presented in Table 4.2. Similar to the mortar sample, for the sand-lime samples higher adsorption properties are also obtained for the case containing chloride. However, the effect of the presence of chloride is less significant. For example, for RH = 20% and RH = 70%, the absolute difference is about 2.1 kg/m^3 and 1.8 kg/m^3, respectively. In addition, for both cases, the adsorption curves are BET Type II.

The difference in the adsorption properties of sand-lime with and without chloride is in line with the results of the previous studies by Rijniers [23] and Franzen and Mirwald [24]. The main reason for such differences can be related to the tendency of chloride to adsorb water [9-10].

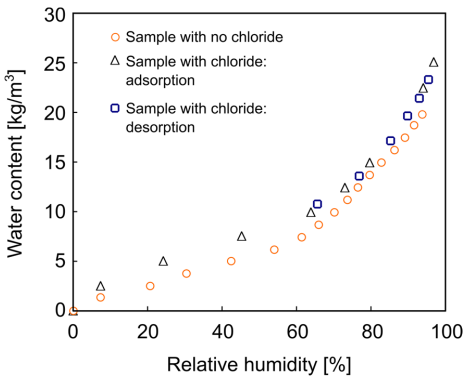

Figure 4.13: Comparison of sorption between a sand-lime sample containing chloride and a sample containing no chloride.

Furthermore, Figure 4.13 also shows the desorption curve for sand-lime containing chloride. No hysteresis effect can be observed for the sand-lime material.

The adsorption isotherm of the sand-lime sample with no chloride is also compared with the results provided by Pel [44], as shown in Figure 4.14. Similar trends can be seen in the behaviour of the adsorption properties as a function of relative humidity. In [44] no specific details on the used sand-lime sample could be found, so that there may be a difference in used samples, so the sample used here and that in [44]. Obviously, a difference in materials will lead to a different outcome in adsorption properties.

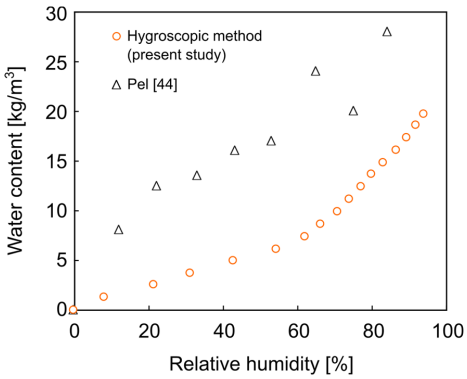

Figure 4.14: Adsorption isotherm of sand-lime containing no chloride.

4.5 Conclusions

In this study, a hygroscopic technique is introduced to measure the sorption behaviour of porous materials. To the best knowledge of the authors, the accuracy of the hygroscopic technique has not yet been investigated for porous materials. Therefore, this study introduces a novel hygroscopic technique to measure the sorption behaviour of porous materials. In this technique, the sorption isotherm can be obtained by injecting water with a high level of control into a controlled environment where a sample is positioned. The amount of water can be added in steps resulting in high-resolution data for the sorption properties of the sample.

The technique is evaluated for two porous materials: Portland cement mortar and sand-lime brick. The results are compared with similar measured data published in the literature. Given the fact that the presence of chloride can significantly increase the level of complexity of the sorption behaviour of porous materials, in this study, the performance of the new technique is also investigated for samples containing chloride.

It is found that the samples containing chloride have higher sorption properties. The significant increase is because some chloride can be bounded to the surface of the pore walls. The bounded chloride is then capable of absorbing some water. This phenomenon, therefore, can significantly increase the adsorption properties of the material. The larger sorption as a consequence of the presence of chloride in the sample is also observed in other studies in the literature.

The results show that the new technique is capable of predicting the sorption properties of porous materials with and without chloride.

4.6 References

[1] Janssen H., A discussion of “moisture diffusion in cement pastes with hydrophobic agent”, Construction and Building Materials 344 (2022) 128241.

[2] Akkaya A., Çağatay İ.H., Investigation of the density, porosity, and permeability properties of pervious concrete with different methods, Construction and Building Materials 294 (2021) 123539.

[3] Nguyen M.H., Nishio S., Nakarai K., Effect of temperature on nondestructive measurements for air permeability and water sorptivity of cover concrete, Construction and Building Materials 334 (2022) 127361.

[4] Tedjditi A.K., Ghomari F., Belarbi R., Cherif R., Boukhelf F., Bouhraoua R.T., Towards understanding cork concrete behaviour: Impact of considering cork absorption during mixing process, Construction and Building Materials 317 (2022) 125905.

[5] Baroghel-Bouny V., Water vapour sorption experiments on hardened cementitious materials: part I: essential tool for analysis of hygral behaviour and its relation to pore structure, Cement and Concrete Research 37 (2007) 414-437.

[6] Poyet S., Experimental investigation of the effect of temperature on the first desorption isotherm of concrete, Cement and Concrete Research 39 (2009) 1052-1059.

[7] De Belie N., Kratky J., Vlierberghe S.V., Influence of pozzolans and slag on the microstructure of partially carbonated cement paste by means of water vapour and nitrogen sorption experiments and BET calculations, Cement and Concrete Research 40 (2010) 1723-1733.

[8] De Burgh J.M., Foster S.J., Influence of temperature on water vapour sorption isotherms and kinetics of hardened cement paste and concrete, Cement and Concrete Research 92 (2017) 37-55.

[9] Moussaoui H., Bahammou Y., Idlimam A., Lamharrar A., Abdenouri N, Investigation of hygroscopic equilibrium and modeling sorption isotherms of the argan products: A comparative study of leaves, pulps, and fruits, Food and Bioproducts Processing 114 (2019) 12-22.

[10] Wadsö L., Svennberg K,. Dueck A., An experimentally simple method for measuring sorption isotherms, Drying Technology 22 (2004) 2427-2440.

[11] Van der Zanden A.J.J., Goossens E.L.J., The measurement of water in paint films, Chemical Engineering and Processing 43 (2004) 739-743.

[12] Broom D.P., Hydrogen storage materials, Gas sorption measurement techniques (Chapter 4), Springer-Verlag, London (2011) 117-139.

[13] Porion P., Faugère A.M., Levitz P., van Damme H., Raoof A., Guilbaud J.P., Chevoir F., A NMR investigation of adsorption/desorption hysteresis in porous silica gels, Journal of Magnetic Resonance Imaging 16 (1998) 679.

[14] Leisen J., Haskell Beckham W., Benham M., Sorption Isotherm Measurements by NMR, Solid State Nuclear Magnetic Resonance 22 (2002) 409-422.

[15] Al-Muhtaseb A.H., McMinn W.A.M., Magee T.R.A., Moisture Sorption Isotherm Characteristics of Food Products: A Review, Food and Bioproducts Processing 80 (2002) 118-128.

[16] Li D., Liu Q., Weniger P., Gensterblum Y., Busch A., Krooss B., High-pressure sorption isotherms and sorption kinetics of CH4 and CO2 on coals, Fuel 89 (2010) 569-580.

[17] Thommes M., Kaneko K., Neimark K., Alexander V., Olivier J.P., Rodriguez-Reinoso F., Rouquerol J., Kenneth S.W., Physisorption of gases, with special reference to the evaluation of surface area and pore size distribution, Pure and Applied Chemistry 87 (2015) 1051-1069.

[18] Crank J., Park G.S., Diffusion in polymers, in: Crank J., Park G.S. (Eds.), Methods of Measurement (Chapter 1), Academic Press, London (1968) 1-39.

[19] Scarpa F., Tagliafico L.A., A new procedure to measure water adsorption isotherms of porous fibrous materials, Journal of Porous Materials 15 (2008) 451-456.

[20] Zhu Y., Wan X., Han X., Ren J., Luo J., Yu Q., Solidification of chloride ions in alkali-activated slag, Construction and Building Materials 320 (2022) 126219.

[21] Bai L., Xie J., Liu J., Xie Y., Effect of salt on hygroscopic properties of cement mortar, Construction and Building Materials 305 (2021) 124746.

[22] Sun H., Liu S., Yu F., Zhang X., Wu C., Xing F., Ren J., Behaviour of cement binder exposed to semi-immersion in chloride-rich salt solutions and seawater with different RH levels, Cement and Concrete Composites 131 (2022) 104606.

[23] Rijniers L.A., Salt crystallization in porous materials: an NMR study, PhD Thesis, Eindhoven University of Technology, the Netherlands (2004).

[24] Franzen C., Mirwald P.W., Moisture sorption behaviour of salt mixtures in porous stone, Chemie der Erde 69 (2009) 91-98.

[25] Koniorczyk M., Wojciechowski M., Influence of salt on desorption isotherm and hygral state of cement mortar – Modelling using neural networks, Construction and Building Materials 23 (2009) 2988-2996.

[26] Villani C., Spragg R., Pour-Ghaz M., Weiss W.J., The role of deicing salts on the non-linear moisture diffusion coefficient of cementitious materials, Brittle Matrix Composites 10 (2012) 101-114.

[27] NT Build 492, Concrete, mortar and cement-based repair materials: Chloride migration coefficient from non-steady-state migration experiments. Nord test method. Finland (1999).

[28] ASTM C1202 Standard Test Method for Electrical Indication of Concrete's Ability to Resist Chloride Ion Penetration. In Annual Book of ASTM Standards. American Society for Testing and Materials 04.02, Philadelphia, USA (2005).

[29] Yu Q.L., Design of environmentally friendly calcium sulfate-based building materials - Towards an improved indoor air quality, PhD thesis, Eindhoven University of Technology, the Netherlands (2012).

[30] Townshend A., Titrimetric analysis, Encyclopedia of analytical science, Academic Press 9 (1995) 5240-5248.

[31] Parvinen P., Virtanen V., Lajunen L.H.J., Chlorine, in Townshend A, Encyclopedia of analytical science, Academic Press 2 (1995) 687-699.

[32] Hulanicki A., Glab S., Potentiometry: Titrations, in: Townshend A, Encyclopedia of analytical science, Academic Press 7 (1995) 4106-4112.

[33] Dean J.A., Analytical Chemistry Handbook, Electroanalytical methods, The McGraw-Hill Companies, New York (1995).

[34] Reid, R.C., Prausnitz, J.M. & Sherwood, T.K., The pressure of gases and liquids, 3rd edition, The McGraw-Hill Companies, New York (1977).

[35] Bridgeman, O.C., Aldrich, E.W.,Vapor Pressure Tables for Water, Journal of Heat Transfer 86 (1964) 279-286.

[36] Gregg S.J., Sing K.S.W., Adsorption, Surface Area and Porosity, 2nd edition, Academic Press, London (1982).

[37] Brunauer S., Emmett P.H, Teller E., Adsorption of gases in multimolecular layers, Journal of the American Chemical Society 60 (1938) 309-319.

[38] Benavente D., Garcia del Cura M.A, Bernabeu A., Ordonez S., Quantification of salt weathering in porous stones using an experimental continuous partial immersion method, Engineering Geology 59 (2001) 313-325.

[39] Benavente D., Garcia del Cura M.A., Ordonez S., Salt Influence on evaporation from porous building rocks, Construction and Building Materials 17 (2003) 113-122.

[40] Selander A., Hydrophobic impregnation of concrete structures, Effect on concrete properties, Ph.D. Thesis, Royal Institute of Technology, Stockholm, Sweden (2010).

[41] Spragg R., Castro J., Li W., Pour-Ghaz M., Huang P.T, Weiss J., Wetting and drying of concrete using aqueous solutions containing de-icing salts, Cement and Concrete Composites 33 (2011) 535-542.

[42] Tada S., Watanabe K, Dynamic determination of sorption isotherm of cement-based materials, Cement and Concrete Research 35 (2005) 2271-2277.

[43] Daian J.F., Condensation and isothermal water transfer in cement mortar, Transport in Porous Media 3 (1988) 563– 589.

[44] Pel L., Moisture transport in porous building materials, PhD Thesis, Eindhoven University of Technology, the Netherlands (1995).

[45] Brouwers H.J.H., The work of Powers and Brownyard revisited: Part 1, Cement and Concrete Research 34 (2004) 1697-1716.

[46] Brouwers H.J.H., A hydration model for Portland cement using the work of Powers and Brownyard, Eindhoven University of Technology/Portland Cement Association Report SN3039 (2011).

5

5. Moisture and chloride transport during wetting/drying cycles

This chapter has been published as:

Van der Zanden, A.J.J., Taher, A. & Arends, T. *Construction and Building Materials* 81 (2015) 120-129.

5.1 Introduction

A large threat for the durability of concrete is the corrosion process of the steel reinforcement. The corrosion is initiated by the presence of chloride. Most often, the chloride comes from outside the concrete during the lifetime of the structure. An overview of the literature regarding the factors influencing the chloride transport in concrete is given by Song et al. [1]. The chloride can also be bound to the cement hydration products. A review on this topic is the work of Yuan et al. [2].

It has been described by Baessler et al. [3] how the corrosion of the reinforcement can be analysed with electrochemical measurements. The corrosion process around the steel in concrete has been studied numerically by Kim and Kim [4]. Also, the bond between the reinforcement and the surrounding concrete depends on the status of corrosion of the steel, as studied by Fang et al. [5]. The relation between the various parameters and the time to corrosion initiation of the reinforcement has been given by Zhang and Lounis [6]. How the time to corrosion depends on the surface chloride concentration has been examined by Ann et al. [7].

The reinforcement of a concrete structure can be protected against corrosion by a high quality covering layer of concrete or by the sufficiently deep covering layer. Very often, concrete has small cracks due to the production and curing processes or caused by mechanical stress. The chloride penetration in cracked concrete and around the cracks in concrete has been measured by Win et al. [8]. The crack width in the covering layer of concrete can be used to analyse how much the corrosion of the reinforcement has proceeded, as it has been shown by Vidal et al. [9]. The service life of repaired concrete structures under chloride environment has been studied by Song et al. [10].

An additional factor in the transport of chloride in concrete is the question whether the surface of the concrete is exposed to wetting and drying or not. During the wetting process, additional chloride can enter the concrete and stays behind when water is evaporating during the drying process. This way, the surface chloride concentration can rise to high values. There is not so much research yet on this point.

Most often, the concentration of chloride in concrete is measured with a destructive technique. However, Montemor et al. [11] showed that with Ag/AgCl electrodes the concentration can be measured in situ. Pel et al. [12] showed that NaCl concentration profiles in fired-clay brick can be measured with Nuclear Magnetic Resonance. Climent et al. [13] presented a method to measure the diffusion coefficient of chloride in non-saturated concrete. Also, Azari et al. [14] measured the diffusion coefficient of chloride in a wide range of micro silica concrete. Measurements of Hong and Hooton [15] showed that chloride not only can enter concrete, but that it can also, to a certain extent, be washed out of the concrete with fresh water. It has been shown experimentally by Marsavina et al. [16] and by Djerbi et al. [17] that the transport of chloride in concrete is increased by the presence of cracks in the concrete. The coupled transport of water and chloride in concrete was measured by Cerny et al. [18]. The influence of wetting/drying cycles with water with a chloride concentration on the rebars of concrete was characterized by Polder and Peelen [19].

Huinink et al. [20] put forward a simple model for ion distribution in drying porous materials which was based on convection and diffusion. Oh and Jang [21] gave a model including the binding of chloride to the cement hydration products and the water flux in concrete and compared the prediction of this model with the chloride concentration profile in concrete structures of ten years old. The transport properties of interacting ions in unsaturated cement systems were modelled by Marchand [22]. A model for the chloride ion ingress in concrete, including the adsorption of the chloride on the concrete and the

desorption from the concrete, as well as the chemical reaction of the chloride with the concrete, was given by Shin and Kim [23]. Johannesson [24] made a complex model for describing ion transport in a pore solution using the mixture theory, where the transport of moisture is taken into account explicitly also. Conciatori et al. [25] also put forward a complex model based on capillary suction and diffusion to describe the chloride ingress into concrete. A model for the ingress of chloride in concrete, including convection, drying/wetting cycles and carbonation was given by Meijers et al. [26]. The predictions of this model were compared with experimental results. Their conclusion was that models which take into account explicitly the moisture transport are more accurate than models which use only one diffusion coefficient for chloride transport. This conclusion was also the result of the work of Wang et al. [27]. The predictions of a model incorporating the fine or coarse network structure of the porous concrete were given by O'Neill and Ishida [28] for a cyclic exposure with wetting and drying. The theory and experimental results about the chloride transport in concrete under the influence of an external electric field was given by Stanish et al. in respectively [29] and [30].

The models described in the preceding paragraph are very often so complex that almost always an analytical solution is impossible, and that only a numerical solution can be given. Also, the material properties, which are used in these models, can be a strong function of other parameters which makes an analytical solution impossible. For instance, the diffusion coefficient of water in concrete and the diffusion coefficient of chloride in concrete depend strongly on the moisture content.

The present study puts forward a model for the transport of chloride in concrete that is not saturated with water. The transport of water is described with a diffusion coefficient. The transport of chloride includes the transport of chloride dissolved in the pore water migrating through the concrete and the transport of chloride caused by a gradient in the pore water chloride concentration. The first process of chloride convection through the concrete is modelled with keeping in mind that the larger water filled pores contribute (relatively) more to the chloride transport than the smaller water filled pores. It is a first simple model for a complex process. The second process of chloride diffusion is modelled with Fick's law, which is adapted for the non-ideal situation.

The model is applied on concrete with a daily and a yearly cycle of wetting and drying. The equations are solved numerically using the Crank-Nicolson method. The numerical results are given. A final discussion ends the chapter.

5.2 Water transport

In a partially saturated porous material, the water flux, n_w, is influenced by differences in the water concentration, C. In the present work, it is assumed that the water flux is, according to Fick's first law, proportional to the concentration gradient of water

$$n_w = -D\frac{\partial C}{\partial x} \tag{5.1}$$

where x is the position coordinate and D the diffusion coefficient of water in concrete. It is recognized that also a presence of chloride and a gradient in the chloride concentration can influence the water transport, but in this study, these influences are ignored, because they are not well known and are probably mostly of minor importance. Using a micro mass balance and Eq. (5.1), the result is Fick's second law, which describes the time evolution of a water concentration as

$$\frac{\partial C}{\partial t} = \frac{\partial}{\partial x}\left(D\frac{\partial C}{\partial x}\right) \tag{5.2}$$

where t is time.
Eq. (5.2) will be applied between $x = 0$ and $x = L$, where L is the length of a sample of the studied material. The boundary condition at $x = 0$ is given by

$$C = C_{x=0} \tag{5.3}$$

where $C_{x=0}$ is a prescribed concentration. At $x = L$, the sample is isolated against water transport, and the corresponding boundary condition is

$$\left.\frac{\partial C}{\partial x}\right|_{x=L} = 0 \tag{5.4}$$

At the start of a process, the concentration in the sample is prescribed with

$$C = C_{t=0} \tag{5.5}$$

where $C_{t=0}$ is the begin concentration, a function of x.
For use in the next section, the volume flux of water, $n_{v,w}$, is given by

$$n_{v,w} = \frac{n_w}{\rho_w} \tag{5.6}$$

where ρ_w is the density of water.

5.3 Chloride transport

In the model, the chloride is dissolved in the water in the pores. This is the only chloride present. It is assumed that there is no chloride bound to the surface of the pore walls. The concentration of chloride in the pore water is denoted s. This makes that the chloride concentration in the concrete, S, is described with

$$S = \varphi_w s \tag{5.7}$$

where φ_w is the volume fraction water of the concrete. The mass flux of chloride is formed by a convective and a dispersive component. The convective component arises when water with dissolved chloride is being transported through the concrete. The convective mass flux of chloride is

$$n_{s,convective} = n_{v,w}s = \frac{n_w}{\rho_w}\frac{S}{\varphi_w} = \frac{n_w}{\rho_w}\frac{S}{\frac{C}{\rho_w}} = n_w\frac{S}{C} \tag{5.8}$$

The dispersive component of the chloride flux arises due to differences of the chloride concentration in the pore water, i.e. in s, and because of differences in the local water velocity in the pores. The total chloride flux in concrete is then given by

$$n_s = -D\frac{\partial C}{\partial x}\frac{S}{C} - D_s\frac{\partial S}{\partial x} \tag{5.9}$$

where D_s is, in the present work, called the dispersion coefficient of chloride in the partially saturated concrete, which depends also on the water transport. The equation for the chloride transport is

$$\frac{\partial S}{\partial t} = \frac{\partial}{\partial x}\left(D\frac{\partial C}{\partial x}\frac{S}{C} + D_s\frac{\partial S}{\partial x}\right) \tag{5.10}$$

which is a differential equation for S coupled to Eq. (5.2) for the water transport.
The chloride flux at $x = L$ must be zero. The convective chloride flux at $x = L$ is zero, because the water flux is zero. Thus, the dispersive chloride flux at $x = L$ must be zero, which leads to the boundary condition

$$\left.\frac{\partial S}{\partial x}\right|_{x=L} = 0 \tag{5.11}$$

At $x = 0$, various boundary conditions can be applied for the wetting situation and for the drying situation, depending on the physics of the outside environment working on the sample. Water entering the sample can take chloride from the outside environment into the sample. Also, water leaving the sample can take chloride with it in more or less degrees. In this study, two types of boundary conditions are studied. The first one is sweet water transport, where the water entering or leaving the sample contains no chloride. In this case, the total chloride flux at $x = 0$ is zero, i.e.

$$-D\left.\frac{\partial C}{\partial x}\right|_{x=0}\frac{S}{C} - D_s\left.\frac{\partial S}{\partial x}\right|_{x=0} = 0 \tag{5.12}$$

This boundary condition holds for both wetting and drying, which is then reflected in the sign of $\partial C/\partial x$. For drying, it means that water is, for instance, being evaporated at the surface of the sample and that the chloride remains in the sample. Probably, the chloride concentration at the surface will rise in such a situation. The second type of boundary condition is salt water transport. If the water added to the sample takes with it a chloride concentration $s_{outside}$, the boundary condition at $x = 0$ becomes

$$\frac{n_w}{\rho_w}s_{outside} = -D\left.\frac{\partial C}{\partial x}\right|_{x=0}\frac{S}{C} - D_s\left.\frac{\partial S}{\partial x}\right|_{x=0} \tag{5.13}$$

The condition for salt water transport leaving the sample is not so straightforward. The condition that the water leaving the sample would have a concentration $s_{outside}$ is physically unrealistic. The most realistic condition is that the chloride concentration in the water leaving the sample is equal to the chloride concentration in the pore water. This leads to the boundary condition

$$\frac{n_w}{\rho_w}s = \frac{n_w}{\rho_w}\frac{S}{\varphi_w} = -D\left.\frac{\partial C}{\partial x}\right|_{x=0}\frac{S}{C} - D_s\left.\frac{\partial S}{\partial x}\right|_{x=0} \tag{5.14}$$

which leads, because $\rho_w\varphi_w = C$ to

$$\left.\frac{\partial S}{\partial x}\right|_{x=0} = 0 \tag{5.15}$$

5.4 Physical properties

5.4.1 Diffusion coefficient

Differences in the water concentration in concrete lead to differences in the capillary pressure. This means that the pressure in the liquid water phase inside the concrete is different and that, as a result of these pressure differences, liquid water flows through the pores that are filled with water. There is a

large flow through the large water filled pores and a small flow through the small water filled pores. This process has been modelled by van der Zanden et al. [31] and van der Zanden [32], with the result the diffusion coefficient as a function of the water concentration. For very small water concentrations in concrete, the water vapor diffusion through the concrete can also contribute significantly to the water transport. The structure of the concrete determines the value of the diffusion coefficient as a function of the water concentration.
However, in the present study, just to be sure about the correctness of the value of the diffusion coefficient, the value as it was reported in the literature will be used, as it will be explained in a later section.

5.4.2 Dispersion coefficient

The dispersion coefficient has its lowest value when there is no water transport through the concrete. In this case, there can only be chloride transport caused by the molecular diffusion of chloride in water, originating from chloride concentration differences in the water. The chloride flux in the stagnant water, $n_{s,w}$, is, using Eq. (5.7), described with

$$n_{s,w} = -\frac{D_m}{\tau}\frac{\partial s}{\partial x} = -\frac{D_m}{\tau}\frac{1}{\varphi_w}\frac{\partial S}{\partial x} + \frac{D_m}{\tau}\frac{S}{{\varphi_w}^2}\frac{\partial \varphi_w}{\partial x} \tag{5.16}$$

where D_m is the molecular diffusion coefficient of chloride in water, and where τ, the tortuosity, has been added to incorporate deviations from the ideal situation. With

$$n_s = \varphi_w n_{s,w} \tag{5.17}$$

and neglecting the last term in Eq. (5.16), n_s becomes

$$n_s = -\frac{D_m}{\tau}\frac{\partial S}{\partial x} \tag{5.18}$$

Comparison of Eq. (5.18) with Eq. (5.9) shows that the lower limit for the dispersion coefficient is given by

$$D_s = \frac{D_m}{\tau} \tag{5.19}$$

The last term in Eq. (5.16) has been neglected in order to arrive at the neat expression of Eq. (5.19). This is only valid when this term is much smaller than the preceding term, i.e. when

$$\left|\frac{\partial \varphi_w}{\varphi_w}\right| \ll \left|\frac{\partial S}{S}\right| \tag{5.20}$$

The lower limit of the dispersion coefficient is supposed to be relevant only in the case where the chloride transport is dominated by molecular diffusion, and the convective term caused by water transport is small. This is exactly what inequality (5.20) tales. When the numerical results of the model are available, inequality (5.20) can be verified.
To obtain a value for the dispersion coefficient when the water flux is not zero, a situation is studied where $\partial s/\partial x$ has a negative value, as it is shown in Figure 5.1.

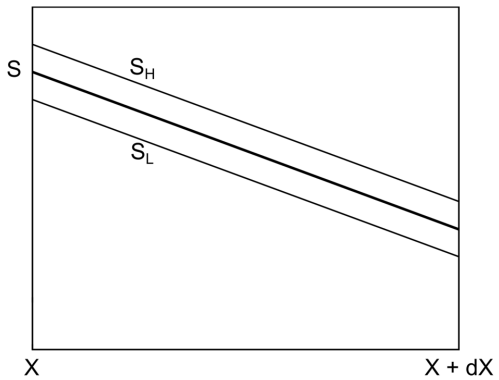

Figure 5.1: The chloride concentration of the pore water as a function of x, where the subscript $_H$ indicates a concentration in water with a higher velocity and subscript $_L$ with lower velocity.

At position x, there is a value of s and at position $x+dx$, there is a value of $s+ds$, where, in this case, ds is negative. It is now assumed that the water flows into the positive x-direction. In a partially saturated porous material, the velocity of the water is not the same everywhere. The velocity in the larger water filled pores is larger than the velocity in the smaller ones. This is the reason, in the case of Figure 5.1, why the pores with a high velocity have a higher s, indicated s_H, than the s in the pores with a low velocity, indicated s_L. The larger pores form better channels for water coming from a smaller x value, and therefore a larger s value. The exact distribution of the water flow over the different pores is quite complex. Here, to arrive at an expression for the dispersion coefficient, the total water filled pore space is assumed to consist of two extremes, one half of the water filled pore space is flowing homogeneously with velocity v_H, and the other half is stagnant. The assumption of the division in half / half is assumed in view of the lack of better arguments leading to a different division. This case is illustrated in Figure 5.2 with a sketch of the division of the total available pore space in air filled pores, pores with homogeneously flowing water, and pores with stagnant water.

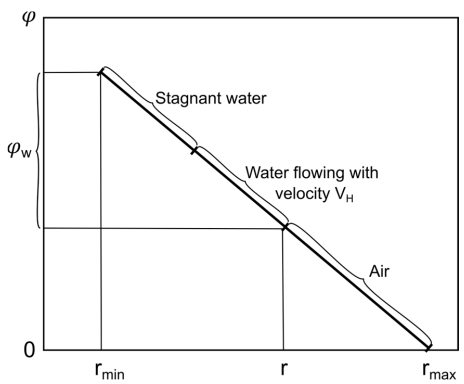

Figure 5.2: The division of the total available pore space in air filled pores, pores with homogeneously flowing water, and pores with stagnant water.

Figure 5.1 now also shows the profile of s_H and s_L. It can now be assumed and later verified that the value of s_H-s_L is independent of x. s is the average of s_H and s_L. The chloride is being transported with the water in the pores with the moving water in the x-direction, and the pores with the stagnant water are supplied

with chloride by a diffusion process caused by the difference between s_H and s_L. This process causes a rise in s_H and s_L as a function of time. It can be verified later that the rise in time of s_H is equal to the rise in time of s_L. The difference between s_H and s_L is constant in time. A chloride balance over the water filled pore volume per surface unit between x and $x+dx$ gives

$$\left(s_{H,x} - s_{H,x+dx}\right) v_H \frac{1}{2} \varphi_w \partial t = -\partial s_H v_H \frac{1}{2} \varphi_w \partial t = \frac{\partial s_H}{\partial t} \varphi_w \partial x \partial t \tag{5.21}$$

which can be written as

$$\frac{\partial s_H}{\partial t} = -\frac{\partial s_H}{\partial x} \frac{v_H}{2} \tag{5.22}$$

Because

$$\frac{\partial s_H}{\partial t} = \frac{\partial s_L}{\partial t} = \frac{\partial s}{\partial t} \tag{5.23}$$

Eq. (5.22) leads to

$$\frac{\partial s}{\partial t} = -\frac{\partial s}{\partial x} \frac{v_H}{2} \tag{5.24}$$

Eq. (5.24) seems to be the differential equation for the chloride transport. However, it is only valid in the case of Figure 5.1. The general differential equation for the chloride transport is Eq. (5.10).
The transport of chloride from the high velocity part to the low velocity part is modelled as a diffusion flux over a distance r, the largest filled pore radius, with the molecular diffusion coefficient of chloride in water, D_m, at a specific exchanging surface area, a. A chloride balance over the low velocity part then gives

$$(s_H - s_L) \frac{D_m}{r} a = \frac{1}{2} \varphi_w \frac{\partial s_L}{\partial t} \tag{5.25}$$

Because s is the average of s_H and s_L, with Eq. (5.25) it can be written that

$$s_H = s + \frac{1}{4} \varphi_w \frac{\partial s_L}{\partial t} \frac{r}{D_m a} \tag{5.26}$$

which, with Eq. (5.24), becomes

$$s_H = s - \frac{1}{8} \varphi_w v_H \frac{\partial s}{\partial x} \frac{r}{D_m a} \tag{5.27}$$

which, substituted in the expression for the total chloride flux

$$n_s = s_H v_H \frac{1}{2} \varphi_w \tag{5.28}$$

gives

$$n_s = s v_H \frac{1}{2} \varphi_w - \frac{1}{16} \varphi_w^2 v_H^2 \frac{\partial s}{\partial x} \frac{r}{D_m a} \tag{5.29}$$

With Eq. (5.7), Eq. (5.29) becomes

$$n_s = \frac{1}{2} S v_H - \frac{1}{16} \varphi_w v_H^2 \frac{\partial S}{\partial x} \frac{r}{D_m a} + \frac{1}{16} v_H^2 \frac{\partial \varphi_w}{\partial x} S \frac{r}{D_m a} \tag{5.30}$$

Because

$$v_H \frac{1}{2} \varphi_w = n_{v,w} = -\frac{D}{\rho_w} \frac{\partial C}{\partial x} \tag{5.31}$$

or

$$v_H = -\frac{2D}{C} \frac{\partial C}{\partial x} \tag{5.32}$$

Eq. (5.30) can be rewritten as

$$n_s = -\frac{D}{C} \frac{\partial C}{\partial x} S - \frac{1}{4} \frac{C}{\rho_w} \left(\frac{D}{C} \frac{\partial C}{\partial x} \right)^2 \frac{\partial S}{\partial x} \frac{r}{D_m a} + \frac{1}{4} \left(\frac{D}{C} \frac{\partial C}{\partial x} \right)^2 \frac{1}{\rho_w} \frac{\partial C}{\partial x} S \frac{r}{D_m a} \tag{5.33}$$

or as

$$n_s = -\frac{D}{C} \frac{\partial C}{\partial x} S \left(1 - \frac{1}{4} \frac{D}{C} \frac{\partial C}{\partial x} \frac{1}{\rho_w} \frac{r}{D_m a} \right) - \frac{1}{4} \frac{C}{\rho_w} \left(\frac{D}{C} \frac{\partial C}{\partial x} \right)^2 \frac{\partial S}{\partial x} \frac{r}{D_m a} \tag{5.34}$$

It can now be verified that in most cases the second term of the expression between the first pair of brackets is much smaller than 1, and can thus be neglected. Comparing Eq. (5.34) with Eq. (5.9) shows that the dispersion coefficient is given by

$$D_s = \frac{1}{4} \frac{C}{\rho_w} \left(\frac{D}{C} \frac{\partial C}{\partial x} \right)^2 \frac{r}{D_m a} \tag{5.35}$$

Now, an expression will be derived for the specific exchanging surface, a, between s_H and s_L. In 1 m³ of concrete, the volume with s_H is $\varphi_w/2$. These pores have a cross sectional surface area of πr^2 and a total length of $(\varphi_w/2)/\pi r^2$. The side surface area of these pores is $((\varphi_w/2)/\pi r^2) 2\pi r = \varphi_w/r$. If it is assumed that half of the pore walls is exposed to air and to concrete, and that the other half is available for diffusion towards the stagnant water, it follows that

$$a = \frac{\varphi_w}{2r} = \frac{C}{2r\rho_w} \tag{5.36}$$

Using Eq. (5.36) in Eq. (5.35) gives

$$D_s = \frac{D_m}{\tau} + \frac{1}{2} \left(\frac{D}{C} \frac{\partial C}{\partial x} \right)^2 \frac{r^2}{D_m} \tag{5.37}$$

where the term D_m/τ has been added as the lower limit as derived in Eq. (5.19).
The parameter r depends also on the water concentration, but cannot be expressed now because the relation between r and C depends on the concrete. In a later section, this dependence will be given for the studied concrete.

5.5 Case study

5.5.1 Studied concrete

In order to proceed with the analysis, the diffusion coefficient of water in concrete is needed while the pore size distribution of that same concrete is given also. A literature research did not get such a result. However, Pel [33] measured the diffusion coefficient of water in a few types of mortar and also measured the pore size distribution of these mortars. These results will be used below to obtain an estimation of the diffusion coefficient and pore size distribution of a fictitious concrete.

The studied concrete is formed of 25 volume percent gravel and 75 volume percent mortar as studied by Pel [33]. The diffusion coefficient in mortar type MZ from the work of Pel is approximated as a parabola for low water concentrations and as a straight line for high water concentrations on a log(D) versus C plot. With Eq. (5.28) of the work of Van der Zanden [34] and the assumption that the gravel is impermeable to water, it can be calculated that the effective diffusion coefficient of water in the studied concrete is 0.89 times the diffusion coefficient of water in the mortar of Pel. This leads to the two equations

$$\begin{aligned} D &= 10^{0.0017851 \cdot C^2 - 0.093715 \cdot C - 7.551} && \text{for } 0 \text{ kg m}^{-3} \leq C \leq 52.5 \text{ kg m}^{-3} \\ D &= 10^{0.023895 \cdot C - 8.806} && \text{for } 52.5 \text{ kg m}^{-3} < C \leq 157.5 \text{ kg m}^{-3} \end{aligned} \tag{5.38}$$

with which the diffusion coefficient of the studied concrete is approximated, which is sketched in Figure 5.3a.

In the expression for the dispersion coefficient D_s, a value for r, the largest filled pore radius, is needed. From the work of Pel [33], it follows that, for the studied concrete,

$$\begin{aligned} r &= 10^{-0.04905 \cdot C - 4.0} && \text{for } 0 \text{ kg m}^{-3} \leq C \leq 14.25 \text{ kg m}^{-3} \\ r &= 10^{-0.01141 \cdot C - 4.536} && \text{for } 14.25 \text{ kg m}^{-3} < C \leq 128.25 \text{ kg m}^{-3} \\ r &= 10^{-0.08728 \cdot C + 1.194} && \text{for } 128.25 \text{ kg m}^{-3} < C \leq 157.5 \text{ kg m}^{-3} \end{aligned} \tag{5.39}$$

These three lines are sketched in Figure 5.3b.

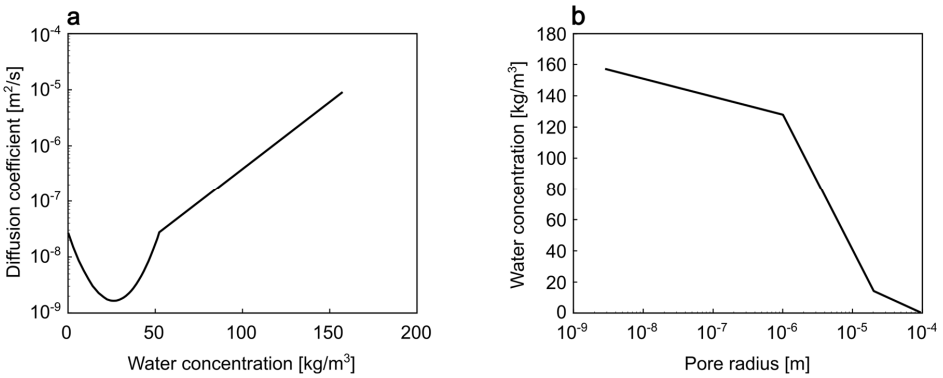

Figure 5.3: a) The diffusion coefficient of the studied concrete as a function of the water concentration. b) The water concentration as a function of the largest filled pore radius of the studied concrete.

The tortuosity of the studied concrete is assumed to be 1, in absence of an experimentally obtained value of the mortar, and because its absolute value does not have a significant influence on the predictions of the model. Concrete samples are studied with a length of 0.1 and 0.2 m.

5.5.2 Boundary conditions

In this study, in order to mimic a wet winter and a dry summer, a repeated cycle of one year is computed in which $C_{x=0}$ is a sine function with a maximum and a minimum concentration of 150 and 10 kg m^{-3} respectively, leading to

$$C_{x=0} = 70\,sin(1.9924 \times 10^{-7} t) + 80 \tag{5.40}$$

The initial water concentration is taken as the average concentration, 80 kg m^{-3} (Figure 5.4).

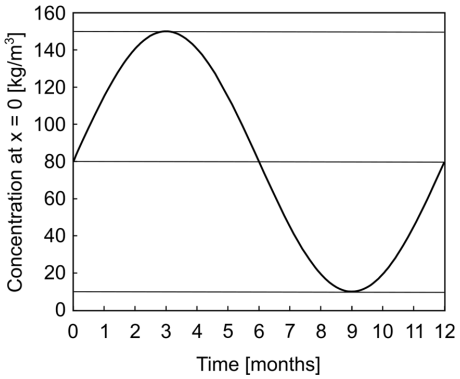

Figure 5.4: One wetting and drying cycle of one year

Because it is very likely that a structure wetted by salt water is located in a marine environment, a realistic value for the chloride concentration of the entering water is the chloride concentration in seawater, which has a typical value of approximately 19 kg m^{-3}. The molecular diffusion coefficient of sodium chloride in water has a value of 1.26×10^{-9} m^2 s^{-1} at 20 °C [35].

With all the possible boundary conditions for the chloride transport, water in, water out, and initial chloride concentration, eight situations can be distinguished as sketched in Figure 5.5.

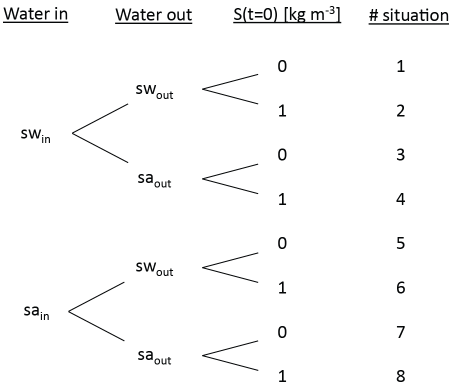

Figure 5.5: Eight situations are distinguished with the boundary conditions of the water moving into the sample sweet or salt (sw, sa), the water moving out of the sample sweet or salt, and the initial chloride content of the sample 0 or 1 kg m^{-3}.

For a sweet water environment, Situations 1 and 3 will not be studied, because there is no chloride present in these situations. In Situation 2, there is initial chloride in the concrete that is redistributed with the water flow, while in situation 4, the chloride is washed out with the water flow. The initial

concentration is chosen as 1 kg m^{-3}, because this implies a chloride concentration in the pore water of 12.5 kg m^{-3} at the initial water concentration of 80 kg m^{-3}, below the saturation concentration.
For a salty water environment, the situations with an initial chloride concentration, Situations 6 and 8, are not studied, because they are less interesting than the studied Situations 5 and 7. Situation 5 will surely lead to an ever increasing chloride concentration in the concrete, because chloride can enter the sample with the water, but cannot leave the sample.

5.6 Numerical solution technique

The numerical solution for this model is obtained using the Crank-Nicholson method. First, a dimensionless length scale is introduced as an equidistant grid with grid points numbered from 0 to N. The position $x = 0$ corresponds to $z = 0$ and $x = L$ corresponds to $z = N$:

$$z = \frac{N}{L}x \tag{5.41}$$

Fick's second law of diffusion thus becomes

$$\frac{L^2}{N^2}\frac{\partial C}{\partial t} = \frac{\partial D}{\partial z}\frac{\partial C}{\partial z} + D\frac{\partial^2 C}{\partial z^2} \tag{5.42}$$

The Crank-Nicolson method requires that the right hand side of Eq. (5.42) is approximated with half the values before a time step, at t, and half the values after the time step, at $t + \Delta t$, as

$$\frac{L^2}{N^2}\frac{\partial C}{\partial t} = \frac{1}{2}\frac{\partial D}{\partial z}\bigg|_t \frac{\partial C}{\partial z}\bigg|_t + \frac{1}{2}D_t\frac{\partial^2 C}{\partial z^2}\bigg|_t + \frac{1}{2}\frac{\partial D}{\partial z}\bigg|_{t+\Delta t}\frac{\partial C}{\partial z}\bigg|_{t+\Delta t} + \frac{1}{2}D_{t+\Delta t}\frac{\partial^2 C}{\partial z^2}\bigg|_{t+\Delta t} \tag{5.43}$$

where Δt is the size of the time step.
Assuming a parabola through three consecutive grid points, this parabola becomes

$$C = \left(\frac{C_{-1}}{2} - C_0 + \frac{C_1}{2}\right)z^2 + \left(-\frac{C_{-1}}{2} + \frac{C_1}{2}\right)z + C_0 \tag{5.44}$$

Using this parabola and its first and second derivatives, the expression for the dimensionless Fick's second law becomes upon rearrangement

$$\begin{aligned} &C_{-1,t+\Delta t}\left(-\frac{D_{-1,t+\Delta t}}{4} - D_{0,t+\Delta t} + \frac{D_{1,t+\Delta t}}{4}\right) + C_{0,t+\Delta t}\left(\frac{2L^2}{N^2\Delta t} + 2D_{0,t+\Delta t}\right) \\ &\quad + C_{1,t+\Delta t}\left(\frac{D_{-1,t+\Delta t}}{4} - D_{0,t+\Delta t} - \frac{D_{1,t+\Delta t}}{4}\right) \\ &= \frac{2L^2 C_{0,t}}{N^2\Delta t} + \left(-\frac{D_{-1,t}}{2} + \frac{D_{1,t}}{2}\right)\left(-\frac{C_{-1,t}}{2} + \frac{C_{1,t}}{2}\right) + D_{0,t}\left(C_{-1,t} - 2C_{0,t} + C_{1,t}\right) \end{aligned} \tag{5.45}$$

With the boundary conditions expressed as

$$\begin{aligned} &C_{0,t+\Delta t} = C_{x=0}, \\ &C_{N-1,t+\Delta t} - C_{N,t+\Delta t} = 0 \end{aligned} \tag{5.46}$$

these expressions are implemented in MATLAB in the matrix form as

$$\begin{pmatrix} 1 & 0 & 0 & 0 & 0 & L & 0 & 0 & 0 \\ - & - & - & 0 & 0 & L & 0 & 0 & 0 \\ 0 & - & - & - & 0 & L & 0 & 0 & 0 \\ 0 & 0 & - & - & - & L & 0 & 0 & 0 \\ 0 & 0 & 0 & - & - & L & - & 0 & 0 \\ M & M & M & M & M & L & M & M & M \\ 0 & 0 & 0 & 0 & 0 & L & - & - & 0 \\ 0 & 0 & 0 & 0 & 0 & L & - & - & - \\ 0 & 0 & 0 & 0 & 0 & L & 0 & 1 & -1 \end{pmatrix} \begin{pmatrix} C_{0,t+\Delta t} \\ C_{1,t+\Delta t} \\ C_{2,t+\Delta t} \\ C_{3,t+\Delta t} \\ C_{4,t+\Delta t} \\ M \\ C_{N-2,t+\Delta t} \\ C_{N-1,t+\Delta t} \\ C_{N,t+\Delta t} \end{pmatrix} = \begin{pmatrix} C_{x=0} \\ - \\ - \\ - \\ - \\ M \\ - \\ - \\ 0 \end{pmatrix} \tag{5.47}$$

For every time step the set of equations is solved using the Gauss elimination to obtain a water concentration profile for the sample.

With the z-coordinate, the differential equation for the chloride transport is written as

$$\frac{L^2}{N^2}\frac{\partial S}{\partial t} = \frac{\partial D}{\partial z}\frac{\partial C}{\partial z}\frac{S}{C} + D\frac{\partial^2 C}{\partial z^2}\frac{S}{C} + D\frac{\partial C}{\partial z}\frac{\partial S}{\partial z}\frac{1}{C} - D\frac{\partial C}{\partial z}\frac{S}{C^2}\frac{\partial C}{\partial z} + \frac{\partial D_s}{\partial z}\frac{\partial S}{\partial z} + D_s\frac{\partial^2 S}{\partial z^2} \tag{5.48}$$

Writing this with the Crank-Nicolson method and rearranging the terms to yield a linear relation gives

$$\begin{aligned} & S_{-1,t+\Delta t}\left(\frac{1}{4}D_{0,t+\Delta t}\left(-C_{-1,t+\Delta t} + C_{1,t+\Delta t}\right)\frac{1}{C_{0,t+\Delta t}} + \frac{1}{4}\left(-D_{s,-1,t+\Delta t} + D_{s,1,t+\Delta t}\right) - D_{s,0,t+\Delta t}\right) \\ & + S_{0,t+\Delta t}\left(\frac{2L^2}{N^2\Delta t} - \frac{1}{4}\left(-D_{-1,t+\Delta t} + D_{1,t+\Delta t}\right)\left(-C_{-1,t+\Delta t} + C_{1,t+\Delta t}\right)\frac{1}{C_{0,t+\Delta t}}\right. \\ & \left. - D_{0,t+\Delta t}\left(C_{-1,t+\Delta t} - 2C_{0,t+\Delta t} + C_{1,t+\Delta t}\right)\frac{1}{C_{0,t+\Delta t}} + \frac{1}{4}D_{0,t+\Delta t}\left(-C_{-1,t+\Delta t} + C_{1,t+\Delta t}\right)^2\frac{1}{C_{0,t+\Delta t}^{\ 2}} + 2D_{s,0,t+\Delta t}\right) \\ & + S_{1,t+\Delta t}\left(-\frac{1}{4}D_{0,t+\Delta t}\left(-C_{-1,t+\Delta t} + C_{1,t+\Delta t}\right)\frac{1}{C_{0,t+\Delta t}} - \frac{1}{4}\left(-D_{s,-1,t+\Delta t} + D_{s,1,t+\Delta t}\right) - D_{s,0,t+\Delta t}\right) \\ & = \frac{2L^2 S_{0,t}}{N^2\Delta t} + \frac{1}{4}\left(-D_{-1,t} + D_{1,t}\right)\left(-C_{-1,t} + C_{1,t}\right)\frac{S_{0,t}}{C_{0,t}} + D_{0,t}\left(C_{-1,t} - 2C_{0,t} + C_{1,t}\right)\frac{S_{0,t}}{C_{0,t}} \\ & + \frac{1}{4}D_{0,t}\left(-C_{-1,t} + C_{1,t}\right)\left(-S_{-1,t} + S_{1,t}\right)\frac{1}{C_{0,t}} - \frac{1}{4}D_{0,t}\left(-C_{-1,t} + C_{1,t}\right)^2\frac{S_{0,t}}{C_{0,t}^{\ 2}} \\ & + \frac{1}{4}\left(-D_{s,-1,t} + D_{s,1,t}\right)\left(-S_{-1,t} + S_{1,t}\right) + D_{s,0,t}\left(S_{-1,t} - 2S_{0,t} + S_{1,t}\right) \end{aligned} \tag{5.49}$$

Eq. (5.11) is converted into

$$S_{N-1,t+\Delta t} - S_{N,t+\Delta t} = 0 \tag{5.50}$$

The boundary condition for sweet water transport is converted into

$$-D\frac{\partial C}{\partial z}\frac{S}{C} - D_s\frac{\partial S}{\partial z}\Big|_{z=0} = 0 \tag{5.51}$$

which is upon rearrangement approximated by

$$S_{0,t+\Delta t}\left(-D_{0,t+\Delta t}\left(C_{1,t+\Delta t} - C_{0,t+\Delta t}\right) + D_{s,0,t+\Delta t}C_{0,t+\Delta t}\right) - D_{s,0,t+\Delta t}C_{0,t+\Delta t}S_{1,t+\Delta t} = 0 \tag{5.52}$$

For a chloride flux into the sample, Eq. (5.51). is converted into

$$-\frac{D}{\rho_w}\frac{\partial C}{\partial z}s_{outside} = -D\frac{\partial C}{\partial z}\frac{S}{C} - D_s\frac{\partial S}{\partial z}\Big|_{z=0} \tag{5.53}$$

which is approximated and rearranged to yield

$$S_{0,t+\Delta t}\left(\frac{D_{0,t+\Delta t}(C_{1,t+\Delta t}-C_{0,t+\Delta t})}{C_{0,t+\Delta t}} - D_{s,0,t+\Delta t}\right) + D_{s,0,t+\Delta t}S_{1,t+\Delta t} = \frac{D_{0,t+\Delta t}s_{outside}}{\rho_w}\left(C_{1,t+\Delta t} - C_{0,t+\Delta t}\right) \tag{5.54}$$

For a chloride flux out of the sample, Eq. (5.15) results in

$$S_{0,t+\Delta t} - S_{1,t+\Delta t} = 0 \tag{5.55}$$

Just like for the water transport, the equations discussed above are written in matrix form and solved using the Gauss elimination method.

5.7 Results

Eqs. (5.2) and (5.10) are solved numerically using the Crank-Nicolson method and implemented in MATLAB with a mesh of 0.2 mm and a time step of 10000 s.

Because the water transport is not influenced by the chloride transport in the present model, in this section, the results of the water transport will be presented first, because it is identical in all the situations, after which the situations where only sweet water can enter the sample, sweet water environment, and the situations where only salt water can enter the sample, salt environment, are treated consecutively for the chloride transport.

5.7.1 Water transport

The water concentration profiles for the first year are shown in Figure 5.6. For a sample length of 0.1 m, the water is almost homogeneously distributed throughout the sample. For a sample of 0.2 m, there is a nonhomogeneous water distribution over the sample after 9 months. This is caused by the fact that after 9 months the sample is dry and that the corresponding diffusion coefficient of water in concrete is small, and the diffusion of water through the sample is not fast enough to create a homogeneous water distribution. For the second and further years, the results are essentially identical to the results of the first year, and are not presented here.

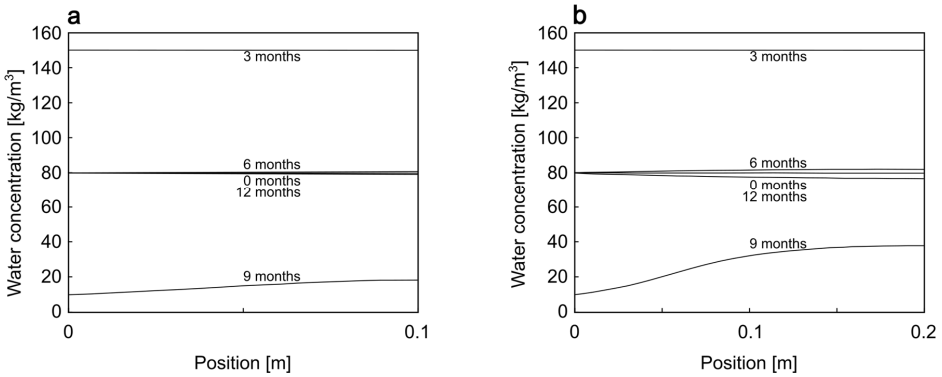

Figure 5.6: Water concentration profiles for a sample length of a) 0.1 m and b) 0.2 m.

5.7.2 Sweet water environment

Figure 5.7 shows the chloride concentration profiles for situation 2 of Figure 5.5, (Sw_{in}, Sw_{out}). Although the sample takes up much sweet water from 0 to 3 months, this does not result in a significant chloride redistribution in the sample of 0.1 m. The (molecular) diffusion of chloride through the wet concrete is, in this case, fast enough to redistribute the chloride to a homogeneous distribution. For the sample of 0.2 m, there is a small redistribution of chloride through the sample after 3 months. After 6 months, and even more after 9 months, the sweet water leaving the sample leaves chloride behind and causes a high surface concentration for both sample lengths. Clearly, the (molecular) diffusion of chloride is, in this case, not fast enough to create a homogeneous distribution of chloride in the sample. From 9 months till 12 months, the sample takes up sweet water again, and this is reflected in the profiles which show that after 12 months the chloride is a little bit flushed away from the surface deeper into the sample. This phenomenon is more clearly visible in the larger sample. For further years, this process repeats itself. The water transport causes the chloride profiles to fluctuate in a cyclic way in the sample. The total chloride amount in a sample does not change.

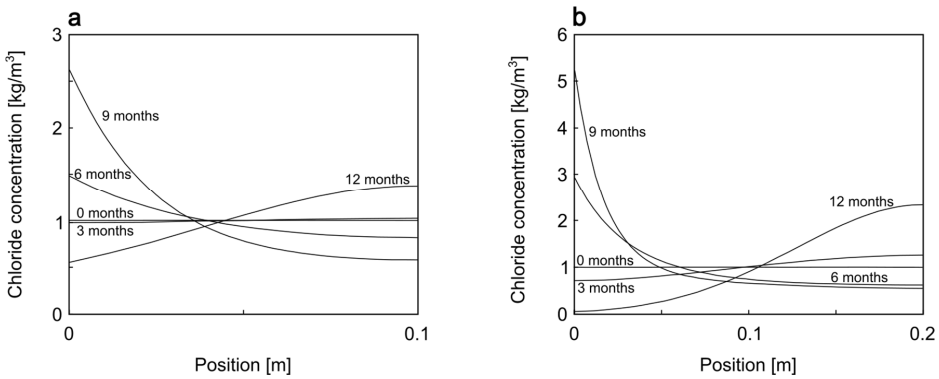

Figure 5.7: Chloride concentration profiles where sweet water enters and sweet water leaves the sample for a sample length of (a) 0.1 m and (b) of 0.2 m.

Chloride concentration profiles for situation 4, (Sw_{in}, Sa_{out}), are shown in Figure 5.8. From 0 to 3 months, only sweet water enters the sample and the result is therefore the same as in Figure 5.6. From 3 months to 9 months, salt water leaves the sample, and because the chloride concentration in the pore water, *s*, is approximately constant for a sample of 0.1 m, the decreasing chloride concentration is proportional with the decreasing water concentration. For a sample of 0.2 m, *s* is not constant, because the graph for 3 months shows no horizontal line, while the water distribution does show a horizontal line. After 12 months, almost all of the chloride has been washed out of the sample. In a sample of 0.1 m, this process is fast and the sample contains only a small amount of chloride after 12 months. In a sample of 0.2 m, this process is slower, and the sample still contains a considerable amount of chloride. For further years, the chloride concentration decreases further.

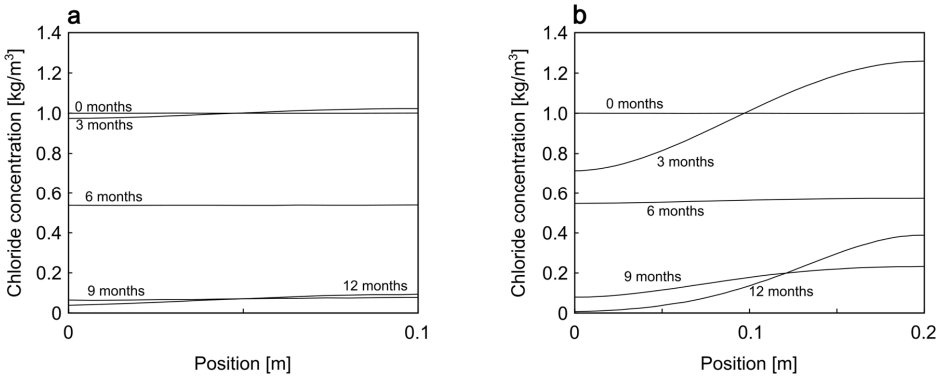

Figure 5.8: Chloride concentration profiles where sweet water enters and salt water leaves the sample for sample lengths of a) 0.1 m and b) 0.2 m.

5.7.3 Salt water environment

For situation 5, (Sa_{in}, Sw_{out}), the chloride profiles in the first year in the sample of 0.l m are shown in Figure 5.9 a) and for the second year in Figure 5.9 b). After 3 months, there is still a homogeneous chloride distribution. This is caused by the homogeneous water distribution in the sample. After 3 months, the sample dries without losing chloride. This causes the rise in the surface chloride concentration in the profiles of 6 and 9 months. After 9 months, the sample takes in again salt water, which results in a higher total amount of chloride after 12 months. This process repeats itself in the second year on a higher chloride concentration level. For further years, the total amount of chloride in the sample increases further, because the incoming water takes chloride into the sample and the outgoing water takes no chloride with it. For the same situation, Figures 5.9c) and 5.9d) show that the differences are larger for a sample of 0.2 m.

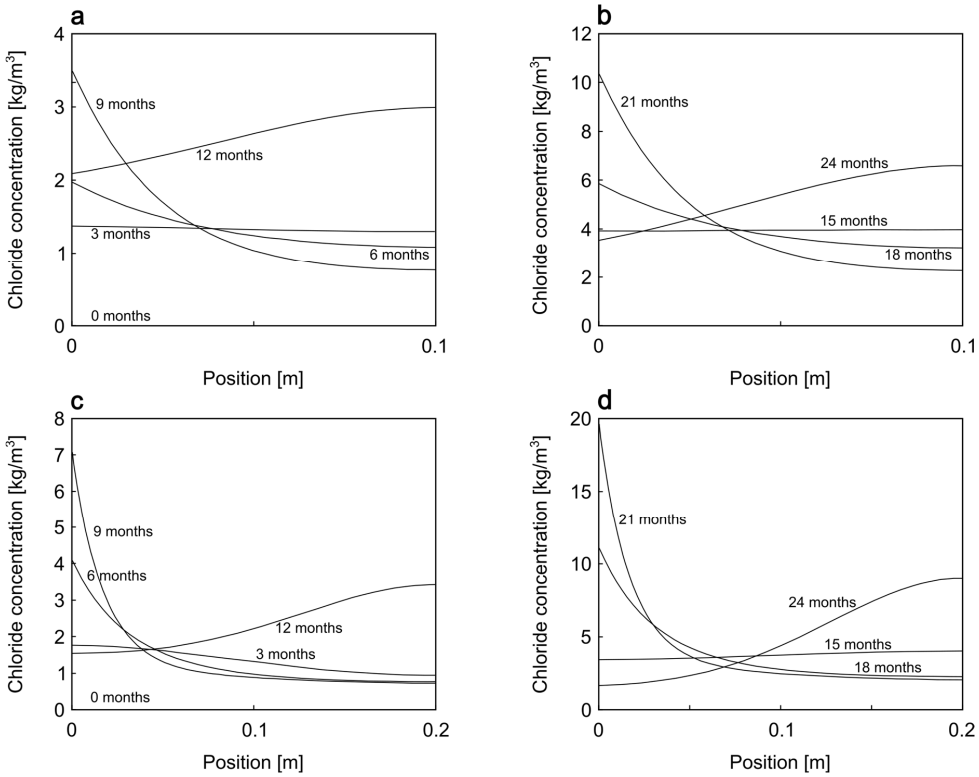

Figure 5.9: Chloride concentration profiles where salt water enters the sample, but only sweet water leaves, for a sample length of 0.1 m (top) and 0.2 m (bottom).

Figure 5.10 shows the chloride profiles for situation 7, (Sa_{in}, Sa_{out}). For a sample of 0.1 m, the chloride concentration varies only slightly throughout the sample. This is caused by the homogeneous water distribution throughout the sample and by the fact that the chloride concentration in the pore water is approximately constant. The profiles for a sample of 0.2 m show larger differences, especially in the first year, because the chloride concentration in the pore water is not a constant yet. For longer times, 18 months and further, the concentration in the pore water has become constant, equal to $s_{outside}$, and the chloride concentration then depends only on the water concentration in the concrete.

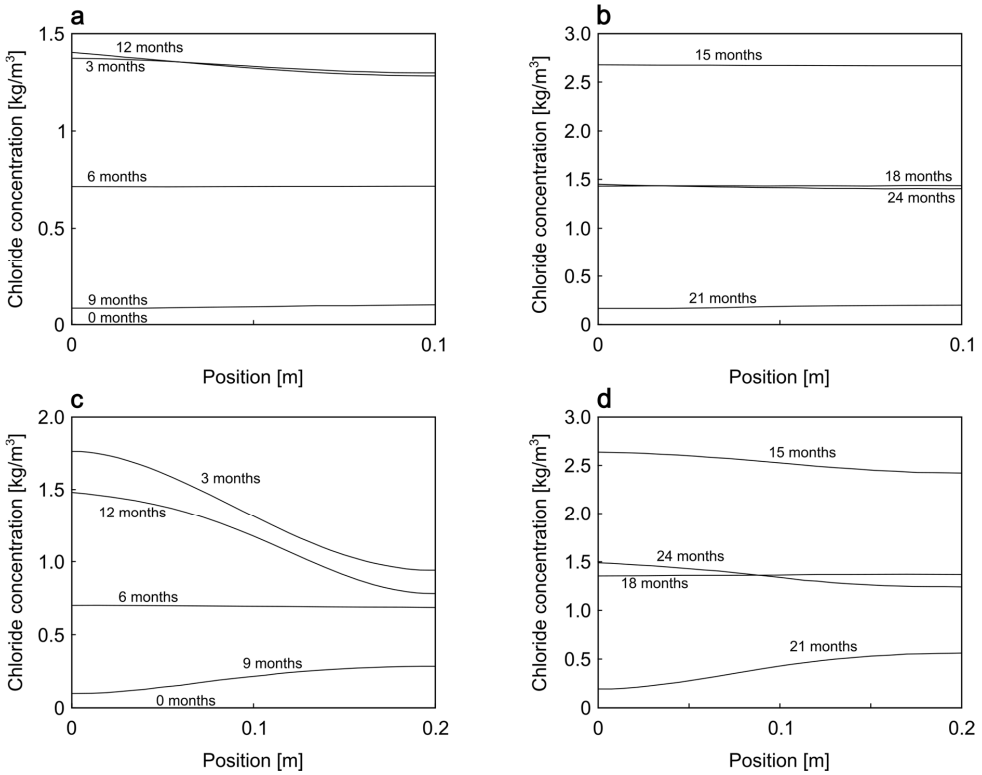

Figure 5.10: Chloride concentration profiles where salt water enters and salt water leaves the sample. Upper graphs are for a sample length of 0.1 m, the lower graphs are for a sample length of 0.2 m.

In the figures above, the chloride concentration in the concrete is shown. The chloride concentration in the pore water, however, is considerably higher, particularly at a low water concentration. Figure 5.11 shows the chloride concentration in the pore water in the situation of salt water going into the sample and sweet water leaving the sample, for a sample of 0.1 m. At 9 months, the surface chloride concentration of the pore water is very high, because the sample is relatively dry and the chloride cannot leave the sample and can only diffuse backward into the sample, for which a large gradient in the chloride concentration of the pore water is needed. The given value of 350 kg m^{-3}, or even higher values, can lead to crystallization of the chloride. The crystallization product will be in such a case a solid near the surface of the sample. This is not incorporated in the present model.

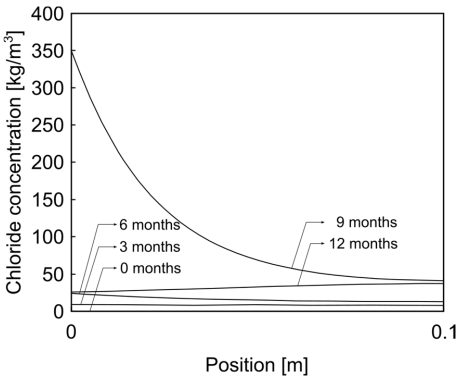

Figure 5.11: Profiles of the chloride concentration in the pore water, where salt water enters and sweet water leaves the sample.

5.7.4 Remarks

Eq. (5.10) with its boundary conditions is a linear set of equations for the chloride transport. Thus, multiplying the solution of one of the situations presented in the Figures. 5.7 to 5.10 gives also a solution of the set of equations.

Figure 5.6 showed that the water distribution throughout the sample is quite homogeneous compared to the distribution of chloride according to most chloride profiles. Thus inequality (5.20) is satisfied in most cases. Exceptions seem to be Figures. 5.8a) and 5.10a) and 5.10b). However, because of the homogeneous water distribution, the chloride concentration in the pore water is homogeneous and therefore the transport of chloride is dominated by the convective chloride flux and the exact value of the diffusive flux is not so relevant then.

5.8 Two water diffusion coefficients approach

The modelling of moisture and chloride is simulated with another approach. In this case, two boundary conditions arise in describing the water transport. The first is a prescribed water content at the exposed surface of the sample. In this model, a wetting/drying cycle is considered. Corresponding to a tidal cycle, the sample gets wet during one half of the day and dries during the other half. During wetting, i.e. during the first half of a cycle, the water saturation at the surface is 1. During drying, the saturation is 0.1. In conclusion, the boundary condition for water transport is

$$U_{x=0} = \begin{cases} 1 & \text{during wetting} \\ 0.1 & \text{during drying} \end{cases} \tag{5.56}$$

with the saturation

$$U = \frac{C}{C_{sat}} \tag{5.57}$$

where C_{sat} is the saturated water content of the studied concrete. It is assumed that the porosity is not dependent on x, therefore C_{sat} is constant. In a later section, the properties of the studied concrete are discussed.

The second boundary condition states that no water transport occurs at the isolated surface of the sample, i.e.,

$$\left.\frac{\partial C}{\partial x}\right|_{x=L} = 0 \tag{5.58}$$

At the start of the process, the water content in the concrete sample is prescribed.
It is assumed that two types of chloride are present in the medium: dissolved free chloride in the pore solution and chloride bound to the surface of the pore walls. Whereas free chloride is available for transport, bound chloride is immobile. Furthermore, equilibrium between free and bound chloride is assumed. Also, a linear relation between the free and bound chloride is assumed. This linear relation is

$$s_b = K_b s_f \tag{5.59}$$

where s_b is the concentration of bound chloride [kg/m^3 concrete], s_f the concentration of free chloride [kg/m^3 pore solution] and K_b an binding constant. The total chloride concentration [kg/m^3 concrete] is written as

$$S_{tot} = s_f \frac{C}{\rho_w} + K_b s_f = s_f \left(\frac{C}{\rho_w} + K_b\right) \tag{5.60}$$

The chloride mass flux consists of an advective and a diffusive component. The advective component arises if the dissolved free chloride is transported through the concrete due to the bulk motion of the water. The advective chloride mass flux is

$$n_{c,advective} = n_{v,w} s_f = -\frac{D}{\rho_w}\frac{\partial C}{\partial x} s_f \tag{5.61}$$

The diffusive component arises due to differences in the chloride concentration of the pore solution. The diffusive chloride mass flux in the pore solution is, proportional to the chloride concentration gradient, written as

$$n_{c,solution} = -D_m \frac{\partial s_f}{\partial x} \tag{5.62}$$

where D_m is the molecular diffusion coefficient of chloride in water, which has a value of 1.26×10^{-9} m^2/s [9]. The diffusive chloride mass flux in the concrete is

$$n_{c,diffusive} = n_{c,solution} \frac{C}{\rho_w \cdot \tau} = -\frac{D_m}{\tau}\frac{\partial s_f}{\partial x}\frac{C}{\rho_w} \tag{5.63}$$

where the tortuosity τ has been added to the expression to incorporate deviations from the ideal situation. With Eqs. (5.61) and (5.63), the total chloride mass flux in concrete can be written as

$$n_c = -\frac{D}{\rho_w}\frac{\partial C}{\partial x} s_f - \frac{D_m}{\tau}\frac{\partial s_f}{\partial x}\frac{C}{\rho_w} \tag{5.64}$$

With the aid of a micro mass balance and Eq. (5.64), the result is a partial differential equation describing the time- evolution of the chloride concentration as

$$\frac{\partial}{\partial t}\left(s_f\left(\frac{C}{\rho_w} + K_b\right)\right) = \frac{\partial}{\partial x}\left(\frac{D}{\rho_w}\frac{\partial C}{\partial x} s_f + \frac{D_m}{\tau}\frac{\partial s_f}{\partial x}\frac{C}{\rho_w}\right) \tag{5.65}$$

The boundary condition for the surface where the sample is isolated against water transport states that the chloride mass flux at $x = L$ is zero. Because the advective chloride flux is zero, the diffusive chloride flux must be zero as well. This leads to the boundary condition

$$\left.\frac{\partial s_f}{\partial x}\right|_{x=L} = 0 \tag{5.66}$$

At the exposed boundary of the sample, salt or fresh water can enter the sample during wetting and salt or fresh water can leave the sample during drying. In this study, the situation in which salt water, for instance seawater, enters the sample will be considered. When the sample dries, water with a certain amount of chloride leaves the sample.

During wetting, it is assumed that the surface of the concrete sample is in contact with external water having a chloride concentration $s_{outside}$. There are two ways for chloride to enter the sample: by advection if external water containing chloride is adsorbed by the sample, and by diffusion, due to a difference in the chloride concentration of the external water and the pore solution at the surface. The boundary condition at x = 0 is

$$n_{v,w}|_{x=0} s_{outside} + D_m\left(s_{outside} - s_f|\right)_{x=0} = n_c|_{x=0} \tag{5.67}$$

which, with Eqs. (5.1) and (5.64), transforms into

$$-\frac{D}{\rho_w}\left.\frac{\partial C}{\partial x}\right|_{x=0} s_{outside} + D_m\left(s_{outside} - s_f\right)\frac{C}{\rho_w} = -\frac{D}{\rho_w}\left.\frac{\partial C}{\partial x}\right|_{x=0} s_f - \frac{D_m}{\tau}\left.\frac{\partial s_f}{\partial x}\right|_{x=0}\frac{C}{\rho_w} \tag{5.68}$$

The value for $s_{outside}$ is chosen to be the value of the chloride concentration in seawater, which is approximately 19 kg/m^3 in the North Sea.

During drying, the chloride concentration of the water leaving the sample equals the chloride concentration of the pore solution at the surface, i.e., s_f. The boundary condition during drying becomes

$$n_c|_{x=0} = n_{v,w}|_{x=0} s_f \tag{5.69}$$

which, with Eqs. (5.1) and (5.64), transforms into

$$-\frac{D}{\rho_w}\left.\frac{\partial C}{\partial x}\right|_{x=0} s_f - \frac{D_m}{\tau}\left.\frac{\partial s_f}{\partial x}\right|_{x=0}\frac{C}{\rho_w} = -\frac{D}{\rho_w}\left.\frac{\partial C}{\partial x}\right|_{x=0} s_f \tag{5.70}$$

and thus the final form of this boundary condition is

$$\left.\frac{\partial s_f}{\partial x}\right|_{x=0} = 0 \tag{5.71}$$

5.8.1 Studied concrete

In order to simulate the water and chloride transport in concrete, a concrete with known diffusion coefficient and chloride binding capacity is needed. Since no such concrete is found in the literature, a combination of properties is used. Zibara [10] studied the chloride binding of various kinds of cement pastes. Samples were exposed to water with a chloride concentration of 0.5 M, which corresponds well to the chloride concentration of the external water used in the present model. The experimental data for cement paste were translated to a concrete with an evaporable water content of 8%. It is therefore

assumed that the concrete in the present study has a saturated water content θ_{sat} of 0.08 m^3/m^3. The binding constant K_b then has a value of 0.19. Li et al. [11] used two experimentally determined diffusion coefficients in their model. These diffusion coefficients will be used in the present model. The diffusivity during wetting is given by the relation

$$D^+ = 10^{-10} \cdot e^{6U} \tag{5.72}$$

The diffusion coefficient during drying is described with

$$D^- = 10^{-10} \cdot \left(0.025 + \frac{0.975}{1 + \left(\frac{1-U}{0.208}\right)^6} \right) \tag{5.73}$$

In absence of a specific value, the tortuosity of the studied concrete is assumed to be 1.0.

5.8.2 Results of the two diffusion coefficients approach

The equations in the previous sections are discretized and numerically solved using MATLAB. In the computations, a sample length of 0.1 m is considered, with an equidistant grid of 0.5 mm.

Figure 5.12 shows the water content profiles after 1, 5 and 10 cycles, where the sample was initially half-saturated, i.e., the water content at $t = 0$ was 0.04 m^3/m^3. Since the diffusivity during drying is much smaller than during wetting, the sample drains only a small amount of water during the drying period. It is therefore seen that water accumulates rapidly, and after 10 cycles, the sample is almost completely saturated in the bulk of the sample.

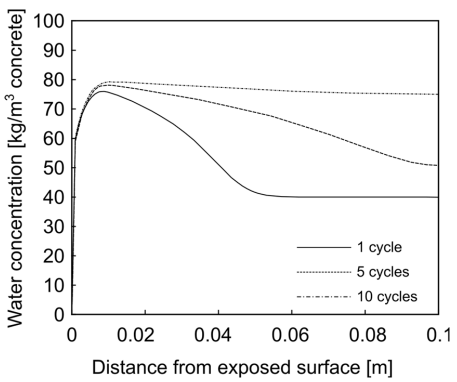

Figure 5.12: Water content profiles after 1, 5 and 10 cycles.

The free chloride concentration of the pore solution, i.e., c_f, after 1, 5 and 10 cycles is illustrated in Figure 5.13. The sample initially contained no chloride. It can be seen that the chloride concentration has the highest value at the surface of the sample. After 10 cycles, chloride is diffused towards the back of the sample. A more constant water content decreases the water transport, and therefore the influence of advection on chloride transport. Diffusion then dominates over advection.

Since the bound chloride concentration is the multiplication of the chloride concentration with the constant K_b, the shape of the bound chloride profiles is equal to the shape presented in Figure 5.13, only the values are different. Therefore, these graphs will not be illustrated in a Figure.

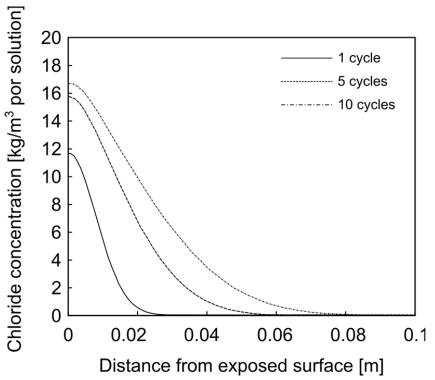

Figure 5.13: Free chloride concentration profiles.

In Figure 5.14, the profiles of the total chloride concentration in concrete, i.e. C_{tot}, are shown after 1, 5 and 10 cycles. These profiles illustrate that the total chloride concentration has the highest value just below the surface. Since the water content at the surface is small at the end of a cycle, the amount of free chloride per m^3 concrete at the surface is small as well. A similar chloride concentration profile for a concrete sample subjected to a wetting/drying cycle is found by Polder and Peelen [19].

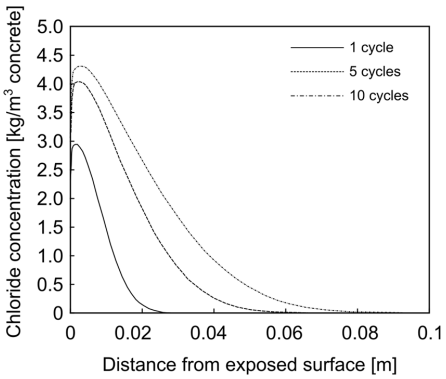

Figure 5.14: Total chloride concentration profiles.

5.9 Conclusions and discussion

A model for the water and chloride transport in concrete is put forward in this study. The water transport is modelled with a diffusion coefficient and the chloride transport is modelled as the sum of a convective term and a diffusive term. The model is applied in the case of yearly wetting/drying cycles with various boundary conditions for the chloride transport. The resulting equations are solved numerically using the Crank-Nicolson method and implemented in MATLAB, which results in water and chloride concentration profiles.

The model recognizes that convective chloride transport is formed by water transport through mainly the largest water filled pores. The smaller water filled pores contribute relatively less. The division of the chloride transport over the pores as a function of the pore radius is a very complex process and has been modelled here with a division over two extremes, i.e. the half of the water filled pore volume with the largest water filled pores is flowing homogeneously with a constant velocity and the half of the water

filled pore volume with the smallest pores is stagnant. These two halves are connected with a diffusion process.

A model is always a simplification of all the physical processes that are operating in a real concrete structure. Processes to be incorporated in a possible extension of the present model can be:

1. Crystallization. In a few situations studied here, the chloride concentration in pore water can exceed the solubility so that the chloride comes out of solution and forms solid particles. These particles can probably hinder the transport of water and chloride. When there is more water present later, the chloride concentration goes down and the solid particles can dissolve again. There is not so much research yet on this topic.
2. The influence of chloride on water transport. Even if there is no crystallization, the presence of chloride can influence the water transport. This is probably a thermodynamic property. It is often said that salt attracts water.
3. Adsorption, desorption, reaction, carbonation. In the present model, there is no interaction between the chloride and the concrete pore walls. However, it is known that chloride can adsorb to the concrete pore surface and can be bound there. Also, desorption has been reported. The phenomenon of carbonation plays an important role here.
4. Heat effects. The application of the model on a situation with a yearly cycle does not need to incorporate heat effects, because the differences in the temperature over the structure will be very small. In a daily wetting/drying cycle however, the effects due to differences in temperature will probably be relatively much more important. In this case, there are larger temperature differences in the structure.
5. Surface boundary conditions. In the present study, the surface boundary conditions were taken as extremes, i.e., water takes no chloride with it, or all the chloride. More research is needed on what is happening outside the concrete structure regarding the transport of water and chloride there. Also, the heat effects play a role here.
6. Dispersion coefficient. The dispersion coefficient has been modelled with a simple process. In the concrete research there is not so much literature on the processes underlying this physical phenomenon. However, it would be interesting to see if other fields of science have theories or experiments that would shed any light on the process. Maybe theories or experiments of the distribution of pollutants in wet soil already give some information.
7. 2D effects. The present model is one dimensional. Many constructions, however, are built in an marine environment. Part of the construction is underneath the water line and part of it is above the water line. It is imaginable that water is absorbed by the concrete structure underneath the water line, is then transported upwards through the structure, and leaves the structure again above the water line. This seems to show the need for a two-dimensional model. (Tidal) waves make such a two-dimensional situation even more complex.
8. In the assumptions on chloride binding, some phenomena are simplified. For instance, a linear binding isotherm is assumed. In the literature [14-16], other types of binding isotherms have been found that correspond well to experimental data. These other types (Langmuir, Freundlich) are considered as a better description of reality by many authors. Furthermore, equilibrium between free and bound chloride is assumed. Since the exposure period of chloride in concrete during a daily wetting/drying cycle is small due to the motion of chloride, it is expected that the application

of a chloride mass transfer rate between free and bound chloride would describe the phenomenon of chloride binding more accurately.

5.10 References

[1] Song H.W., Lee C.H., Ann K.Y., Factors influencing chloride transport in concrete structures exposed to marine environments, Cement and Concrete Composites 30 (2008) 113-121.

[2] Yuan Q., Shi C.G., De Schutter G., Audenaert K., Deng D., Chloride binding of cement-based materials subjected to external chloride environment – A review. Construction and Building Materials 23 (2009) 1-13.

[3] Baessler R., Burkert A., Isecke B., Electrochemical devices for determination of corrosion related values for reinforced concrete structures, in Proceedings of Nace Corrosion, Nashville, USA (2017) 07377.

[4] Kim C.Y., Kim J.K., Numerical analysis of localized steel corrosion in concrete, Construction and Building Materials 22 (2008) 1129-1136.

[5] Fang C., Lundgren K., Chen L., Zhu C., Corrosion influence on bond in reinforced concrete. Cement and Concrete Research 34 (2004) 2159-2167.

[6] Zhang J., Lounis Z., Nonlinear relationships between parameters of simplified diffusion-based model for service life design of concrete structures exposed to chlorides. Cement and Concrete Composites 31 (2009) 591-600.

[7] Ann K.Y., Ahn J.H., Ryou J.S., The importance of chloride content at the concrete surface in assessing the time to corrosion of steel in concrete structures, Construction and Building Materials 23 (2009) 239-245.

[8] Win P.P., Watanabe M., Machida A., Penetration profile of chloride ion in cracked reinforced concrete. Cement and Concrete Research 4 (2004) 1073-1079.

[9] Vidal T., Castel A., Francois R., Analyzing crack width to predict corrosion in reinforced concrete. Cement and Concrete Research 34 (2004) 165-174.

[10] Song H.W., Shim H.B., Petcherdchoo A., Park S.K., Service life prediction of repaired concrete structures under chloride environment using finite difference method, Cement and Concrete Composites 31 (2009) 120-127.

[11] Montemor M.F., Alves J.H., Simoes A.M., Fernandes J.C.S., Lourenco Z., Costa A.J.S., Appleton A.J., Ferreira M.G.S., Multiprobe chloride sensor for in situ monitoring of reinforced concrete structures, Cement and Concrete Composites 28 (2006) 233-236.

[12] Pel L., Huinink H., Kopinga K., Salt transport and crystallization in porous building materials, Magnetic Resonance Imaging 21 (2003) 317-320.

[13] Climent M.A., de Vera G., Lopez J.F., Viqueira E., Andrade C., A test method for measuring chloride diffusion coefficients through nonsaturated concrete Part I. The instantaneous plane source diffusion case, Cement and Concrete Research 32 (2002) 1113-1123.

[14] Azari M.M., Mangat E.S., Tu S.C., Chloride ingress in microsilica concrete. Cement and Concrete Composites 15 (1993) 215-221.

[15] Hong K., Hooton R.D., Effects of fresh water exposure on chloride contaminated concrete, Cement and Concrete Research 30 (2000) 1199-1207.

[16] Marsavina L., Audenaert K., De Schutter G., Faur N., Marsavina D., Experimental and numerical determination of the chloride penetration in cracked concrete, Construction and Building Materials 23 (2009) 264-274.

[17] Djerbi A., Bonnet S., Khelidj A., Baroghel-Bouny V., Influence of traversing crack on chloride diffusion into concrete, Cement and Concrete Research 38 (2008) 877-883.
[18] Cerny R., Pavlik Z., Rovnanikova P., Experimental analysis of coupled water and chloride transport in cement mortar, Cement and Concrete Composites 26 (2004) 705-715.
[19] Polder R.B., Peelen W.H.A., Characterisation of chloride transport and reinforcement corrosion in concrete under cyclic wetting and drying by electrical resistivity, Cement and Concrete Composites 24 (2004) 427-435.
[20] Huinink H.P., Pel L., Michels M.A.J., How ions distribute in a drying porous medium: a simple model. Physics of Fluids 14 (2002) 1389-1395.
[21] Oh B.H., Jang S.Y., Effects of material and environmental parameters on chloride penetration profiles in concrete structures, Cement and Concrete Research 37 (2007) 47-53.
[22] Marchand J., Modelling the behaviour of unsaturated cement systems exposed to aggressive chemical environments. Materials and Structures 34 (2001) 195-200.
[23] Shin C.B., Kim E.K., Modelling of chloride ion ingress in coastal concrete, Cement and Concrete Research 32 (2002) 757-762.
[24] Johannesson B.F., A theoretical model describing diffusion of a mixture of different types of ions in pore solution of concrete coupled to moisture transport, Cement and Concrete Research 33 (2003) 481-488.
[25] Conciatori D., Sadouki H., Brühwiler E., Capillary suction and diffusion model for chloride ingress into concrete, Cement and Concrete Research 38 (2008) 1401-1408.
[26] Meijers S.J.H., Bijen J.M.J.M., de Borst R., Fraaij A.L.A., Computational results of a model for chloride ingress in concrete including convection, drying-wetting cycles and carbonation. Materials and Structures 38 (2005) 145-154.
[27] Wang Y, Li L.Y., Page C.L., Modelling of chloride ingress into concrete from a saline environment, Building and Environment 40 (2005) 1573-1582.
[28] O'Neill Iqbal P., Ishida T., Modelling of chloride transport coupled with enhanced moisture conductivity in concrete exposed to marine environment, Cement and Concrete Research 39 (2009) 329-339.
[29] Stanish K., Hooton R.D., Thomas M.D.A., A novel method for describing chloride ion transport due to an electrical gradient in concrete: Part 1. Theoretical description, Cement and Concrete Research 34 (2004) 43-49.
[30] Stanish K., Hooton R.D., Thomas M.D.A., A novel method for describing chloride ion transport due to an electrical gradient in concrete: Part 2. Experimental study, Cement and Concrete Research 34 (2004) 51-57.
[31] Van der Zanden A.J.J., Coumans W.J., Kerkhof P.J.A.M., Schoenmakers A.M.E., Isothermal moisture transport in partially saturated porous media, Drying Technology 14 (1996) 1525-1542.
[32] Van der Zanden A.J.J., A possible revision of the results of a model for moisture transport in partially saturated porous media, Drying Technology 13 (1995) 2227-2231.
[33] Pel L., Moisture transport in porous building materials, PhD Thesis, Eindhoven University of Technology, The Netherlands (1995).
[34] Van der Zanden A.J.J., Heat and mass transfer in heterogeneous media where a phase transition takes place, Chemical Engineering Science 55 (2000) 6235-6241.
[35] Treybal R.E., Mass Transfer Operations, McGraw - Hill Book Company, Malaysia (1980).

6

6. Experimental study on moisture and chloride transport

This chapter has been published as:

Taher, A. van der Zanden, A.J.J. & Brouwers, H.J.H. Chloride transport in mortar at low moisture concentration. *Chemistry and Materials Research* 5 (2013) 53-56.

6.1 Introduction

Wetting/drying cycles shorten the lifetime of concrete structures [1-7], and it is, therefore, essential to understand this process. During these cycles, there is always an interaction between the moisture transport and the chloride (Figure 6.1). Many authors [8-14] investigated the durability of marine structures by means of chloride penetrating into concrete. All these cases deal with a combined transport of moisture and chloride. Nevertheless, the data considering the influence of chloride on moisture transport is lacking in the literature.

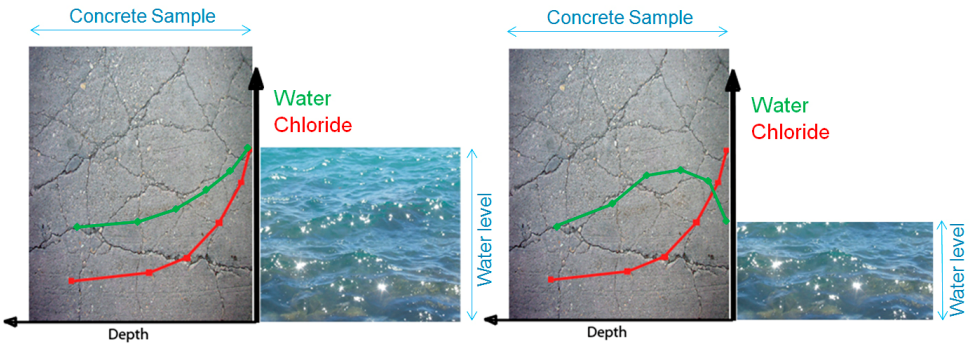

Figure 6.1: Wetting/drying cycles.

The purpose of the present study is to investigate the influence of chloride on the moisture transport in concrete for low moisture concentrations. To achieve this, an experimental set-up is designed to measure the moisture transport in thin specimens. Because concrete contains gravel, the use of concrete as a thin specimen is difficult. By using mortar specimens in the experiment, thin specimens are obtained more easily and the results will apply also to concrete. The experiment is carried out by comparing the moisture transport through mortar specimens with and without chloride. A material with a higher porosity, sand-lime, is also examined in this study. Moisture transport in sand-lime is faster, and, therefore, reliable results can be obtained faster.

6.2 Experiment

An experiment is designed to create a moisture flux through specimens with or without chloride. The moisture flux through the specimens is obtained by creating a low and a high relative humidity, as it is shown in Figure 6.2. This leads to an upward moisture flux.

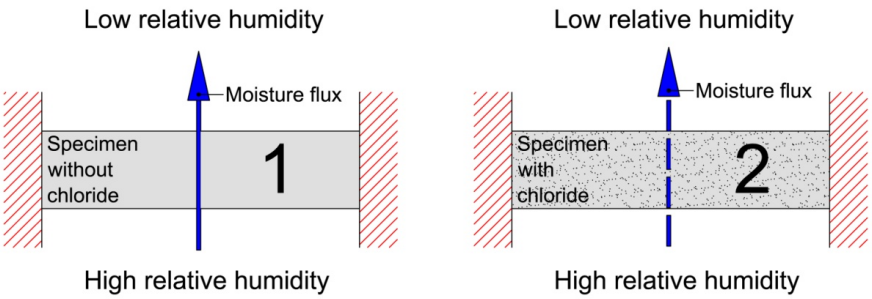

Figure 6.2: A moisture flux is created by applying a high relative humidity below the specimen and a low relative humidity above the specimen. Specimens containing chloride are compared with specimens without chloride.

The desired relative humidity is obtained by using oversaturated salt solutions. By using magnesium nitrate, an equilibrium relative humidity of 54% at 20 ºC is obtained [15]. By using sodium chloride, an equilibrium relative humidity of 75% at 20 ºC is obtained [15]. The specimens are cylinders with a diameter of 100 mm and thickness of 10 mm. The side of the specimens is sealed to ensure a one dimensional flux. As shown in Figure 6.3, the specimens are fixed in a glass container with the oversaturated sodium chloride solution. The glass container is placed in a large container with the oversaturated magnesium nitrate solution. The attachment of the sample on the glass container is shown in detail in Figure 6.4.

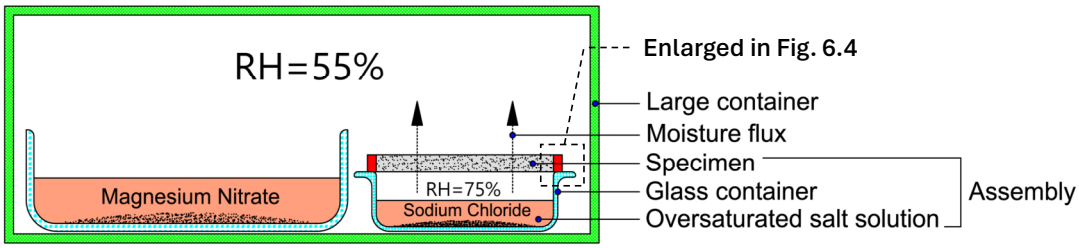

Figure 6.3: Schematic view of the experiment.

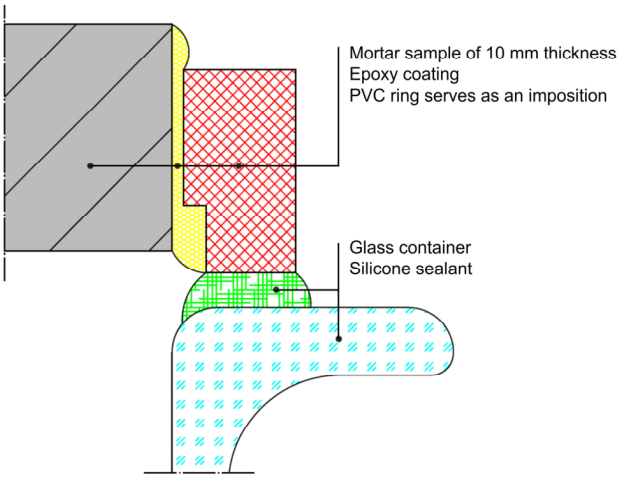

Figure 6.4: Placing the sample on the glass container.

Due to the moisture flux, the mass of the assembly (specimen, glass container and oversaturated salt solution) decreases during the experiment. The assemblies are weighed at least once a month to determine the mass. In the beginning, the mass of the assemblies decreases quickly because of evaporation of the water from the saturated specimen. Approximately after 1 d, the specimen is in a steady state between its surrounding relative humidity.

6.3 Specimen preparation

In this experiment, two porous materials are examined: cement-based mortar specimens and sand-lime specimens. The specimens have the same composition and properties as shown in Table 4.2 in Chapter 4. These specimens are immersed into various chloride solutions to obtain specimens with various chloride concentrations.

6.3.1 Mortar preparation

Mortar is cast in PVC tubes with a diameter of 100 mm. The mortar is cured for 28 days. Specimens of 10 mm thickness are cut from the mortar cylinder, and provided with a chloride mass percentage 2.0%. These chloride concentrations [16], S_t ($kg_{Cl}/100\ kg_{solid}$ or %), are calculated as

$$S_t = \frac{\phi \cdot s_f + s_B \cdot (100 - \phi) \cdot \rho_s}{\rho_m} \tag{6.1}$$

where ϕ ($m^3_{solution}/100\ m^3_{mortar}$) is the porosity, s_f ($kg_{Cl}/m^3_{solution}$) the concentration of free chlorides, s_B (kg_{Cl}/kg_{solid}) the concentration of bound chlorides, ρ_s (kg_{solid}/m^3_{solid}) the specific density and ρ_m (kg_{solid}/m^3_{mortar}) the apparent density, where the subscript mortar includes the solid and the pore solution.

It is assumed that s_B is a function of s_f [5] given by

$$s_B = K \cdot {s_f}^b \tag{6.2}$$

where K (m^{3b}/kg^b) is the chloride binding capacity and b (-) the chloride binding intensity parameter.

Due to the negative effect of calcium chloride solutions, which increases the volumetric shrinkage of concrete by 10-50% [17] mainly because of the higher degree of hydration, and changes in hydration products [18], sodium chloride solutions are used to provide the specimens with chloride.

In order to obtain 2.0% chloride content on the mass of mortar specimen, s_f is calculated from Eqs. (6.1) and (6.2) for $K = 0.53\times10^{-3}\ m^{3b}/kg^b$ [19], $b = 0.52$ [19], $\phi = 17\ m^3_{solution}/100\ m^3_{mortar}$, $\rho_s = 2062\ kg_{solid}/m^3_{solid}$ and $\rho_m = 2412\ kg_{solid}/m^3_{mortar}$, so that $s_f = 144\ kg_{Cl}/m^3_{solution}$.

Due to the use of the sodium chloride solution, the values of the concentration of free chlorides s_f are recalculated. To obtain 2.0% chloride by mass of mortar, sodium chloride solution of 237 kg/m^3 is used.

After penetrating chloride into the mortar by using vacuum saturation, the chloride concentration profiles of mortar specimens are measured in five positions in the specimens by Metrohm MET 702 automatic titration [20].

The chloride concentration is calculated as:

$$S_t = \frac{V_{AgNO_3} \cdot N_{AgNO_3} \cdot M_{Cl}}{m_s} \cdot 100 \tag{6.3}$$

where S_t ($kg_{Cl}/100kg_{solid}$) is the chloride concentration, V_{AgNO_3} ($m^3_{AgNO_3}$) the volume of the titrated silver nitrate solution, N_{AgNO_3} ($mol_{AgNO_3}/m^3_{AgNO_3}$) the molarity of silver nitrate solution, M_{CL} (kg_{Cl}/mol_{Cl}) the molar mass of chloride and m_s (kg_{solid}) the mass of the sample.

With Eq. (6.3), the chloride concentration is determined as a function of the position for mortar, as it is shown in Figure 6.5.

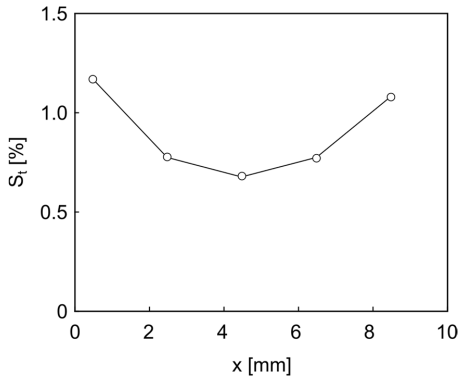

Figure 6.5: Chloride concentration profile in mortar.

The measured chloride profiles are clearly different through the sample. However, the concentration of chloride is lower than expected, especially in the middle of the specimen. The high chloride concentration profile in the surface layer occurs due to the use of a specimen that was not completely dry in the beginning of the experiment (as explained in Chapter 4). However, the drying procedure requires much attention because drying causes micro cracks in the specimen, which must be avoided in this experiment. Furthermore, the increased porosity at the surface of the specimen, which is generated by cutting in layers of 10 mm, could also cause this effect. Another possible reason for the high chloride concentration in the surface layer is that part of the free-chloride entering the specimen can be bound in the external layers, and, therefore, the chloride concentration in the solution entering the deeper layers is automatically decreased.

Another method for obtaining the needed chloride concentration in the sample is by adding chloride directly into the fresh mortar. This is executed by pouring a known amount of $CaCl_2$ into fresh mortar, calculating the right dosage of this salt based on the mass of chloride. The hardening in this case is accelerated by placing the mortar in oven (40ºC and 100% RH) for 10 days.

Table 6.1: Chloride concentrations.

Added	**Measured**	**Measured**
Cl [mass % of mortar]	Total Cl [%]	Free Cl [%]
0	0.000	0.000
0.25	0.295	0.201
0.5	0.541	0.456
0.75	0.831	0.773
1	1.019	0.919
1.5	1.464	1.341

Hereafter the total chloride concentration is measured by titration (Table 2.1 in Chapter 2). Also, the free chloride concentration is measured by adding 2g of dry mortar powder into 35 ml water for 24 h, then filtering and titration (Figure 6.6).

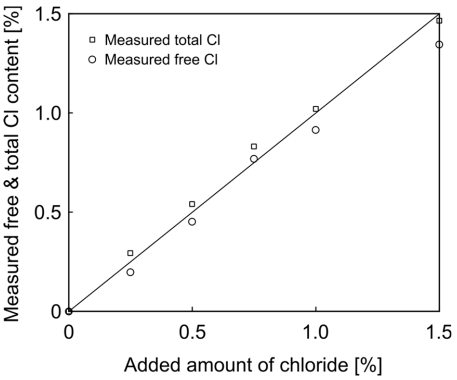

Figure 6.6: Measured chloride concentration.

The results show that the added amount of chloride to the fresh mortar is similar to the measured concentrations. Therefore, this method can also be used for penetrating chloride into mortar. Furthermore, by subtracting the measured total chloride from the free chloride, the bound chloride can be calculated. The average bound chloride in this experiment is 0.1% of the mass of mortar.

6.3.2 Sand-lime preparation

Cylindrical cores with a diameter of 100 mm are drilled from blocks sand-lime, and specimens of 10 mm thickness are cut from the cores. The same method is used for penetrating chloride into the sand-lime specimen. Sand-lime specimens are also exposed to the 2.0% chloride solution concentration, which means that the specimens are saturated in the 237 kg/m^3 sodium chloride solution. It is expected that in these specimens the chloride concentration is higher than in the mortar specimens due to the higher porosity (Table 4.2 in Chapter 4). The chloride concentration in the sand-lime specimen is, as a function of the position, shown in Figure 6.7.

The high chloride concentration in the surface layer occurs due to the same reasons as in the mortar specimens.

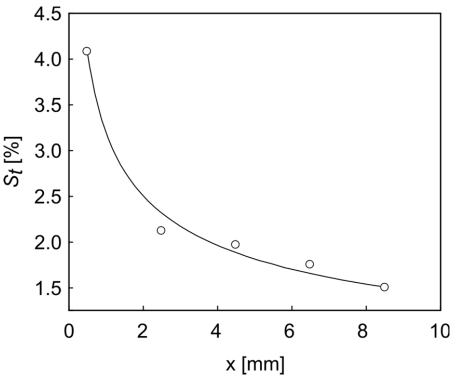

Figure 6.7: Chloride concentration in the sand-lime.

6.4 Results

The accuracy of the relative humidity created by oversaturated salt solutions, is of major importance because of their large influence on the moisture flux. Therefore, the equilibrium relative humidities are

measured before starting the experiment. An escort logger EJ-HS-B-8 is used to measure the relative humidity in the glass container (Figure 6.8) and the large container.

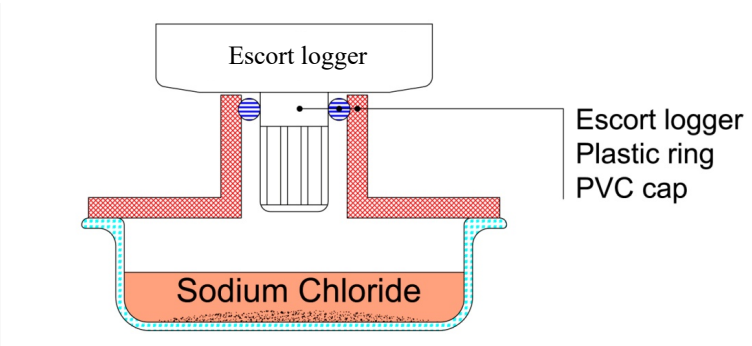

Figure 6.8: Measurement of relative humidity in the glass container.

The measurement in the glass containers is performed for 3 days and shown in Figure 6.9. The same measurements are performed for the large container. The duration in this case is 27 days. Figure 6.10 indicates these measurements. Furthermore, the influence of opening the door of the large container is investigated as well. From these measurements, it can be concluded that the equilibrium state inside the container is reached after 2.5 h, as shown in Figure 6.11.

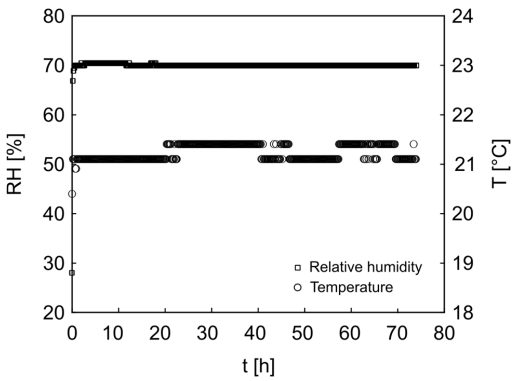

Figure 6.9: Relative humidity and temperature measurements in the glass container.

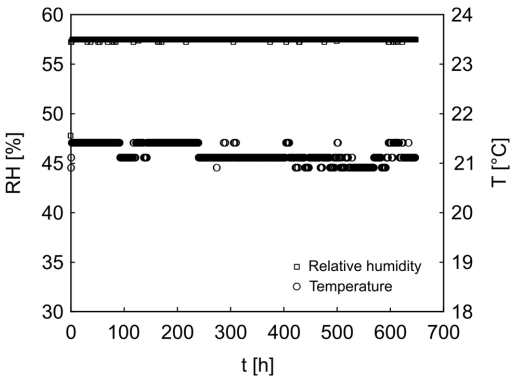

Figure 6.10: Relative humidity and temperature measurements in the large container.

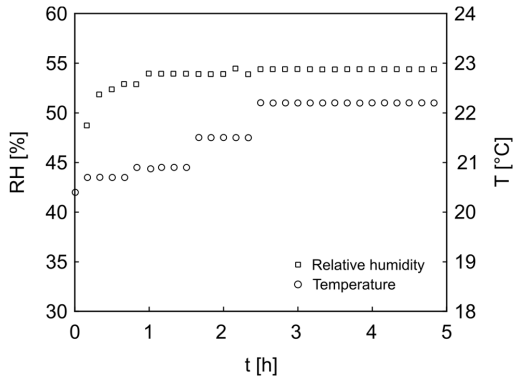

Figure 6.11: Equilibrium relative humidity and constant temperature inside the large container reached after 2.5 h.

6.4.1 Results of mortar specimens

The glass containers with specimens are weighed three times in the first month, twice in the second month, and once a month after that. Figure 6.12 shows the mass loss (M_l) of the assembly with mortar specimens with various chloride concentrations.

Figure 6.12 also shows that the results of the mortar specimen with and without chloride are substantially similar. This indicate that the chloride concentration of 2.0% in the specimen has only a limited influence on the moisture transport in mortar.

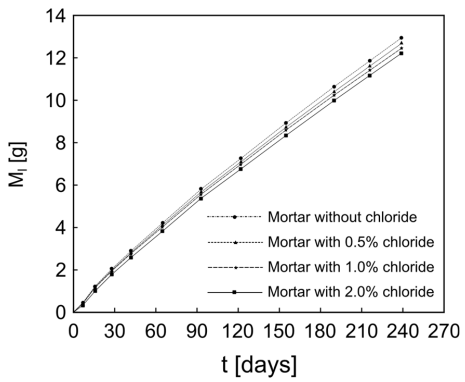

Figure 6.12: Mass loss M_l on mortar disk with various amount of chloride.

Furthermore, the chloride profiles in the mortar specimens are measured by titration before the start of the experiment, as shown in Figure 6.5. The chloride profile for two specimens after a moisture flux of 10 months through the specimen is also measured, as shown in Figure 6.13. The moisture flux during these 10 months is measured by the mass of the assembly. This mass decreases during the experiment. The moisture flow, which is the time derivative of the decreased mass, is calculated and is approximately 0.05 g/d.

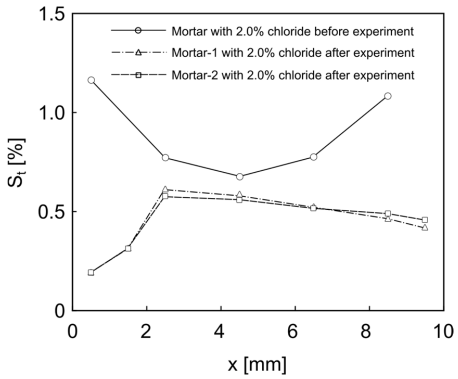

Figure 6.13: Chloride concentration profiles before and after the experiment.

Figure 6.13 shows two interesting behaviours after 10 months. Firstly, it shows that the average chloride concentration in the specimen has decreased. Secondly, the chloride concentration at the surface is also decreased. It is unclear how the chloride content decreased in the specimen. Due to the uncertainty of this result, the chloride concentrations after 10 months are measured with methods other than titration. Ion chromatography is one of other techniques that are used to measure the chloride concentrations in the specimen. This technique is similar to titration due to the measuring the chloride ions in a liquid. With this technique, the first layers from the surface are measured, as it is shown in Figure 6.14.

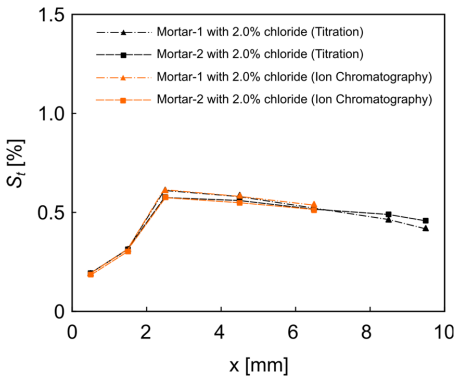

Figure 6.14: Measurement of chloride concentration profiles with titration and Ion chromatography.

The measurements with both techniques, titration and ion chromatography, are similar. From this result, it is clear that the amount of the free chloride in the solution is measured. But to measure the total chloride, the bound chloride must also be taken into account. It is assumed in the measurement with these two techniques that all the bound chloride is unbound by using nitric acid. To examine this, the powders of the ground layers are measured again by XRF. XRF is a technique which can be used to determine chloride content. However, a calibration is needed to obtain reliable results. First measurement in powder form of the layer close to the surface is carried out to compare the three techniques (Titration, Ion chromatography and XRF), as it is shown in Figure 6.15.

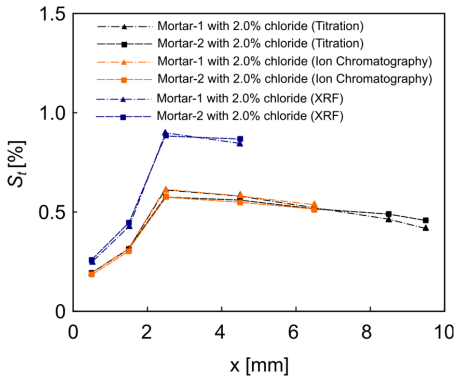

Figure 6.15: Comparison of different techniques to measure chloride concentration profiles.

The measurement of chloride concentration in the specimen with XRF shows a higher chloride concentration by approximately 30%, but with the same trend as the previous two techniques. The accuracy of this technique is however questionable as mentioned earlier. To obtain more reliable results, a calibration method is designed. Layer of mortar specimens without chloride is ground with the Profile Grinder 110. By adding a known amount of sodium chloride to the powder, the exact amount of chloride is then known (Table 6.2). By measuring the chloride concentration of the mixed powder, the calibration of XRF can be obtained.

Table 6.2: Samples with various amount of sodium chloride.

Sample	Cl%
1	0
2	0.25
3	0.5
4	0.75
5	1
6	1.5
7	2

Figure 6.16 shows the results of the measuring the chloride concentrations in the 7 samples with XRF.

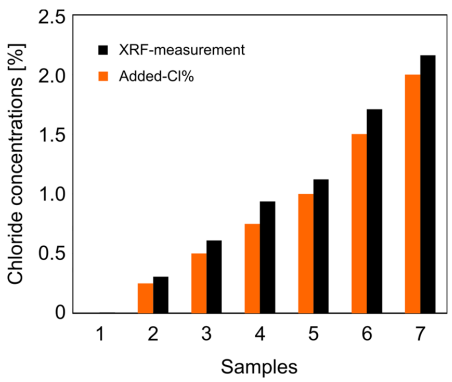

Figure 6.16: XRF measurements.

The calibration is done by fitting the results in one graph as shown in Figure 6.17. With the calibration of XRF, there is still a large difference between the chloride concentrations at the start of the experiment

and at the end of the experiment. Therefore, another test is devolved to examine the evaporation of chloride (Figure 6.18).

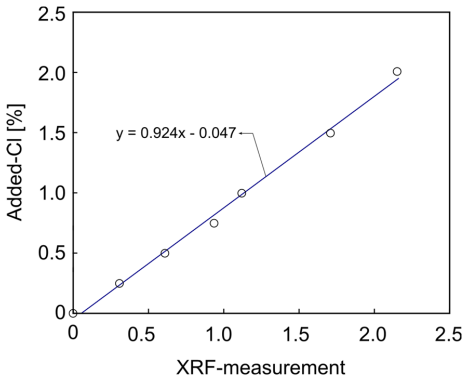

Figure 6.17: Calibration of XRF.

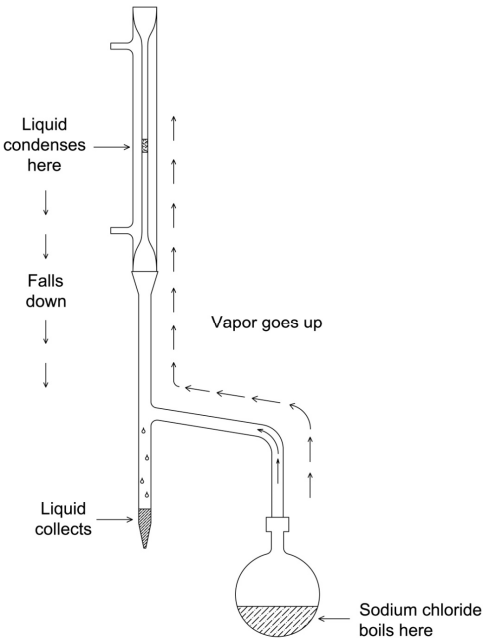

Figure 6.18: Testing evaporation of chloride.

Sodium chloride solution is prepared and boiled. The created vapor cools down in a condenser. The resulting liquid is collected and used for titration to measure the chloride concentration. The obtained result gives 0% chloride concentration, which means that chloride does not evaporate.

More research is needed to explain the decreased chloride concentration. Therefore, a new experiment is designed to examine the decrease of the chloride concentration towards the end of the experiment. In this experiment, mortar samples with initial chloride are tested in four different exposure conditions during 7 months. The applied exposure conditions are: sealed, fresh water, low relative humidity and

CO_2. The sealed exposure condition is obtained by sealing the mortar sample completely. The fresh water exposure condition is obtained by placing the sample in water. The low relative humidity exposure condition is obtained by placing the samples in a desiccator and by blowing dry air with a relative humidity of 7% and flow rate of 5 l/min through it. The CO_2 exposure condition is obtained also by placing the samples in a desiccator and by blowing CO_2 with flow rate of 0.5 l/min, and by placing a small fan in the desiccators to create a stable environment (Figure 6.19).

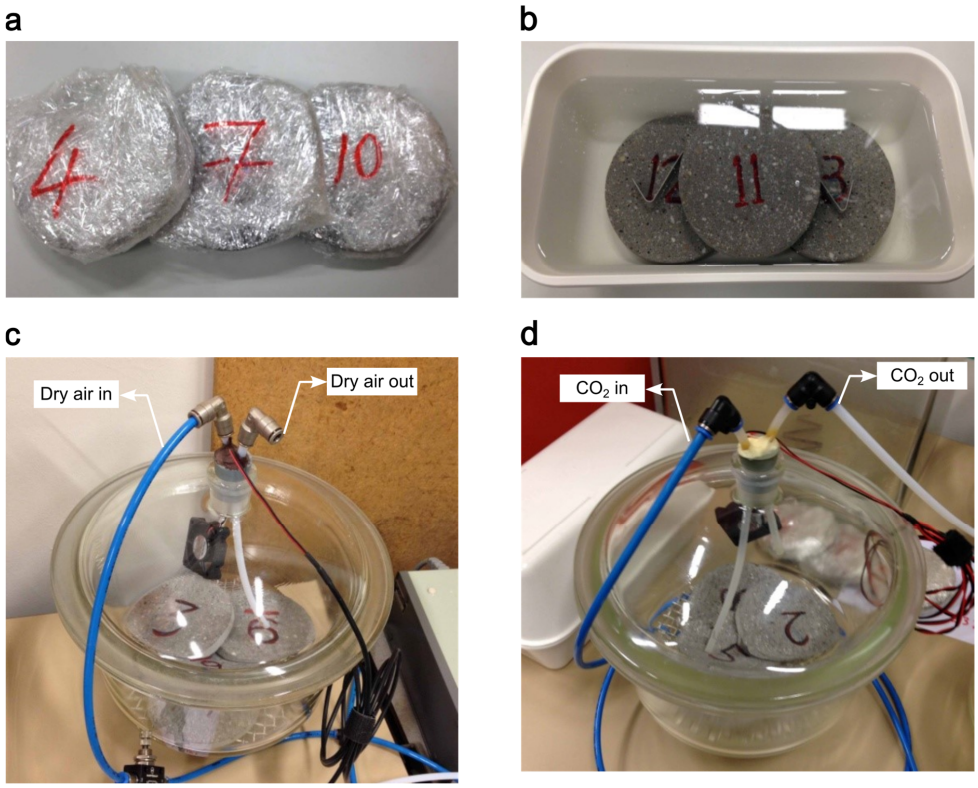

Figure 6.19: Experiment set-up. (a) The sealed mortar samples of the sealed exposure condition. (b) Fresh water exposure condition. (c) Low relative humidity exposure condition. (d) CO2 exposure condition.

The chloride concentrations profiles in the sample that are exposed to various conditions are measured by titration and shown in the Figures 6.20, 6.21 and 6.22.

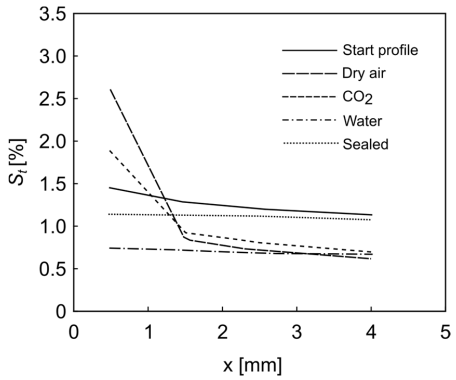

Figure 6.20: Chloride concentration profile after 1 month.

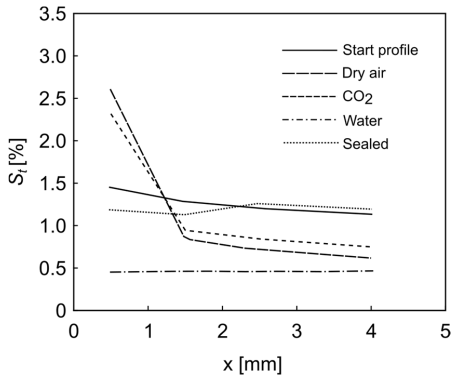

Figure 6.21: Chloride concentration profile after 3 months.

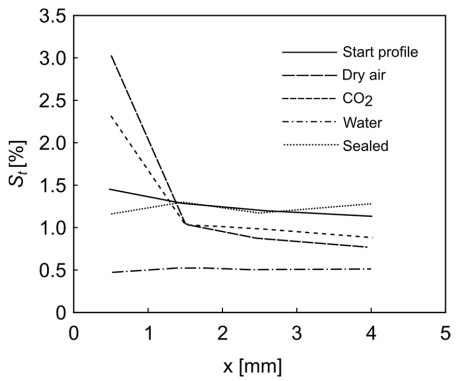

Figure 6.22: Chloride concentration profile after 7 months.

The new experiment shows no decrease of chloride during the exposure period. The initial chloride content is remaining stable. The experiment shows that the chloride is transported towards the surface of the sample. The sample stored in water shows a reduction of the initial chloride concentration, but that is expected due to the transport of chloride through the pores filled with water out the sample (diffusion from high concentration to low concentration regions). The chloride profile in the sealed sample is similar to the start sample, which means there was no chloride transport inside the sample

during 7 months. In the sample with dry air, the highest chloride concentration at the surface is measured. That can be explained by water transport, which moves towards the surface carrying chloride along. The same effect can be observed on the sample with CO_2.

6.4.2 Results of sand-lime specimens

The glass containers with sand-lime specimens are weighed in the same way as mortar specimens. Figure 6.23 shows the mass loss of three specimens of 0.0% sand-lime and two specimens of 2.0% sand-lime. Figure 6.23 indicates that the mass loss of the specimens with 2.0% of chloride is much lower than the mass loss of the specimens with 0.0% of chloride. This implies that the moisture flux in the specimens with a 2.0% of chloride concentration is much smaller than in the specimens without chloride.

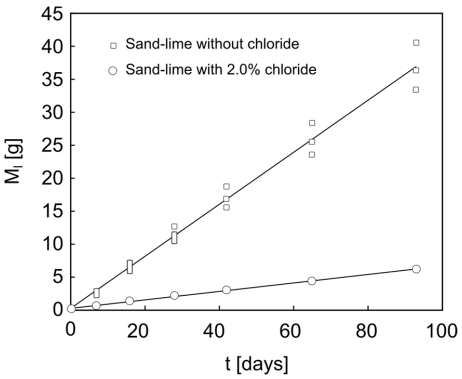

Figure 6.23: Mass loss M_l of the assembly with sand-lime specimens.

To indicate better the difference in flux between specimens with chloride and specimens without chloride, the mass flow (M_f) is compared, as is shown in Figure 6.24. Mass flow is the time derivative of the average results of mass loss. The mass flow of the specimens with chloride is approximately 0.05 $\times 10^{-3}$ kg/d. On the other hand, the mass flow of the reference specimens is approximately 0.4 $\times 10^{-3}$ kg/d. The 237 kg/m^3 of the solution sodium chloride, which is applied to the specimens at the start of the experiment, decreases the moisture flow by a factor of 75%. The chloride present in the specimens moves, because of the moisture transport, to the surface. At the surface of the specimen, the chloride becomes crystallized, forming a layer that blocks the pore. This leads to a smaller transport of moisture.

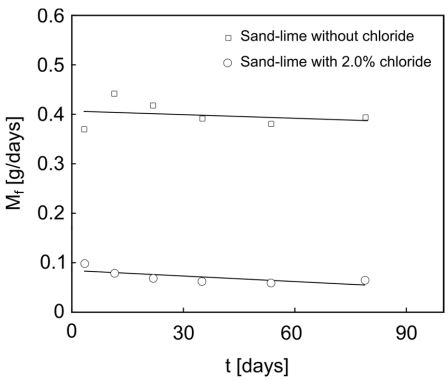

Figure 6.24: Mass flow of the assembly with sand-lime specimens.

The diffusion coefficient of water in sand-lime for samples without chloride is calculated with Fick's first law of diffusion as

$$n_m = -D \cdot \frac{\partial C_m}{\partial x} \tag{6.4}$$

where n_m is the moisture flux [kg/s·m^2], D the diffusion coefficient [m^2/s], C_m the moisture concentration [kg/m^3], and x the position coordinate [m]. Eq. (6.4) is written as,

$$n_m = -D \cdot \frac{\partial C_m}{\partial RH} \cdot \frac{dRH}{dx} \tag{6.5}$$

where RH is the relative humidity [%].

For the determination of the moisture concentration in the specimens, it is assumed that the relative humidity at the surface is equal to the surroundings, which means at the top of the specimen the relative humidity is 55% and at the bottom 70%, as it is shown in Figure 6.3. The sorption isotherm of sand-lime (Figure 6.25) [21] is used to determine the $\partial C_m/\partial RH$. Because in the experiment a saturated specimen is used in the drying phase, the desorption curve is used to calculate $\partial C_m/\partial RH$.

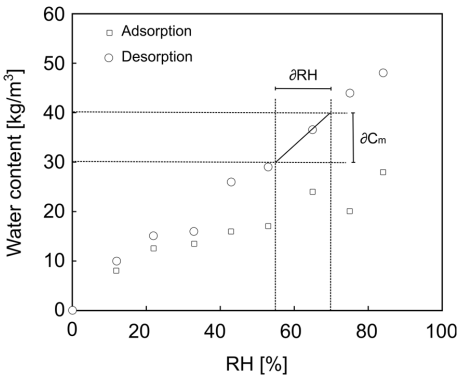

Figure 6.25: Sorption isotherm of sand-lime brick [21].

Figure 6.25 shows that the slope of the sorption isotherm, $\partial C_m/\partial RH$, for sand-lime bricks is equal to 0.667 kg/m^3. The diffusion coefficient is calculated with Equation 6.5 for the specimen with a thickness of 0.01 m, and it is approximately 5.9×10^{-10} m^2/s. In the literature [21], a diffusion coefficient of water in sand-lime of 7.9×10^{-11} m^2/s can be found.

More results are obtained by comparing 2.0% chloride specimen before and after the experiment. Figure 6.26 shows the two chloride profiles. The two specimens went through the same procedure of penetrating chloride, as explained in the section specimen preparation. The chloride profile of the 2.0% sand-lime specimen (after the experiment) is measured after 93 days.

Figure 6.26 shows that the concentration of chloride inside the specimen is reduced while the concentration at the top of the specimen is increased. This indicates that chloride has been transported with the moisture to the top of the specimen.

The chloride profiles before the experiment are measured soon after performing the vacuum saturation. However, the experiment is started after reaching the steady-state conditions in the specimen, which

could mean that the chloride profiles before the experiment are slightly changed. Furthermore, it is not clear whether the chloride profiles have reached a steady state during the experiment.

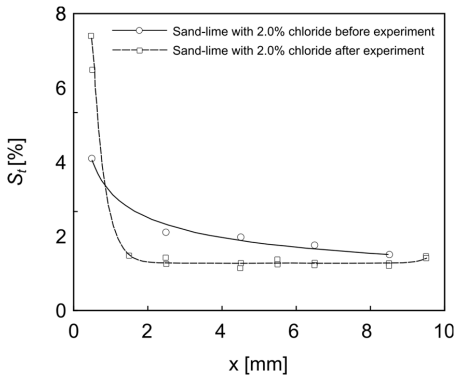

Figure 6.26: Chloride concentrations of sand-lime specimens with the moisture flux to the left.

6.5 Conclusions

The presented experiments are performed to investigate the influence of chloride on moisture transport in mortar and sand-lime. This is carried out by comparing moisture transport through specimens with chloride with specimens without chloride. The results of this study show that chloride, with a concentration of 2.0%, has a large influence on moisture transport in sand-lime specimens, but a limited influence on the moisture transport in mortar specimens. It appears that the precipitating chloride salt blocks the pores in the sand-lime specimens, which leads to a limited transport of moisture. The difference in the results between the two materials can be explained by their properties. In mortar, chloride can be bound, and the amount of the bound chlorides constitutes about 50% of the total chloride amount in the material, as explained in [16]. However, in sand-lime, there is only free chloride (sand-lime has no binding capacity). This means that the amount of free chloride, which can crystallize in a form of salts, in sand-lime is much higher than in mortar. Further research is needed regarding the influence of chloride with the total concentration higher than 2.0% on the moisture transport in mortar.
Furthermore, in this study the specimen is exposed on its both ends to different conditions in order to create moisture flux through the specimen. After 10 months, the chloride concentration profiles are measured by titration and compared with the chloride concentration profiles from the start of the experiment. The results show that the chloride concentration is decreased at the end of the experiment. Because of the seemingly disappearance of chloride, the chloride concentrations profiles are measured with different techniques. Ion chromatography is used to measure the profiles. The result of this technique is similar to the titration technique. In these two techniques, the chloride is measured from liquid solution, where it is assumed that all the bound chloride is unbound due to the use of nitric acid. To investigate this, XRF technique is used to measure the chloride concentration profile. With this technique, chloride concentration can be measured in solid state, which means directly from the ground powder. With all the different technique, the disappearance of chloride remains without explanation. Therefore, a new experimental set-up is designed to investigate this case. The results of these experiments show no disappearing chloride during a moisture flux of 7 months. This is why it can be assumed that the results of the first experiment contain an error.

6.6 References

[1] Polder R.B., Peelen W.H.A., Characterization of chloride transport and reinforcement corrosion in concrete under cyclic wetting and drying by electrical resistivity, Cement and Concrete Composites 24 (2002) 427-435.

[2] Ann K.Y., Ahn J.H., Ryou J.S., The importance of chloride content at the concrete surface in assessing the time to corrosion of steel in concrete structures, Construction and Building Materials 23 (2009) 239-245.

[3] Bohni H., Corrosion in reinforced concrete structures, Woodhead publishing Ltd and CRC press LLC Boca Raton (2005).

[4] Meijers S.J.H., Bijen J.M.J.M., de Borst R., Fraaij A.L.A., Computational results of a model chloride ingress in concrete including convection, drying-wetting cycles and carbonation, Materials and Structures 38 (2005) 145-154.

[5] Seung-Woo P., Min-Sun J., Ha-Won S., Sang-Hyo K., Ki Yong A., Prediction of time dependent chloride transport in concrete structures exposed to a marine environment, Cement and Concrete Research 40 (2010) 302-312.

[6] Hong K., Hooton R.D., Effects of cyclic chloride exposure on penetration of concrete cover, Cement and Concrete Research 29 (1999) 1379-1386.

[7] Pel L., Sawdy A., Voronina V., Physical principles and efficiency of salt extraction by poulticing, Journal of Cultural Heritage 11 (2010) 59-67.

[8] Weheeb Al-Khaja A., Influence of temperature, cement type and level of concrete consolidation on chloride ingress in conventional and high-strength concrete, Construction and Building Materials 11 (1997) 9-13.

[9] Tamimi A.K., Abdalla J.A., Sakka Z.I., Prediction of long term chloride diffusion of concrete in harsh environment, Construction and Building Materials 22 (2008) 829-836.

[10] Yuzer N., Akoz F., Kabay N., Prediction of time to crack initiation in reinforced concrete exposed to chloride, Construction and Building Materials 22 (2008) 1100-1107.

[11] Ha-Won S., Chang-Hong L., Ki Yong A., Factors influencing chloride transport in concrete structures exposed to marine environments, Cement and Concrete Composites 30 (2008) 113-121.

[12] Marsavina L., Audenaert K., De Schetter G., Faur N., Marsavina D., Experimental and numerical determination of chloride penetration in cracked concrete, Construction and Building Materials 23 (2009) 264-274.

[13] Guneyisi E., Gesoglu M., Ozturan T., Ozbay E, Estimation of chloride permeability of concretes by empirical modeling: Considering effects of cement type, curing condition and age, Construction and Building Materials 23 (2009) 469-481.

[14] Xuemei L., Kok Seng C., Min-Hong Z., Water absorption, permeability, and resistance to chloride-ion penetration of lightweight aggregate concrete, Construction and Building Materials 25 (2011) 335-343.

[15] David Lide R., CRC Handbook of Chemistry and Physics, CRC Press, Washington (2004).

[16] Spiesz P., Ballari M.M., Brouwers H.J.H., RCM: A new model accounting for the non-linear chloride binding isotherm and the non-equilibrium conditions between the free- and bound-chloride concentrations, Construction and Building Materials 27 (2012) 293-304

[17] Shideler J. J., Calcium Chloride in Concrete. Journal proceedings of the American Concrete Institute 48 (1952) 537-559.

[18] Collepardi M., Massida L., Hydration of beta dicalcium silicate alone and in the presence of $CaCl_2$ or C_2H_5OH, Journal of the American Ceramic Society 56 (1973) 181-183.

[19] Tang L., Chloride transport in concrete – measurement and prediction, PhD Thesis, Chalmers University of Technology, Sweden (1996).

[20] Yuan Q., Fundamental studies on test methods for the transport of chloride ions in cementitious materials, PhD Thesis, University of Ghent, Belgium (2009).

[21] Pel L., Moisture transport in porous building materials, PhD Thesis, Eindhoven University of Technology, The Netherlands (1995).

7

7. Experimental study on chloride transport in unsaturated mortar

This chapter has been published as:

Taher, A. Hofstede, J.M. van der Zanden, A.J.J. & Brouwers, H.J.H. The influence of air in mortar on the results of the RCM test. & Influence of air on the chloride penetration in concrete**.** *Proceedings of the 5th International Conference on Non-Traditional Cement and Concrete (NTCC2014)*, June 16-19, 2014, Brno, Czech Republic (pp. 245-248) & *Proceedings of the 9th International Symposium on Cement and Concrete (ISCC 2017)*, November 1-4**,** 2017, Wuhan, China.

7.1 Introduction

Chloride penetration into concrete can influence the durability of reinforced concrete structures. Many experimental techniques have been developed for examining concrete properties in terms of chloride transport, such us long-term and short-term methods. From the practical point of view, short-term methods are often preferred due to the fact that long-term methods are laborious, time consuming and costly. The rapid chloride migration test (RCM-test), developed by Tang [1] and released as a guideline NT Build 492 [2], is the most commonly used short-term test. Many authors [3-7] performed the test with liquid saturated samples (as prescribed in the guideline [2]), while in practice concrete structures/elements are mostly unsaturated. Marine structures in the splash and tidal zones, are typical examples of an unsaturated concrete.

The aim of this study is to experimentally investigate the chloride transport in unsaturated mortar/concrete and to emphasize why the capillary suction mechanism of the chloride transport is dominating in the surface layers of unsaturated concrete. To achieve this, two experiments are designed in this chapter. The first experiment is designed to compare the chloride transport in unsaturated mortar via natural diffusion and capillary suction. Three groups with standard mortar samples having various air percentage (in order to create capillary suction) are obtained and brought into contact with chloride solution to compare the chloride penetration depth and study the influence of capillary suction and diffusion on the chloride penetration.

The second experiment is designed to compare chloride transport in unsaturated mortar via capillary suction and forced migration. Also in this part, standard mortar samples with various air percentage are obtained and tested with the RCM-test.

Furthermore, the chloride penetration depth in the samples is measured with colorimetric method. The titration method is also used for validating the results and measuring the chloride concentration profiles.

7.2 Material

Two batches of mortar samples for two experiments are prepared and tested in this chapter.

7.2.1 Material batch 1

This experiment is designed to study the two chloride transport mechanisms (natural diffusion and capillary suction). To achieve this, cylindrical mortar samples with a water/cement ratio of 0.5 and cement type CEM I 42.5 N are examined in this experiment. The samples are cured in water for 28 days. Samples with 30 mm thickness and 100 mm in diameter are cut from the cylindrical samples. The samples are provided with various air percentages as shown in Table 7.1.

Table 7.1: Samples with various air contents.

Samples	Air content	Duration of sealing
1-6	0%	1 week
7-9	6%	1 week
10-12	10%	1 week

The flowchart of the experiment is shown in Figure 7.1.

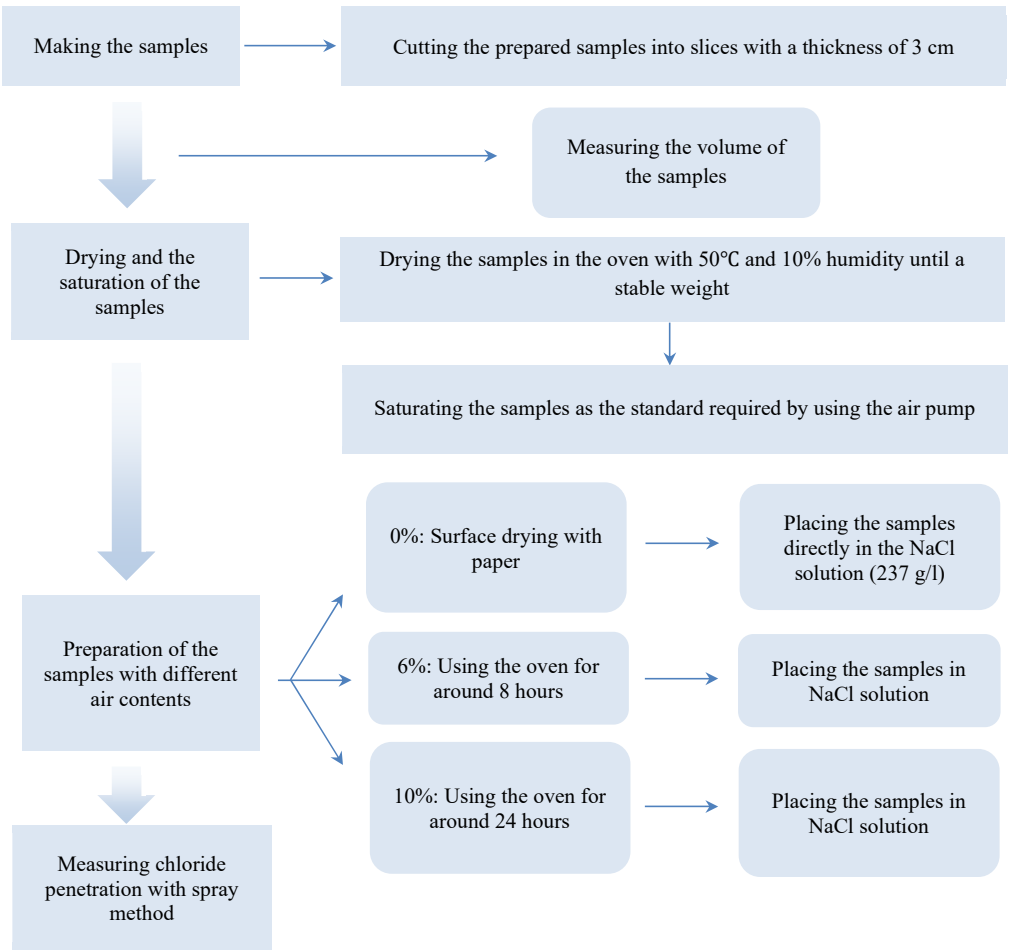

Figure 7.1: Flowchart of the experiment.

The desired air contents in the samples are obtained by first saturating the samples with water, using the vacuum saturation method, as described in chapter 2. When the saturation process is completed, the samples are dried for a short period of time in a climate chamber with a relative humidity of 10% and temperature of 50° C. During the drying process the mass of the samples is monitored closely to obtain the correct air content in the sample.

The air content (V_{air}) in each sample is calculated by.

$$V_{air} = V_{sample} \cdot P_{air} \tag{7.1}$$

where V is the volume and P_{air} is the air content in the sample (%). The volume of the air equals the volume of water that leaves the voids of the sample, and is given by

$$V_{water} = \frac{M_{water}}{\rho_{water}} \tag{7.2}$$

where M is the mass and ρ the density. By measuring the total mass of the sample, the mass of the water that left the sample will also be determined and with this the air volume in the samples is computed. Figure 7.2 shows the air content developed during drying. For instance, to provide a sample with 10% air a drying period of approximately 27 hours (1600 min) is needed. After achieving the desired total air contents, the samples are sealed with plastic foil for one week. This is done to obtain an even air distribution within the whole sample volume.

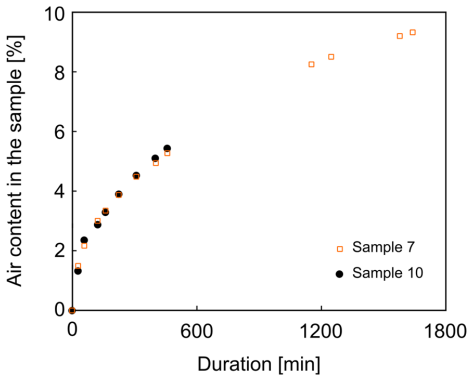

Figure 7.2: Air content in the mortar samples during drying.

Hereafter, a sodium chloride solution (237 kg/m^3) of four liter is prepared. The samples are placed in the solution for a certain period of time, to provide the samples with a concentration of 2% of chloride per the mass of the sample, as discussed in Chapter 6.

7.2.2 Material batch 2

In this part, six cylindrical mortar samples with a water/cement ratio of 0.5 and cement type CEM I 42.5 N are prepared. Slices 20 mm thickness and 100 mm in diameter are cut from cylindrical samples. Thinner samples are chosen because the penetration of chloride will take place from one side (one dimension). The desired air contents in the hardened mortar samples are obtained with the same method as explained in Section 7.2.1 (see Table 7.2).

Table 7.2: Samples with various air contents.

Sample	Air content	Duration of sealing
21	0%	1 week
22	2%	1 week
23	4%	1 week
24	6%	1 week
25	8%	1 week
26	10%	1 week

During the drying process, the mass of the samples is also monitored. Figure 7.3 shows the air content change over time during drying.

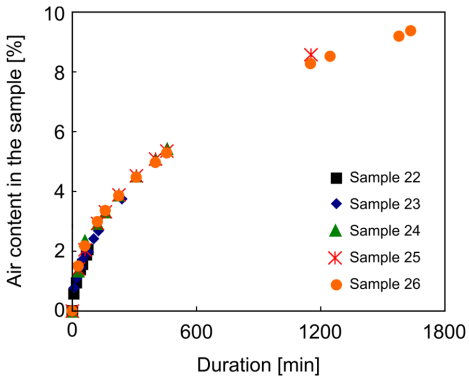

Figure 7.3: Drying time of the mortar samples.

7.3 Methods

7.3.1 Diffusion experiments

In this experiment two transport mechanisms of chloride penetration in mortar are investigated, diffusion and capillary suction.

To obtain an indication about the rate of diffusion of chloride in the sample over time, the samples (1-4, see Table 7.1) are placed in a sodium chloride solution (237 kg/m^3) for various periods of time (3 h, 6 h, 15 h and 30 h). It is noted that the chloride will penetrate from all the sides. The penetration depth is measured with a colorimetric method. The samples are split in half by applying a force. Then, the fractured surface is sprayed with a colorimetric indicator for chlorides (0.1 M $AgNO_3$). The colorimetric indicator visualizes the chloride penetration and makes it possible to measure the penetration depth. With the results of the samples (1-4), an exposure duration can be selected for the remaining samples (5-12, see Table 7.1). After the exposure, the penetration depth in the samples (5-12) is measured and the two transport mechanisms (diffusion and capillary suction) are compared.

7.3.2 Migration experiment (RCM-test)

Another experiment is designed to study migration and capillary suction transport mechanisms of chloride in mortar samples. For this purpose, Rapid Chloride Migration test (RCM-test) is used. RCM-test is a test based on forced ionic migration. This ionic migration is induced by an external electrical voltage applied across the mortar/concrete samples. Due to the potential difference between the electrodes, chloride ions will migrate from the catholyte solution, through the mortar sample, toward the anolyte solution. The set-up of the RCM-test is shown in Figure 7.4. The catholyte solution is 10% NaCl by mass in tap water (100 g NaCl per 900 g water) and the anolyte solution is NaOH in distilled water (12 g NaOH per 1 liter water). The samples are clamped tightly in non-conductive rubber sleeves and then placed on an inclined support. This is done to let the gas bubbles, which will be generated on the cathode (below the sample), evacuate freely. The initial voltage of 30 V is applied on the electrodes to measure the initial current. Based on the value of the current, the duration of the RCM-test and the value of the voltage applied during the test are determined, following the specifications given in the guideline NT Build 492 [2]. The current measured in this study resulted in duration of six hours with a voltage of 10 Volt, taking into account the thickness of the sample.

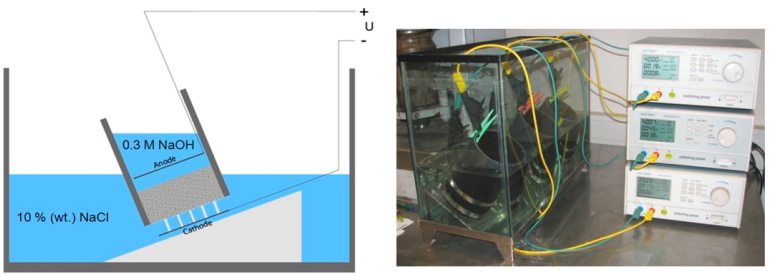

Figure 7.4: RCM test set-up [7].

After the RCM-test, the chloride penetration depth in the samples is measured with two different techniques: colorimetric method and titration method. The penetration depth with colorimetric method is measured on seven evenly spread positions in the sample, as shown Figure 7.5. An average of the seven measurements is calculated and assumed to represent the penetration depth for the whole sample. This procedure is repeated for all the samples.

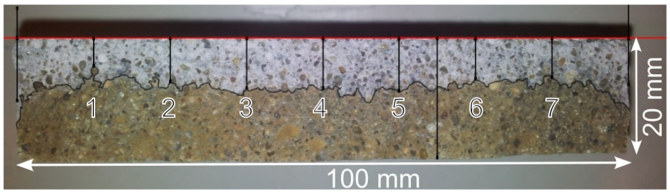

Figure 7.5: Chloride penetration depth in a split mortar sample.

An alternative method is used to compare and validate the colorimetric method. Titration is used to determine the chloride penetration depth and chloride profiles in the samples.

7.4 Results and discussion

7.4.1 Diffusion experiments

The experiment is started by placing the fully saturated (0% air content) samples 1-4 (see Table 7.1) in chloride solution for 3, 6, 15 and 30 hours to examine the diffusion rate over time as shown in Table 7.3.

Table 7.3: Penetration depth.

Samples	Exposure duration [hour]	Average penetration depth [mm]
1	3	2.0
2	6	3.2
3	15	4.2
4	30	7.2

Already at an exposure duration of 6 hours, the chloride penetration depth becomes clearly visible by using the colorimetric method, as shown in Figure 7.6 (b). Therefore, the exposure duration of 6 hours is applied for the remaining samples (5-12), see Figures 7.6 and 7.7.

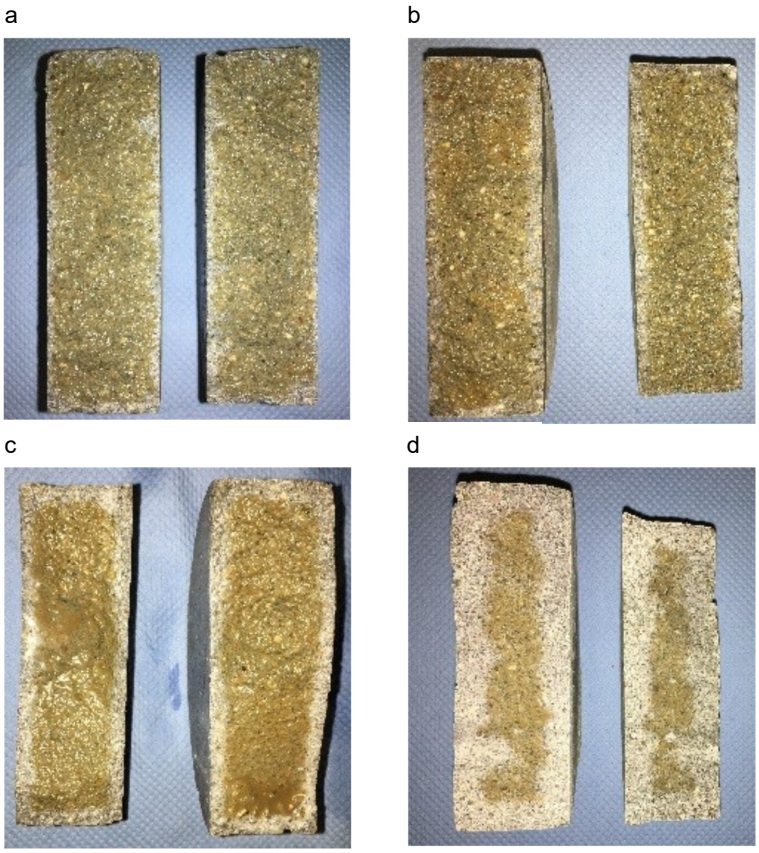

Figure 7.6: Chloride penetration into the samples at various exposure duration. (a) Exposure duration of 3 h and penetration of 2 mm. (b) Exposure duration of 6 h and chloride penetration of 3.2 mm. (c) Exposure duration of 15 h and chloride penetration of 4.2 mm. (d) Exposure duration of 30 h and chloride penetration of 7.2 mm.

Subsequently, three samples from each group (0%, 6% and 10% air content, see Table 7.1) are placed in a chloride solution for 6 hours. Hereafter, the penetrations are measured with the colorimetric method as shown in Figure 7.7.

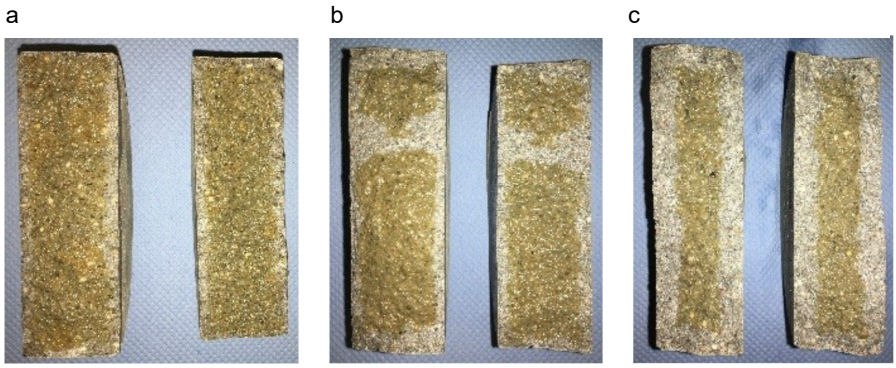

Figure 7.7: Chloride penetration into samples at various air percentage, exposure duration 6 hours. (a) Saturated sample (0% air) and chloride penetration of 3.2 mm. (b) Sample with 6% air and chloride penetration of 3.9 mm. (c) Sample with 10% air and chloride penetration of 6.5 mm.

Figure 7.7 shows that an increment in the air content in the samples leads to an increment of the chloride penetration depth. Figure 7.8 shows the relation between the air content and the average chloride penetration depth into the samples.

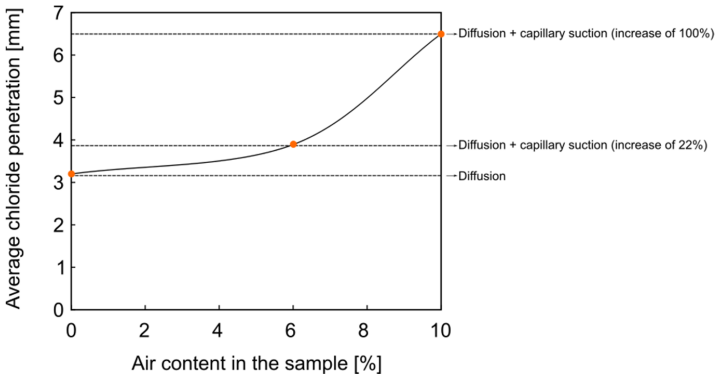

Figure 7.8: Chloride penetration depth by the colorimetric method.

The results show that the presence of air in the samples leads to a deeper/faster chloride penetration. Chloride penetrated into the samples with 0% air purely by diffusion. On the other hand, the influence of capillary suction is visible for the sample with 6% air, in which an increase of 22% in the penetration depth is observed. At 10% air content in the sample, the chloride penetration depth is double, compared to the sample with no air (thus 100% increase).

7.4.2 Migration experiment (RCM-test)

The experiment is started by testing the samples (21-26, see table 7.2) in the RCM-test. Then, the chloride penetration depth in the samples is measured by the colorimetric method and the total chloride concentration profile is determined using the titration method.

7.4.2.1 Colorimetric method

Figure 7.9 shows the chloride penetration depth in the samples with various air contents measured by the colorimetric method. The results show that the chloride penetrated approximately 7 to 14 mm into the samples and the higher air content leads to deeper penetration of chloride.
Furthermore, the results shows that the influence of the capillary suction becomes more visible for the samples with an air content of 6% air (increase of 14% in the chloride penetration depth). The effect of the capillary suction is the highest in the samples with the air content of 10% (increase of 70%). Similar results are found in Section 7.4.1.

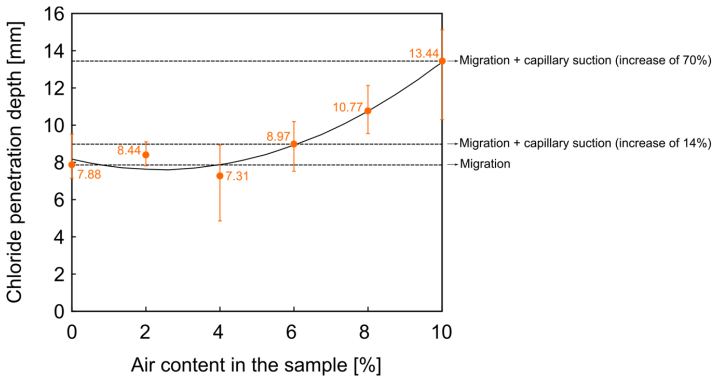

Figure 7.9: Chloride penetration depth by the colorimetric method.

7.4.2.2 Titration method

The results of the chloride penetration depth, determined with the titration method on the samples tested previously using the colorimetric method are shown in Figure 7.10. The results in this case show a chloride penetration of approximately 8.5 to 14.5 mm. Also in this case, higher air content in the sample results in deeper penetration of chloride. The effect of capillary suction is also the same as discussed previously.

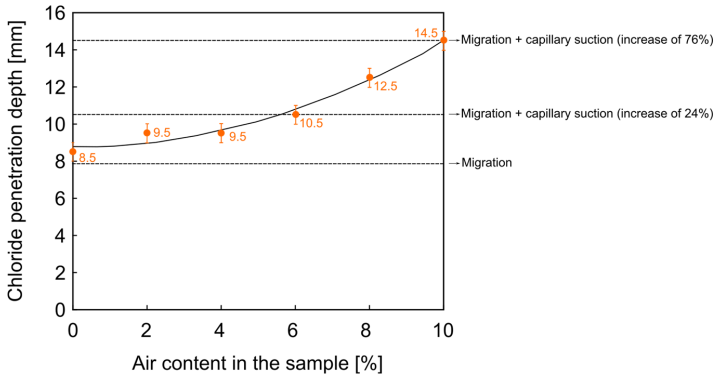

Figure 7.10: Chloride penetration depth by titration method.

7.4.2.3 Comparing the colorimetric method and titration method

The comparison of the colorimetric and titration methods is shown in Figure 7.11. Both methods give similar trends. However, the chloride penetration depth measured by titration is approximately 10% higher. This is because measuring the chloride penetration depth with the colorimetric method is limited to the chloride detection limit of approximately 0.2% of the total chloride concentration in mortar, while with the titration chloride concentration below 0.1% can also be detected [7].

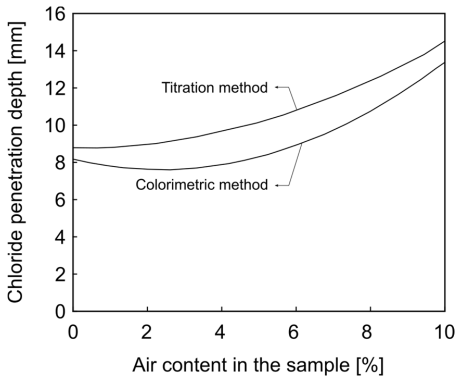

Figure 7.11: Comparison between colorimetric and titration methods.

The differences in the results of the colorimetric and the titration method are also reflected in Figure 7.12, where both methods are compared for each sample with different percentages of air. In Figure 7.12 it can be seen that with the titration method it is possible to obtain more accurate results than with the colorimetric method.

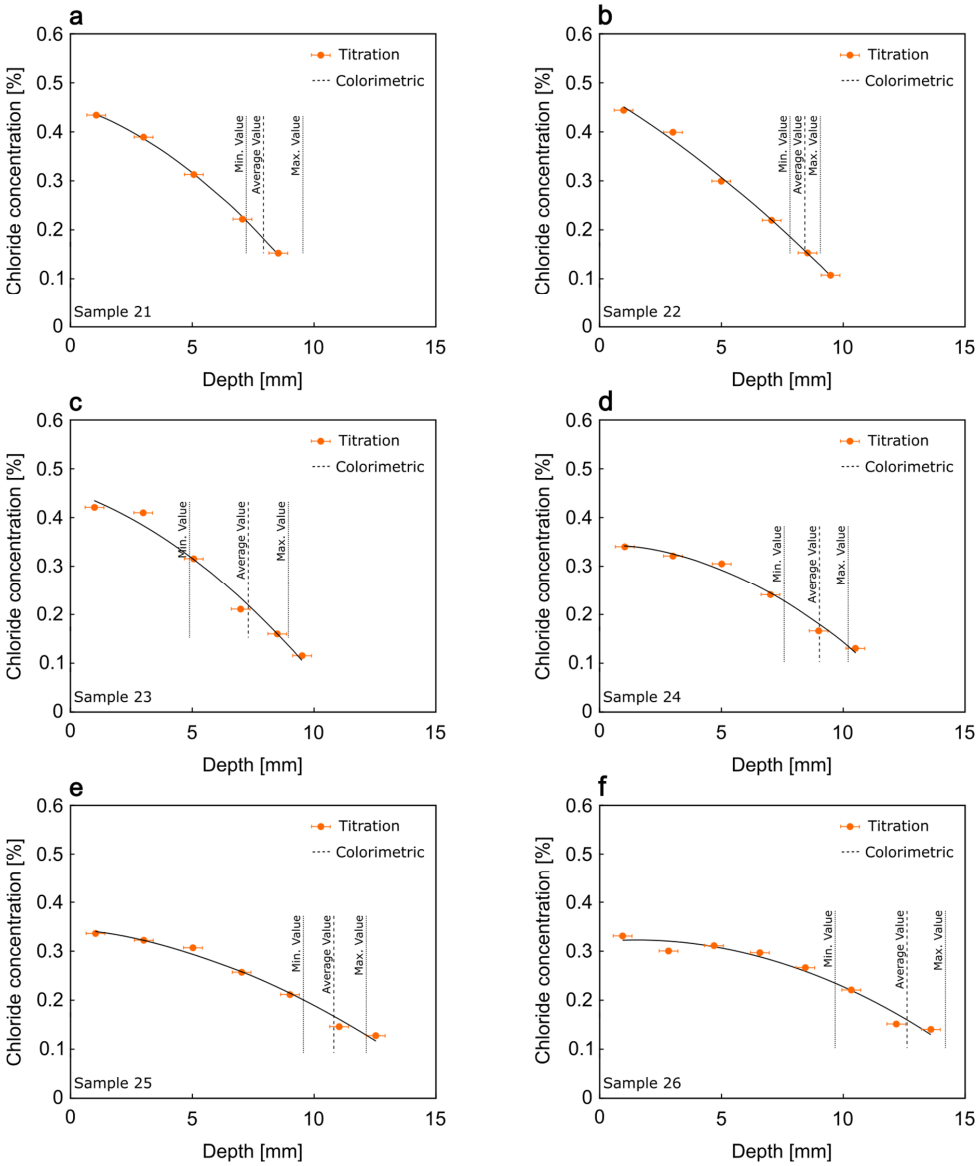

Figure 7.12: Chloride concentration profiles in samples with different percentages of air.

7.5 Conclusions

In this chapter two experimental studies are executed. In the first experiment, two transport mechanisms (diffusion and capillary suction) are compared for the chloride penetration into unsaturated mortar samples. This is executed by providing sample with various air contents (0%, 6% and 10%) and exposing them to a chloride solution for 6 hours. Chloride penetrated into the samples with 0% purely by diffusion as the governing transport mechanism. On the other hand, capillary suction and diffusion are the driving transport mechanisms for the samples with 6% and 10%. The results shows that the presence of air in the samples leads to deeper chloride penetrations (20% –100%).

In the second experiment a study on the RCM-test is executed. In this experiment, capillary suction and forced electric migration are compared for the chloride penetration into mortar samples.
Samples with various air content are tested. The chloride penetration depth in the samples is measured with colorimetric and titration methods. The results of both methods show similar results. However, the titration method is more accurate, because this technique measures also the chloride concentration below 0.1%, while the colorimetric method is limited to 0.2% [7]. Moreover, from the results, it can be concluded that a higher air content in the samples results in deeper chloride penetrations (14% – 76%). This can be explained by the capillary suction. If air is present in mortar/concrete sample, then capillary suction is an additional chloride transport mechanism besides the electrical migration.

7.6 References

[1] Luping T., Chloride transport in concrete – measurement and prediction, PhD Thesis, Chalmers University of Technology, Sweden (1996).

[2] NT Build 492, Concrete, mortar and cement-based repairmaterials: chloride migration coefficient from non-steady-state migration experiments, Nordtest method (1999).

[3] Edvardsen C., Tange Jepsen M., Chloride migration coefficients from non-steady-state migration experiments at environment-friendly "Green" concrete, Proceedings of the 2nd international RILEM workshop, France (2000) 203-209.

[4] Yu Z., Ye G., Chloride penetration and microstructure development of fly ash concrete, Proceedings of the 2nd international conference on Microstructural-related Durability of Cementitious Composites, The Netherlands (2012).

[5] Spiesz P.R., Brouwers H.J.H., Evaluation of the rapid chloride migration (RCM) test, Proceedings of the 17th Ibausil, International Conference on Building Materials, Germany (2009).

[6] Spiesz P.R., Brouwers H.J.H., Influence of the applied voltage on the Rapid Chloride Migration (RCM) test, Cement and Concrete Research 42 (2012) 1072-1082.

[7] Spiesz P.R., Brouwers H.J.H., Analysis of the theoretical model of the Rapid Chloride Migration test, Proceedings 8th fib International PhD Symposium in Civil Engineering, Denmark (2010).

8. Summary and conclusions

This thesis aims to experimentally and numerically assess the individual and combined impacts of moisture transport and chloride transport in concrete.

In Chapter 2, two methods are used and compared to describe moisture transport in concrete structures. Two methods (standard method and hysteretic method) are implemented to describe moisture transport in concrete during wetting/drying cycles. Diffusion coefficients retrieved from the literature are used in the models. One cycle of wetting/drying is compared. The duration of the wetting phase is one day and drying is six days. The results show that using the standard model with one diffusion coefficient or using the hysteretic model with two diffusion coefficients, can have a large influence on the results. After one cycle, the hysteretic model gives clearly a higher amount of moisture content in the structure. An experimental setup is developed to obtain measured data for validation purposes. From the experimental results it can be concluded that models with hysteretic properties give more accurate results compared with models with one diffusion coefficient only.

In Chapter 3, a measuring procedure is proposed to obtain the diffusion coefficient of water in porous materials. In this procedure, a centrifuge is used to create a non-homogenous water distribution inside a porous material. After preparation of the sample, which is the first step, a non-equilibrium situation inside a partially saturated porous sample is created using a centrifuge. Finally the sample is taken out of the centrifuge and how fast the water distribution inside the sample reaches its new equilibrium is measured by hanging the sample from two cables, each connected to a balance. Fick's second law is used to compute the diffusion coefficient. The proposed measurement procedure can be used to measure the diffusion coefficient for any porous materials.

Chapter 4 presents a new experimental setup to measure sorption isotherm in which more points can be measured with an adjustable measurement resolution. Two porous materials are considered: mortar and sand-lime, where the results are compared with the results documented in the literature. In addition, the effect of chloride on the sorption isotherm is investigated and compared with the case without chloride. Samples with chloride present in the pores of the material are prepared with vacuum saturation and a sodium chloride solution. A more homogeneously distributed chloride concentration throughout the sample is obtained by first drying the sample completely before wetting by a sodium chloride solution. More points on the adsorption curve can be obtained by decreasing the amount of added water to the system. This would, however, increase the time required to obtain the sorption curve. After addition of water, equilibrium is awaited and the water content of the sample is calculated with a mass balance and the amount of water in the air of the vessel, which is obtained from the relative humidity. After reaching final equilibrium, the desorption of the sample is obtained by blowing dry air through the vessel and calculating the water loss. The adsorption isotherm of mortar and sand-lime is measured and compared with results found in the literature. There is a slight difference in the results for mortar samples, which can be explained by the composition of the used samples. Apart from this, the results show similarities in the shape of the curves. The higher sorption of a sample containing sodium chloride is explained with the decreased equilibrium relative humidity of a pore containing a sodium chloride solution. In this way, water condensation occurs at a lower relative humidity compared to a sample containing pure water.

Chapter 5 presents a model for the transport of chloride in unsaturated concrete. The transport of water is described with a diffusion coefficient. The transport of chloride includes the transport of chloride dissolved in the pore water migrating through the concrete and the transport of chloride caused by a gradient in the pore water chloride concentration. Two processes are taken into account: (i) chloride convection, and (ii) chloride diffusion (modelled with the Fick's law). The model is applied to concrete

with a daily and yearly cycle of drying and wetting. The water transport is modelled with a diffusion coefficient and the chloride transport is modelled as the sum of a convective term and a diffusive term. The model is applied with various boundary conditions for the chloride transport. The resulting equations are solved numerically using the Crank-Nicolson method which results in water and chloride concentration profiles. The model recognizes that convective chloride transport is formed by water transport through mainly the largest water filled pores. The smaller water filled pores contribute relatively less. The division of the chloride transport over the pores as a function of the pore radius is a very complex process and has been modelled here with a division over two extremes, i.e. the half of the water filled pore volume with the largest water filled pores is flowing homogeneously with a constant velocity and the half of the water filled pore volume with the smallest pores is stagnant. These two halves are connected with a diffusion process. The results show that the chloride concentration at the surface can rise considerably, when water leaves the concrete sample, while chloride stays behind. Crystallization and a few other possible model extensions are discussed in this chapter.

Chapter 6 investigates the impact of chloride on moisture transport in concrete for low moisture concentration. An experimental setup is developed to measure moisture transport in thin specimens. Two materials are considered, mortar and sand-lime, where the measurements are performed for samples with and without chloride. The results show that chloride, with a concentration of 2.0%, has a large influence on moisture transport in sand-lime specimens, but its influence on the moisture transport in mortar specimens is limited. It appears that the precipitating chloride salt blocks the pores in the sand-lime specimens, which leads to a smaller transport of moisture. The difference in the results between the two materials can be explained by their properties. In mortar, chloride can be bound, and the amount of the bound chlorides constitutes about 50% of the total chloride amount in the material. However, in sand-lime, there is only free chloride. Thus, the amount of free chloride, which can crystallize in a form of salts, in sand-lime is much higher than in mortar.

Chapter 7 experimentally studies the chloride transport in unsaturated concrete to better understand the capillary suction mechanism of the chloride transport in the surface layers. The measurements are performed in two stages. The first experiment compares two transport mechanisms, i.e. natural diffusion and capillary suction, while the second experiment is performed to evaluate forced migration and capillary suction in unsaturated concrete. The results shows that the presence of air in the samples leads to deeper chloride penetrations (20% –100%). In the second experiment a study on the RCM-test is executed. In this experiment, capillary suction and forced electric migration are compared for the chloride penetration into mortar samples. Samples with various air content are tested. The chloride penetration depth in the samples is measured with colorimetric and titration methods. The results of both methods show similar results. However, the titration method is more accurate, because this technique measures also the chloride concentration below 0.1%, while the colorimetric method is limited to 0.2%. Moreover, from the results, it can be concluded that a higher air content in the samples results in deeper chloride penetrations (14% – 76%). This can be explained by the capillary suction. If air is present in mortar/concrete sample, then capillary suction is an additional chloride transport mechanism besides the electrical migration.

List of publication

Journal publications

1. **Taher, A.** & Brouwers, H.J.H. (2022). Sorption isotherm measurements for porous materials: A new hygroscopic method. *Construction and Building Materials, 379, 131166.*

2. Van der Zanden, A.J.J. **Taher, A**. & Arends, T. (2015). Modelling of water and chloride transport in concrete during yearly wetting/drying cycles. *Construction and Building Materials*, *81*, 120-129.

3. Van der Zanden, A.J.J. & **Taher, A.** (2014). A gravitational procedure to measure the diffusion coefficient of mater in porous materials: a case study on concrete. *Drying Technology*, *32*(6), 708-712.

4. **Taher, A.** van der Zanden, A.J.J. & Brouwers, H.J.H. (2013). Chloride transport in mortar at low moisture concentration. *Chemistry and Materials Research*, *5*, 53-56.

5. **Taher, A**. Cao, X. Pop, I.S. van der Zanden, A.J.J. & Brouwers, H.J.H. (2013). Moisture transport in concrete during wetting/drying cycles. *Chemistry and Materials Research*, *5*, 86-90.

Conference proceedings

1. **Taher, A.** Qu, Z. & Brouwers, H.J.H. (2017). Influence of air on the chloride penetration in concrete. Proceedings of the 9th International Symposium on Cement and Concrete (ISCC 2017), November 1-4 2017, Wuhan, China.

2. **Taher, A.** Hofstede, J.M. van der Zanden, A.J.J. & Brouwers, H.J.H. (2014). The influence of air in mortar on the results of the RCM test. Proceedings of the 5th International Conference on Non-Traditional Cement and Concrete (NTCC2014), June 16-19 2014, Brno, Czech Republic (pp. 245-248).

3. Arends, T. **Taher, A.** van der Zanden, A.J.J. & Brouwers, H.J.H. (2014). A model describing water and chloride migration in concrete during wetting/drying cycles. Proceedings of the 5th International Conference on Non-Traditional Cement and Concrete (NTCC2014), June 16-19 2014, Brno, Czech Republic (pp. 5-8).

4. **Taher, A.** Arends, T. van der Zanden, A.J.J. & Brouwers, H.J.H. (2014). Measuring water sorption isotherm of mortar containing chloride. XIII International Conference on Durability of Building Materials and Components, (XIII/DBMC), 2-5 September 2014, São Paulo, Brazil (pp. 1093-1100).

5. **Taher, A.** Cao, X. Pop, I.S. van der Zanden, A.J.J. Brouwers, H.J.H., Moisture transport in concrete during wetting/drying cycles, International Congress on Materials & Structural Stability CMSS-2013, 27-30 November 2013, Rabat, Morocco.

6. **Taher, A**. van der Zanden, A.J.J. Brouwers, H.J.H. Chloride transport in mortar at low moisture concentration, International Congress on Materials & Structural Stability CMSS-2013, 27-30 November 2013, Rabat, Morocco.

7. **Taher, A.** van der Zanden, A.J.J. & Brouwers, H.J.H. A hygroscopic method to measure the adsorption isotherm of porous construction materials. 1st International Conference on the Chemistry of Construction Materials, 7-8 October 2013, Berlin, Germany (pp. 241-244).

8. **Taher, A.** van der Zanden, A.J.J. & Brouwers, H.J.H. (2012). The influence of chloride on the moisture transport in mortar and sand-lime. 12th International conference on building materials, IBAUSIL, Weimar, Germany (pp. 2-0609-2-0616).

Poster publications

1. **Taher, A.** van der Zanden, A.J.J. & Brouwers, H.J.H. The influence of chloride on the moisture transport in mortar and sand-lime, Berlin (2012).

2. **Taher, A**. Blagojevic, A. van der Zanden, A.J.J. Fennis-Huijben, S. Brouwers, H.J.H. & Walraven, J.C. Chloride penetration in cracked and uncracked concrete structures, Kick-off IS2C (2011).

Curriculum Vitae

Azee Taher was born on 20 October 1982 in Erbil, Iraq. In 2008, he embarked upon his pursuit of a Master's degree at the Department of the Built Environment, in the unit Structural Engineering and Design at Eindhoven University of Technology. In September 2010, he successfully obtained his Master's degree on the thesis entitled "Aluminium Tube Constructions."

In October 2010, he started as a PhD candidate in the chair Building Materials of the unit Building Physics and Services at Eindhoven University of Technology, the Netherlands, under the supervision of prof.dr.ir. H.J.H. Brouwers and dr.ir. A.J.J. van der Zanden. Since 2018 he works as Senior Consultant in Concrefy B.V., The Netherlands.

Bouwstenen is een publicatiereeks
van de Faculteit Bouwkunde,
Technische Universiteit Eindhoven.
Zij presenteert resultaten van
onderzoek en andere activiteiten op
het vakgebied der Bouwkunde,
uitgevoerd in het kader van deze
Faculteit.

Bouwstenen en andere proefschriften van de
TU/e zijn online beschikbaar via:
https://research.tue.nl/

Reeds verschenen in de serie
Bouwstenen

nr 1
Elan: A Computer Model for Building Energy Design: Theory and Validation
Martin H. de Wit
H.H. Driessen
R.M.M. van der Velden

nr 2
Kwaliteit, Keuzevrijheid en Kosten: Evaluatie van Experiment Klarendal, Arnhem
J. Smeets
C. le Nobel
M. Broos
J. Frenken
A. v.d. Sanden

nr 3
Crooswijk: Van 'Bijzonder' naar 'Gewoon'
Vincent Smit
Kees Noort

nr 4
Staal in de Woningbouw
Edwin J.F. Delsing

nr 5
Mathematical Theory of Stressed Skin Action in Profiled Sheeting with Various Edge Conditions
Andre W.A.M.J. van den Bogaard

nr 6
Hoe Berekenbaar en Betrouwbaar is de Coëfficiënt k in x-ksigma en x-ks?
K.B. Lub
A.J. Bosch

nr 7
Het Typologisch Gereedschap: Een Verkennende Studie Omtrent Typologie en Omtrent de Aanpak van Typologisch Onderzoek
J.H. Luiten

nr 8
Informatievoorziening en Beheerprocessen
A. Nauta
Jos Smeets (red.)
Helga Fassbinder (projectleider)
Adrie Proveniers
J. v.d. Moosdijk

nr 9
Strukturering en Verwerking van Tijdgegevens voor de Uitvoering van Bouwwerken
ir. W.F. Schaefer
P.A. Erkelens

nr 10
Stedebouw en de Vorming van een Speciale Wetenschap
K. Doevendans

nr 11
Informatica en Ondersteuning van Ruimtelijke Besluitvorming
G.G. van der Meulen

nr 12
Staal in de Woningbouw, Korrosie-Bescherming van de Begane Grondvloer
Edwin J.F. Delsing

nr 13
Een Thermisch Model voor de Berekening van Staalplaatbetonvloeren onder Brandomstandigheden
A.F. Hamerlinck

nr 14
De Wijkgedachte in Nederland: Gemeenschapsstreven in een Stedebouwkundige Context
K. Doevendans
R. Stolzenburg

nr 15
Diaphragm Effect of Trapezoidally Profiled Steel Sheets: Experimental Research into the Influence of Force Application
Andre W.A.M.J. van den Bogaard

nr 16
Versterken met Spuit-Ferrocement: Het Mechanische Gedrag van met Spuit-Ferrocement Versterkte Gewapend Betonbalken
K.B. Lubir
M.C.G. van Wanroy

nr 17
De Tractaten van Jean Nicolas Louis Durand
G. van Zeyl

nr 18
Wonen onder een Plat Dak: Drie Opstellen over Enkele Vooronderstellingen van de Stedebouw
K. Doevendans

nr 19
Supporting Decision Making Processes: A Graphical and Interactive Analysis of Multivariate Data
W. Adams

nr 20
Self-Help Building Productivity: A Method for Improving House Building by Low-Income Groups Applied to Kenya 1990-2000
P. A. Erkelens

nr 21
De Verdeling van Woningen: Een Kwestie van Onderhandelen
Vincent Smit

nr 22
Flexibiliteit en Kosten in het Ontwerpproces: Een Besluitvormingondersteunend Model
M. Prins

nr 23
Spontane Nederzettingen Begeleid: Voorwaarden en Criteria in Sri Lanka
Po Hin Thung

nr 24
Fundamentals of the Design of Bamboo Structures
Oscar Arce-Villalobos

nr 25
Concepten van de Bouwkunde
M.F.Th. Bax (red.)
H.M.G.J. Trum (red.)

nr 26
Meaning of the Site
Xiaodong Li

nr 27
Het Woonmilieu op Begrip Gebracht: Een Speurtocht naar de Betekenis van het Begrip 'Woonmilieu'
Jaap Ketelaar

nr 28
Urban Environment in Developing Countries
editors: Peter A. Erkelens
George G. van der Meulen (red.)

nr 29
Stategische Plannen voor de Stad: Onderzoek en Planning in Drie Steden
prof.dr. H. Fassbinder (red.)
H. Rikhof (red.)

nr 30
Stedebouwkunde en Stadsbestuur
Piet Beekman

nr 31
De Architectuur van Djenné: Een Onderzoek naar de Historische Stad
P.C.M. Maas

nr 32
Conjoint Experiments and Retail Planning
Harmen Oppewal

nr 33
Strukturformen Indonesischer Bautechnik: Entwicklung Methodischer Grundlagen für eine 'Konstruktive Pattern Language' in Indonesien
Heinz Frick arch. SIA

nr 34
Styles of Architectural Designing: Empirical Research on Working Styles and Personality Dispositions
Anton P.M. van Bakel

nr 35
Conjoint Choice Models for Urban Tourism Planning and Marketing
Benedict Dellaert

nr 36
Stedelijke Planvorming als Co-Produktie
Helga Fassbinder (red.)

nr 37
Design Research in the Netherlands
editors: R.M. Oxman
M.F.Th. Bax
H.H. Achten

nr 38
Communication in the Building Industry
Bauke de Vries

nr 39
Optimaal Dimensioneren van Gelaste Plaatliggers
J.B.W. Stark
F. van Pelt
L.F.M. van Gorp
B.W.E.M. van Hove

nr 40
Huisvesting en Overwinning van Armoede
P.H. Thung
P. Beekman (red.)

nr 41
Urban Habitat: The Environment of Tomorrow
George G. van der Meulen
Peter A. Erkelens

nr 42
A Typology of Joints
John C.M. Olie

nr 43
Modeling Constraints-Based Choices for Leisure Mobility Planning
Marcus P. Stemerding

nr 44
Activity-Based Travel Demand Modeling
Dick Ettema

nr 45
Wind-Induced Pressure Fluctuations on Building Facades
Chris Geurts

nr 46
Generic Representations
Henri Achten

nr 47
Johann Santini Aichel: Architectuur en Ambiguiteit
Dirk De Meyer

nr 48
Concrete Behaviour in Multiaxial Compression
Erik van Geel

nr 49
Modelling Site Selection
Frank Witlox

nr 50
Ecolemma Model
Ferdinand Beetstra

nr 51
Conjoint Approaches to Developing Activity-Based Models
Donggen Wang

nr 52
On the Effectiveness of Ventilation
Ad Roos

nr 53
Conjoint Modeling Approaches for Residential Group preferences
Eric Molin

nr 54
Modelling Architectural Design Information by Features
Jos van Leeuwen

nr 55
A Spatial Decision Support System for the Planning of Retail and Service Facilities
Theo Arentze

nr 56
Integrated Lighting System Assistant
Ellie de Groot

nr 57
Ontwerpend Leren, Leren Ontwerpen
J.T. Boekholt

nr 58
Temporal Aspects of Theme Park Choice Behavior
Astrid Kemperman

nr 59
Ontwerp van een Geïndustrialiseerde Funderingswijze
Faas Moonen

nr 60
Merlin: A Decision Support System for Outdoor Leisure Planning
Manon van Middelkoop

nr 61
The Aura of Modernity
Jos Bosman

nr 62
Urban Form and Activity-Travel Patterns
Daniëlle Snellen

nr 63
Design Research in the Netherlands 2000
Henri Achten

nr 64
Computer Aided Dimensional Control in Building Construction
Rui Wu

nr 65
Beyond Sustainable Building
editors: Peter A. Erkelens
Sander de Jonge
August A.M. van Vliet
co-editor: Ruth J.G. Verhagen

nr 66
Das Globalrecyclingfähige Haus
Hans Löfflad

nr 67
Cool Schools for Hot Suburbs
René J. Dierkx

nr 68
A Bamboo Building Design Decision Support Tool
Fitri Mardjono

nr 69
Driving Rain on Building Envelopes
Fabien van Mook

nr 70
Heating Monumental Churches
Henk Schellen

nr 71
Van Woningverhuurder naar Aanbieder van Woongenot
Patrick Dogge

nr 72
Moisture Transfer Properties of Coated Gypsum
Emile Goossens

nr 73
Plybamboo Wall-Panels for Housing
Guillermo E. González-Beltrán

nr 74
The Future Site-Proceedings
Ger Maas
Frans van Gassel

nr 75
Radon transport in Autoclaved Aerated Concrete
Michel van der Pal

nr 76
The Reliability and Validity of Interactive Virtual Reality Computer Experiments
Amy Tan

nr 77
Measuring Housing Preferences Using Virtual Reality and Belief Networks
Maciej A. Orzechowski

nr 78
Computational Representations of Words and Associations in Architectural Design
Nicole Segers

nr 79
Measuring and Predicting Adaptation in Multidimensional Activity-Travel Patterns
Chang-Hyeon Joh

nr 80
Strategic Briefing
Fayez Al Hassan

nr 81
Well Being in Hospitals
Simona Di Cicco

nr 82
Solares Bauen: Implementierungs- und Umsetzungs-Aspekte in der Hochschulausbildung in Österreich
Gerhard Schuster

nr 83
Supporting Strategic Design of Workplace Environments with Case-Based Reasoning
Shauna Mallory-Hill

nr 84
ACCEL: A Tool for Supporting Concept Generation in the Early Design Phase
Maxim Ivashkov

nr 85
Brick-Mortar Interaction in Masonry under Compression
Ad Vermeltfoort

nr 86
Zelfredzaam Wonen
Guus van Vliet

nr 87
Een Ensemble met Grootstedelijke Allure
Jos Bosman
Hans Schippers

nr 88
On the Computation of Well-Structured Graphic Representations in Architectural Design
Henri Achten

nr 89
De Evolutie van een West-Afrikaanse Vernaculaire Architectuur
Wolf Schijns

nr 90
ROMBO Tactiek
Christoph Maria Ravesloot

nr 91
External Coupling between Building Energy Simulation and Computational Fluid Dynamics
Ery Djunaedy

nr 92
Design Research in the Netherlands 2005
editors: Henri Achten
Kees Dorst
Pieter Jan Stappers
Bauke de Vries

nr 93
Ein Modell zur Baulichen Transformation
Jalil H. Saber Zaimian

nr 94
Human Lighting Demands: Healthy Lighting in an Office Environment
Myriam Aries

nr 95
A Spatial Decision Support System for the Provision and Monitoring of Urban Greenspace
Claudia Pelizaro

nr 96
Leren Creëren
Adri Proveniers

nr 97
Simlandscape
Rob de Waard

nr 98
Design Team Communication
Ad den Otter

nr 99
Humaan-Ecologisch Georiënteerde Woningbouw
Juri Czabanowski

nr 100
Hambase
Martin de Wit

nr 101
Sound Transmission through Pipe Systems and into Building Structures
Susanne Bron-van der Jagt

nr 102
Het Bouwkundig Contrapunt
Jan Francis Boelen

nr 103
A Framework for a Multi-Agent Planning Support System
Dick Saarloos

nr 104
Bracing Steel Frames with Calcium Silicate Element Walls
Bright Mweene Ng'andu

nr 105
Naar een Nieuwe Houtskeletbouw
F.N.G. De Medts

nr 106 and 107
Niet gepubliceerd

nr 108
Geborgenheid
T.E.L. van Pinxteren

nr 109
Modelling Strategic Behaviour in Anticipation of Congestion
Qi Han

nr 110
Reflecties op het Woondomein
Fred Sanders

nr 111
On Assessment of Wind Comfort by Sand Erosion
Gábor Dezsö

nr 112
Bench Heating in Monumental Churches
Dionne Limpens-Neilen

nr 113
RE. Architecture
Ana Pereira Roders

nr 114
Toward Applicable Green Architecture
Usama El Fiky

nr 115
Knowledge Representation under Inherent Uncertainty in a Multi-Agent System for Land Use Planning
Liying Ma

nr 116
Integrated Heat Air and Moisture Modeling and Simulation
Jos van Schijndel

nr 117
Concrete Behaviour in Multiaxial Compression
J.P.W. Bongers

nr 118
The Image of the Urban Landscape
Ana Moya Pellitero

nr 119
The Self-Organizing City in Vietnam
Stephanie Geertman

nr 120
A Multi-Agent Planning Support System for Assessing Externalities of Urban Form Scenarios
Rachel Katoshevski-Cavari

nr 121
Den Schulbau Neu Denken, Fühlen und Wollen
Urs Christian Maurer-Dietrich

nr 122
Peter Eisenman Theories and Practices
Bernhard Kormoss

nr 123
User Simulation of Space Utilisation
Vincent Tabak

nr 125
In Search of a Complex System Model
Oswald Devisch

nr 126
Lighting at Work: Environmental Study of Direct Effects of Lighting Level and Spectrum on Psycho-Physiological Variables
Grazyna Górnicka

nr 127
Flanking Sound Transmission through Lightweight Framed Double Leaf Walls
Stefan Schoenwald

nr 128
Bounded Rationality and Spatio-Temporal Pedestrian Shopping Behavior
Wei Zhu

nr 129
Travel Information: Impact on Activity Travel Pattern
Zhongwei Sun

nr 130
Co-Simulation for Performance Prediction of Innovative Integrated Mechanical Energy Systems in Buildings
Marija Trčka

nr 131
Niet gepubliceerd

nr 132
Architectural Cue Model in Evacuation Simulation for Underground Space Design
Chengyu Sun

nr 133
Uncertainty and Sensitivity Analysis in Building Performance Simulation for Decision Support and Design Optimization
Christina Hopfe

nr 134
Facilitating Distributed Collaboration in the AEC/FM Sector Using Semantic Web Technologies
Jacob Beetz

nr 135
Circumferentially Adhesive Bonded Glass Panes for Bracing Steel Frame in Façades
Edwin Huveners

nr 136
Influence of Temperature on Concrete Beams Strengthened in Flexure with CFRP
Ernst-Lucas Klamer

nr 137
Sturen op Klantwaarde
Jos Smeets

nr 139
Lateral Behavior of Steel Frames with Discretely Connected Precast Concrete Infill Panels
Paul Teewen

nr 140
Integral Design Method in the Context of Sustainable Building Design
Perica Savanović

nr 141
Household Activity-Travel Behavior: Implementation of Within-Household Interactions
Renni Anggraini

nr 142
Design Research in the Netherlands 2010
Henri Achten

nr 143
Modelling Life Trajectories and Transport Mode Choice Using Bayesian Belief Networks
Marloes Verhoeven

nr 144
Assessing Construction Project Performance in Ghana
William Gyadu-Asiedu

nr 145
Empowering Seniors through Domotic Homes
Masi Mohammadi

nr 146
An Integral Design Concept for Ecological Self-Compacting Concrete
Martin Hunger

nr 147
Governing Multi-Actor Decision Processes in Dutch Industrial Area Redevelopment
Erik Blokhuis

nr 148
A Multifunctional Design Approach for Sustainable Concrete
Götz Hüsken

nr 149
Quality Monitoring in Infrastructural Design-Build Projects
Ruben Favié

nr 150
Assessment Matrix for Conservation of Valuable Timber Structures
Michael Abels

nr 151
Co-simulation of Building Energy Simulation and Computational Fluid Dynamics for Whole-Building Heat, Air and Moisture Engineering
Mohammad Mirsadeghi

nr 152
External Coupling of Building Energy Simulation and Building Element Heat, Air and Moisture Simulation
Daniel Cóstola

nr 153
Adaptive Decision Making In Multi-Stakeholder Retail Planning
Ingrid Janssen

nr 154
Landscape Generator
Kymo Slager

nr 155
Constraint Specification in Architecture
Remco Niemeijer

nr 156
A Need-Based Approach to Dynamic Activity Generation
Linda Nijland

nr 157
Modeling Office Firm Dynamics in an Agent-Based Micro Simulation Framework
Gustavo Garcia Manzato

nr 158
Lightweight Floor System for Vibration Comfort
Sander Zegers

nr 159
Aanpasbaarheid van de Draagstructuur
Roel Gijsbers

nr 160
'Village in the City' in Guangzhou, China
Yanliu Lin

nr 161
Climate Risk Assessment in Museums
Marco Martens

nr 162
Social Activity-Travel Patterns
Pauline van den Berg

nr 163
Sound Concentration Caused by Curved Surfaces
Martijn Vercammen

nr 164
Design of Environmentally Friendly Calcium Sulfate-Based Building Materials: Towards an Improved Indoor Air Quality
Qingliang Yu

nr 165
Beyond Uniform Thermal Comfort on the Effects of Non-Uniformity and Individual Physiology
Lisje Schellen

nr 166
Sustainable Residential Districts
Gaby Abdalla

nr 167
Towards a Performance Assessment Methodology using Computational Simulation for Air Distribution System Designs in Operating Rooms
Mônica do Amaral Melhado

nr 168
Strategic Decision Modeling in Brownfield Redevelopment
Brano Glumac

nr 169
Pamela: A Parking Analysis Model for Predicting Effects in Local Areas
Peter van der Waerden

nr 170
A Vision Driven Wayfinding Simulation-System Based on the Architectural Features Perceived in the Office Environment
Qunli Chen

nr 171
Measuring Mental Representations Underlying Activity-Travel Choices
Oliver Horeni

nr 172
Modelling the Effects of Social Networks on Activity and Travel Behaviour
Nicole Ronald

nr 173
Uncertainty Propagation and Sensitivity Analysis Techniques in Building Performance Simulation to Support Conceptual Building and System Design
Christian Struck

nr 174
Numerical Modeling of Micro-Scale Wind-Induced Pollutant Dispersion in the Built Environment
Pierre Gousseau

nr 175
Modeling Recreation Choices over the Family Lifecycle
Anna Beatriz Grigolon

nr 176
Experimental and Numerical Analysis of Mixing Ventilation at Laminar, Transitional and Turbulent Slot Reynolds Numbers
Twan van Hooff

nr 177
Collaborative Design Support: Workshops to Stimulate Interaction and Knowledge Exchange Between Practitioners
Emile M.C.J. Quanjel

nr 178
Future-Proof Platforms for Aging-in-Place
Michiel Brink

nr 179
Motivate: A Context-Aware Mobile Application for Physical Activity Promotion
Yuzhong Lin

nr 180
Experience the City: Analysis of Space-Time Behaviour and Spatial Learning
Anastasia Moiseeva

nr 181
Unbonded Post-Tensioned Shear Walls of Calcium Silicate Element Masonry
Lex van der Meer

nr 182
Construction and Demolition Waste Recycling into Innovative Building Materials for Sustainable Construction in Tanzania
Mwita M. Sabai

nr 183
Durability of Concrete with Emphasis on Chloride Migration
Przemysław Spiesz

nr 184
Computational Modeling of Urban Wind Flow and Natural Ventilation Potential of Buildings
Rubina Ramponi

nr 185
A Distributed Dynamic Simulation Mechanism for Buildings Automation and Control Systems
Azzedine Yahiaoui

nr 186
Modeling Cognitive Learning of Urban Networks in Daily Activity-Travel Behavior
Şehnaz Cenani Durmazoğlu

nr 187
Functionality and Adaptability of Design Solutions for Public Apartment Buildings in Ghana
Stephen Agyefi-Mensah

nr 188
A Construction Waste Generation Model for Developing Countries
Lilliana Abarca-Guerrero

nr 189
Synchronizing Networks: The Modeling of Supernetworks for Activity-Travel Behavior
Feixiong Liao

nr 190
Time and Money Allocation Decisions in Out-of-Home Leisure Activity Choices
Gamze Zeynep Dane

nr 191
How to Measure Added Value of CRE and Building Design
Rianne Appel-Meulenbroek

nr 192
Secondary Materials in Cement-Based Products: Treatment, Modeling and Environmental Interaction
Miruna Florea

nr 193
Concepts for the Robustness Improvement of Self-Compacting Concrete: Effects of Admixtures and Mixture Components on the Rheology and Early Hydration at Varying Temperatures
Wolfram Schmidt

nr 194
Modelling and Simulation of Virtual Natural Lighting Solutions in Buildings
Rizki A. Mangkuto

nr 195
Nano-Silica Production at Low Temperatures from the Dissolution of Olivine - Synthesis, Tailoring and Modelling
Alberto Lazaro Garcia

nr 196
Building Energy Simulation Based Assessment of Industrial Halls for Design Support
Bruno Lee

nr 197
Computational Performance Prediction of the Potential of Hybrid Adaptable Thermal Storage Concepts for Lightweight Low-Energy Houses
Pieter-Jan Hoes

nr 198
Application of Nano-Silica in Concrete
George Quercia Bianchi

nr 199
Dynamics of Social Networks and Activity Travel Behaviour
Fariya Sharmeen

nr 200
Building Structural Design Generation and Optimisation including Spatial Modification
Juan Manuel Davila Delgado

nr 201
Hydration and Thermal Decomposition of Cement/Calcium-Sulphate Based Materials
Ariën de Korte

nr 202
Republiek van Beelden:
De Politieke Werkingen van het Ontwerp in Regionale Planvorming
Bart de Zwart

nr 203
Effects of Energy Price Increases on Individual Activity-Travel Repertoires and Energy Consumption
Dujuan Yang

nr 204
Geometry and Ventilation:
Evaluation of the Leeward Sawtooth Roof Potential in the Natural Ventilation of Buildings
Jorge Isaac Perén Montero

nr 205
Computational Modelling of Evaporative Cooling as a Climate Change Adaptation Measure at the Spatial Scale of Buildings and Streets
Hamid Montazeri

nr 206
Local Buckling of Aluminium Beams in Fire Conditions
Ronald van der Meulen

nr 207
Historic Urban Landscapes:
Framing the Integration of Urban and Heritage Planning in Multilevel Governance
Loes Veldpaus

nr 208
Sustainable Transformation of the Cities:
Urban Design Pragmatics to Achieve a Sustainable City
Ernesto Antonio Zumelzu Scheel

nr 209
Development of Sustainable Protective Ultra-High Performance Fibre Reinforced Concrete (UHPFRC):
Design, Assessment and Modeling
Rui Yu

nr 210
Uncertainty in Modeling Activity-Travel Demand in Complex Uban Systems
Soora Rasouli

nr 211
Simulation-based Performance Assessment of Climate Adaptive Greenhouse Shells
Chul-sung Lee

nr 212
Green Cities:
Modelling the Spatial Transformation of the Urban Environment using Renewable Energy Technologies
Saleh Mohammadi

nr 213
A Bounded Rationality Model of Short and Long-Term Dynamics of Activity-Travel Behavior
Ifigeneia Psarra

nr 214
Effects of Pricing Strategies on Dynamic Repertoires of Activity-Travel Behaviour
Elaheh Khademi

nr 215
Handstorm Principles for Creative and Collaborative Working
Frans van Gassel

nr 216
Light Conditions in Nursing Homes: Visual Comfort and Visual Functioning of Residents
Marianne M. Sinoo

nr 217
Woonsporen: De Sociale en Ruimtelijke Biografie van een Stedelijk Bouwblok in de Amsterdamse Transvaalbuurt
Hüseyin Hüsnü Yegenoglu

nr 218
Studies on User Control in Ambient Intelligent Systems
Berent Willem Meerbeek

nr 219
Daily Livings in a Smart Home: Users' Living Preference Modeling of Smart Homes
Erfaneh Allameh

nr 220
Smart Home Design: Spatial Preference Modeling of Smart Homes
Mohammadali Heidari Jozam

nr 221
Wonen: Discoursen, Praktijken, Perspectieven
Jos Smeets

nr 222
Personal Control over Indoor Climate in Offices: Impact on Comfort, Health and Productivity
Atze Christiaan Boerstra

nr 223
Personalized Route Finding in Multimodal Transportation Networks
Jianwe Zhang

nr 224
The Design of an Adaptive Healing Room for Stroke Patients
Elke Daemen

nr 225
Experimental and Numerical Analysis of Climate Change Induced Risks to Historic Buildings and Collections
Zara Huijbregts

nr 226
Wind Flow Modeling in Urban Areas Through Experimental and Numerical Techniques
Alessio Ricci

nr 227
Clever Climate Control for Culture: Energy Efficient Indoor Climate Control Strategies for Museums Respecting Collection Preservation and Thermal Comfort of Visitors
Rick Kramer

nr 228
Fatigue Life Estimation of Metal Structures Based on Damage Modeling
Sarmediran Silitonga

nr 229
A multi-agents and occupancy based strategy for energy management and process control on the room-level
Timilehin Moses Labeodan

nr 230
Environmental assessment of Building Integrated Photovoltaics: Numerical and Experimental Carrying Capacity Based Approach
Michiel Ritzen

nr 231
Performance of Admixture and Secondary Minerals in Alkali Activated Concrete: Sustaining a Concrete Future
Arno Keulen

nr 232
World Heritage Cities and Sustainable Urban Development: Bridging Global and Local Levels in Monitoring the Sustainable Urban Development of World Heritage Cities
Paloma C. Guzman Molina

nr 233
Stage Acoustics and Sound Exposure in Performance and Rehearsal Spaces for Orchestras: Methods for Physical Measurements
Remy Wenmaekers

nr 234
Municipal Solid Waste Incineration (MSWI) Bottom Ash: From Waste to Value Characterization, Treatments and Application
Pei Tang

nr 235
Large Eddy Simulations Applied to Wind Loading and Pollutant Dispersion
Mattia Ricci

nr 236
Alkali Activated Slag-Fly Ash Binders: Design, Modeling and Application
Xu Gao

nr 237
Sodium Carbonate Activated Slag: Reaction Analysis, Microstructural Modification & Engineering Application
Bo Yuan

nr 238
Shopping Behavior in Malls
Widiyani

nr 239
Smart Grid-Building Energy Interactions: Demand Side Power Flexibility in Office Buildings
Kennedy Otieno Aduda

nr 240
Modeling Taxis Dynamic Behavior in Uncertain Urban Environments
Zheng Zhong

nr 241
Gap-Theoretical Analyses of Residential Satisfaction and Intention to Move
Wen Jiang

nr 242
Travel Satisfaction and Subjective Well-Being: A Behavioral Modeling Perspective
Yanan Gao

nr 243
Building Energy Modelling to Support the Commissioning of Holistic Data Centre Operation
Vojtech Zavrel

nr 244
Regret-Based Travel Behavior Modeling: An Extended Framework
Sunghoon Jang

nr 245
Towards Robust Low-Energy Houses: A Computational Approach for Performance Robustness Assessment using Scenario Analysis
Rajesh Reddy Kotireddy

nr 246
Development of sustainable and functionalized inorganic binder-biofiber composites
Guillaume Doudart de la Grée

nr 247
A Multiscale Analysis of the Urban Heat Island Effect: From City Averaged Temperatures to the Energy Demand of Individual Buildings
Yasin Toparlar

nr 248
Design Method for Adaptive Daylight Systems for buildings covered by large (span) roofs
Florian Heinzelmann

nr 249
Hardening, high-temperature resistance and acid resistance of one-part geopolymers
Patrick Sturm

nr 250
Effects of the built environment on dynamic repertoires of activity-travel behaviour
Aida Pontes de Aquino

nr 251
Modeling for auralization of urban environments: Incorporation of directivity in sound propagation and analysis of a framework for auralizing a car pass-by
Fotis Georgiou

nr 252
Wind Loads on Heliostats and Photovoltaic Trackers
Andreas Pfahl

nr 253
Approaches for computational performance optimization of innovative adaptive façade concepts
Roel Loonen

nr 254
Multi-scale FEM-DEM Model for Granular Materials: Micro-scale boundary conditions, Statics, and Dynamics
Jiadun Liu

nr 255
Bending Moment - Shear Force Interaction of Rolled I-Shaped Steel Sections
Rianne Willie Adriana Dekker

nr 256
Paralympic tandem cycling and handcycling: Computational and wind tunnel analysis of aerodynamic performance
Paul Fionn Mannion

nr 257
Experimental characterization and numerical modelling of 3D printed concrete: Controlling structural behaviour in the fresh and hardened state
Robert Johannes Maria Wolfs

nr 258
Requirement checking in the building industry: Enabling modularized and extensible requirement checking systems based on semantic web technologies
Chi Zhang

nr 259
A Sustainable Industrial Site Redevelopment Planning Support System
Tong Wang

nr 260
Efficient storage and retrieval of detailed building models: Multi-disciplinary and long-term use of geometric and semantic construction information
Thomas Ferdinand Krijnen

nr 261
The users' value of business center concepts for knowledge sharing and networking behavior within and between organizations
Minou Weijs-Perrée

nr 262
Characterization and improvement of aerodynamic performance of vertical axis wind turbines using computational fluid dynamics (CFD)
Abdolrahim Rezaeiha

nr 263
In-situ characterization of the acoustic impedance of vegetated roofs
Chang Liu

nr 264
Occupancy-based lighting control: Developing an energy saving strategy that ensures office workers' comfort
Christel de Bakker

nr 265
Stakeholders-Oriented Spatial Decision Support System
Cahyono Susetyo

nr 266
Climate-induced damage in oak museum objects
Rianne Aleida Luimes

nr 267
Towards individual thermal comfort: Model predictive personalized control of heating systems
Katarina Katic

nr 268
Modelling and Measuring Quality of Urban Life: Housing, Neighborhood, Transport and Job
Lida Aminian

nr 269
Optimization of an aquifer thermal energy storage system through integrated modelling of aquifer, HVAC systems and building
Basar Bozkaya

nr 270
Numerical modeling for urban sound propagation: developments in wave-based and energy-based methods
Raúl Pagán Muñoz

nr 271
Lighting in multi-user office environments: improving employee wellbeing through personal control
Sanae van der Vleuten-Chraibi

nr 272
A strategy for fit-for-purpose occupant behavior modelling in building energy and comfort performance simulation
Isabella I. Gaetani dell'Aquila d'Aragona

nr 273
Een architectuurhistorische waardestelling van naoorlogse woonwijken in Nederland: Het voorbeeld van de Westelijke Tuinsteden in Amsterdam
Eleonore Henriette Marie Mens

nr 274
Job-Housing Co-Dependent Mobility Decisions in Life Trajectories
Jia Guo

nr 275
A user-oriented focus to create healthcare facilities: decision making on strategic values
Emilia Rosalia Catharina Maria Huisman

nr 276
Dynamics of plane impinging jets at moderate Reynolds numbers – with applications to air curtains
Adelya Khayrullina

nr 277
Valorization of Municipal Solid Waste Incineration Bottom Ash - Chemical Nature, Leachability and Treatments of Hazardous Elements
Qadeer Alam

nr 278
Treatments and valorization of MSWI bottom ash - application in cement-based materials
Veronica Caprai

nr 279
Personal lighting conditions of office workers - input for intelligent systems to optimize subjective alertness
Juliëtte van Duijnhoven

nr 280
Social influence effects in tourism travel: air trip itinerary and destination choices
Xiaofeng Pan

nr 281
Advancing Post-War Housing: Integrating Heritage Impact, Environmental Impact, Hygrothermal Risk and Costs in Renovation Design Decisions
Lisanne Claartje Havinga

nr 282
Impact resistant ultra-high performance fibre reinforced concrete: materials, components and properties
Peipeng Li

nr 283
Demand-driven Science Parks: The Perceived Benefits and Trade-offs of Tenant Firms with regard to Science Park Attributes
Wei Keat Benny Ng

nr 284
Raise the lantern; how light can help to maintain a healthy and safe hospital environment focusing on nurses
Maria Petronella Johanna Aarts

nr 285
Modelling Learning and Dynamic Route and Parking Choice Behaviour under Uncertainty
Elaine Cristina Schneider de Carvalho

nr 286
Identifying indoor local microclimates for safekeeping of cultural heritage
Karin Kompatscher

nr 287
Probabilistic modeling of fatigue resistance for welded and riveted bridge details. Resistance models and estimation of uncertainty.
Davide Leonetti

nr 288
Performance of Layered UHPFRC under Static and Dynamic Loads: Effects of steel fibers, coarse aggregates and layered structures
Yangyueye Cao

nr 289
Photocatalytic abatement of the nitrogen oxide pollution: synthesis, application and long-term evaluation of titania-silica composites
Yuri Hendrix

nr 290
Assessing knowledge adoption in post-disaster reconstruction: Understanding the impact of hazard-resistant construction knowledge on reconstruction processes of self-recovering communities in Nepal and the Philippines
Eefje Hendriks

nr 291
Locating electric vehicle charging stations: A multi-agent based dynamic simulation
Seheon Kim

nr 292
De invloed van Lean Management op de beheersing van het bouwproces
Wim van den Bouwhuijsen

nr 293
Neighborhood Environment and Physical Activity of Older Adults
Zhengying Liu

nr 294
Practical and continuous luminance distribution measurements for lighting quality
Thijs Willem Kruisselbrink

nr 295
Auditory Distraction in Open-Plan Study Environments in Higher Education
Pieternella Elizabeth Braat-Eggen

nr 296
Exploring the effect of the sound environment on nurses' task performance: an applied approach focusing on prospective memory
Jikke Reinten

nr 297
Design and performance of water resistant cementitious materials– Mechanisms, evaluation and applications
Zhengyao Qu

nr 298
Design Optimization of Seasonal Thermal Energy Storage Integrated District Heating and Cooling System: A Modeling and Simulation Approach
Luyi Xu

nr 299
Land use and transport: Integrated approaches for planning and management
Zhongqi Wang

nr 300
Multi-disciplinary optimization of building spatial designs: co-evolutionary design process simulations, evolutionary algorithms, hybrid approaches
Sjonnie Boonstra

nr 301
Modeling the spatial and temporal relation between urban land use, temperature, and energy demand
Hung-Chu Chen

nr 302
Seismic retrofitting of masonry walls with flexible deep mounted CFRP strips
Ömer Serhat Türkmen

nr 303
Coupled Aerostructural Shape and Topology Optimization of Horizontal-Axis Wind Turbine Rotor Blades
Zhijun Wang

nr 304
Valorization of Recycled Waste Glass and Converter Steel Slag as Ingredients for Building Materials: Hydration and Carbonation Studies
Gang Liu

nr 305
Low-Carbon City Development based on Land Use Planning
Gengzhe Wang

nr 306
Sustainable energy transition scenario analysis for buildings and neighborhoods - Data driven optimization
Shalika Saubhagya Wickramarachchi Walker

nr 307
In-between living and manufactured: an exploratory study on biobuilding components for building design
Berrak Kirbas Akyurek

nr 308
Development of alternative cementitious binders and functionalized materials: design, performance and durability
Anna Monika Kaja

nr 309
Development a morphological approach for interactive kinetic façade design: Improving multiple occupants' visual comfort
Seyed Morteza Hosseini

nr 310
PV in urban context: modeling and simulation strategies for analyzing the performance of shaded PV systems
Ádám Bognár

nr 311
Life Trajectory, Household Car Ownership Dynamics and Home Renewable Energy Equipment Adoption
Gaofeng Gu

nr 312
Impact of Street-Scale Built Environment on Walking/Cycling around Metro Stations
Yanan Liu

nr 313
Advances in Urban Traffic Network Equilibrium Models and Algorithms
Dong Wang

nr 314
Development of an uncertainty analysis framework for model-based consequential life cycle assessment: application to activity-based modelling and life cycle assessment of multimodal mobility
Paul Martin Baustert

nr 315
Variable stiffness and damping structural joints for semi-active vibration control
Qinyu Wang

nr 316
Understanding Carsharing-Facilitating Neighborhood Preferences
Juan Wang

nr 317
Dynamic alignment of Corporate Real Estate to business strategies: An empirical analysis using historical data and in-depth modelling of decision making
Howard Cooke

nr 318
Local People Matter: Towards participatory governance of cultural heritage in China
Ji Li

nr 319
Walkability and Walkable Healthy Neighborhoods
Bojing Liao

nr 320
Light directionality in design of healthy offices: exploration of two methods
Parisa Khademagha

nr 321
Room acoustic modeling with the time-domain discontinuous Galerkin method
Huiqing Wang

nr 322
Sustainable insulating lightweight materials for enhancing indoor building performance: miscanthus, aerogel and nano-silica
Yuxuan Chen

nr 323
Computational analysis of the impact of façade geometrical details on wind flow and pollutant dispersion
Xing Zheng

nr 324
Analysis of urban wind energy potential around high-rise buildings in close proximity using computational fluid dynamics
Yu-Hsuan Jang

nr 325
A new approach to automated energy performance and fault detection and diagnosis of HVAC systems: Development of the 4S3F method
Arie Taal

nr 326
Innovative Admixtures for Modifying Viscosity and Volume Change of Cement Composites
Hossein Karimi

nr 327
Towards houses with low grid dependency: A simulation-based design optimization approach
Zahra Mohammadi

nr 328
Activation of demand flexibility for heating systems in buildings: Real-life demonstration of optimal control for power-to-heat and thermal energy storage
Christian Finck

nr 329
A computational framework for analysis and optimisation of automated solar shading systems
Samuel B. de Vries

nr 330
Challenges and potential solutions for cultural heritage adaptive reuse: a comparative study employing the Historic Urban Landscape approach
Nadia Pintossi

nr 331
Shared control in office lighting systems
Tatiana Aleksandrovna Lashina

nr 332
Comfort in Urban Public Spaces
You Peng

nr 333
Numerical modelling of metal soap formation in historical oil paintings
Gerardus Johannes Anna Maria Eumelen

nr 334
A transdisciplinary decision-making approach to food-water-energy nexus: A guide towards sustainable development
Maryam Ghodsvali

nr 335
Numerical modelling of transient low-frequency sound propagation and vibration in buildings
Indra Sihar

nr 336
Characterization of impact sound from lightweight joist floors
Yi Qin

nr 337
Cities for Children: Supporting Children and Caregivers in Participatory Urban Planning
Özlemnur Ataol

nr 338
Engaging the unengaged: Exploring citizen participation in nature-based solutions in China
Li Dai

nr 339
Municipal Solid Waste Incineration Residues: analysis, treatments, and applications
Ekaterina Loginova

nr 340
Enhancing the Uptake of Nature-Based Solutions in Urban Settings: An Information Systems Approach
Shahryar Ershad Sarabi

nr 341
Work Schedule Arrangements in Two-Adult Households with Children
Bilin Han

nr 342
Increasing awareness of urban cultural heritage using digital technologies: empirical design and analysis of a new multi-media web platform
Benshuo Wang

nr 343
Mechanical and physical properties of fibre-cement composites using alternative natural fibres
Katerina Kochova

nr 344
Numerical and experimental investigation of urban microclimate in a real compact heterogeneous urban area
Nestoras Antoniou

nr 345
Examining in-class activities to facilitate academic achievement in higher education: A framework for optimal indoor environmental conditions
Henk W. Brink

nr 346
High-temperature resistant geopolymers: composition, microstructure and performance
Kinga Malgorzata Klima

nr 347
Individual and household decision-making in shared parking
Qianqian Yan

nr 348
In-situ formation of LDHs in Alkali activated binders
Tao Liu

nr 349
Condition assessment of concrete sewer pipes through an integrated experimental-numerical approach
Irene C. Scheperboer

nr 350
In situ PU-based characterization of sound absorbing materials for room acoustic modeling purposes
Baltazar Briere de La Hosseraye

nr 351
Uncertainty analysis and management in building energy data mining: A bottom-up approach considering the temporal and spatial aspect of data
Waqas Khan

nr 352
Personalized Heating Control Systems to improve thermal comfort and reduce energy consumption
Michal Veselý

nr 353
Restorative value of the urban greenscape: Urban residential streets as restorative environments
Robert P. van Dongen

nr 354
Urban ventilation and the compact Mediterranean city: numerical investigations of the dynamic relationships between density, morphology and wind flow
Olga Palusci

nr 355
Data science for buildings: a multi-scale approach bridging occupants to smart-city energy planning
Julien Leprince

nr 356
Class Association Rule Models for Predicting Transportation Mode Choice
Jiajia Zhang

nr 357
Acceptance and use of autonomous vehicles
Zhihui Tian

nr 358
Consumer Acceptance of Crowdshipping Services
Chenyu Wang

nr 359
Determinants of habitual participation in leisure-time physical activity and active travel in life trajectories
Xiaoyue Chen

nr 360
Analysis of Citizens' Motivation and Intention Using Modern Information Technology in Urban Planning Public Participation
Wenshu Li

nr 361
Linking smart and physical port cities. Port-city interface areas: from obsolete/isolated to smart environments
Mercè de Miguel Capdevila

nr 362
Assessment and improvement of indoor thermal comfort and energy demand of Chinese heritage apartment buildings under climate change
Muxi Lei

nr 363
Indoor airflow and heat transfer in a cross-ventilated generic building: wind tunnel experiments and computational fluid dynamics analyses
Katarina Kosutova

nr 364
A Robotic Construction Simulation Platform for Light-weight Prefabricated Structures. Lifetime prediction of vertical-axis wind turbines based on CFD simulations and high-cycle fatigue modeling
Aiyu Zhu

nr 365
Lifetime prediction of vertical-axis wind turbines based on CFD simulations and high-cycle fatigue modeling
Feiyu Geng

nr 366
Computational modeling of convective heat transfer at building surfaces
Samy Iousef

nr 367
Computational modeling of convective heat transfer at building surfaces
Vasaturo Raffaele

nr 368
Bouwen zonder scrupules. De Nederlandse bouwnijverheid tijdens de bezetting en de eerste jaren van wederopbouw (1940-1950)
Geert-Jan Mellink

nr 369
Factors Promoting a Positive Experienced Neighborhood Public Space--A Virtual Environment-based analysis
Yuwen Zhao

nr 370
Place quality making in high-speed railway station areas: Devising place quality indicators for urban design, beyond the transport-land use divide
Jinglun Du

nr 371
Sustainable Bio-based Adsorptive Concrete for Phosphorus Removal
Fan Wu

nr 372
The physical workplace as a resource for mental health: A salutogenic approach to a mentally healthy workplace design at home and at the office
Lisanne Bergefurt

nr 373
High-end application of basic oxygen furnace steel slag as sustainable building materials
Muhammad Jawad Ahmed

nr 374
Energy-Efficient Urban Rail Transit Operations: Models, Algorithms, and Applications
Kang Huang

Chloride ingress in concrete may lead to corrosion of steel reinforcements and reduced service life. The moisture transport in concrete plays a significant role in this process. Therefore, a lack of comprehensive understanding of moisture transport and the combined impacts of moisture and chloride ingress can lead to reduced durability and service life of concrete structures.

The motivation for the presented research is to address the identified gaps in knowledge and contribute to developing more effective strategies for improving the durability of concrete structures, protecting steel reinforcements from corrosion, and ultimately extending the service life of these structures. This is achieved by comparing different moisture transport models, creating a developing experimental procedures for assessing moisture transport, evaluating the impact of sorption isotherms, assessing the combined effects of moisture and chloride, and examining the interaction between transport mechanisms.

This thesis provides fresh insights into the complex processes of moisture and chloride transport in concrete and presents several new experimental methods and models.

DEPARTMENT OF THE BUILT ENVIRONMENT

TU/e EINDHOVEN UNIVERSITY OF TECHNOLOGY